Synthesis and Photophysics of Functionalized Silicon Nanoparticles

Promotoren

Prof. dr. H. Zuilhof, Hoogleraar in de organische chemie, Laboratorium voor Organische Chemie, Wageningen Universiteit, Nederland.

Prof. dr. L. De Cola, Hoogleraar in de chemie en fysica, Physikalisches Institut**,** Westfälische Wilhelms-Universität, Duitsland.

Samenstelling promotiecommissie

Prof. dr. ir. I. M.C.M. Rietjens	Wageningen Universiteit
Prof. dr. H. van Amerongen	Wageningen Universiteit
Prof. dr. ir. P. H. M. van Loosdrecht	Rijksuniversiteit Groningen
Prof. dr. ir. F. A. M. Leermakers	Wageningen Universiteit

Dit onderzoek is uitgevoerd binnen de onderzoekschool VLAG

Synthesis and Photophysics of Functionalized Silicon Nanoparticles

Milena Rosso-Vasic

Proefschrift

Ter verkrijging van de graad van doctor
op gezag van de Rector Magnificus
van Wageningen Universiteit,
Prof. Dr. M. J. Kropff,
in het openbaar te verdedigen
op maandag 1 december 2008
des namiddags te 13.30 uur in de Aula

Rosso-Vasic, M.

Synthesis and Photophysics of Functionalized Silicon Nanoparticles

PhD Thesis submitted to Wageningen University - with summaries in English and Dutch

ISBN: 978-90-8585-294-0

To my grandfather
Drs. Ir. Zivota Jovanovic
For trying to find the answers to all my questions,
for developing my love and admiration for nature and science,
spending long hours with me in chemical laboratories
and all the laughs we had together

Mom deki
Dipl. Ing. Zivoti Jovanovicu
Za sve odgovore na moja mnogobrojna pitanja,
Zato sto me je naucio da volim prirodu i nauku,
Za sve sate koje smo zajedno proveli eksperimentisuci i racunajuci,
Za sve osmehe.

Contents

Chapter 1

General Introduction

Abstract -To highlight the motivation for studying silicon nanoparticles (Si NPs), this section aims to introduce the reader into nanoscale world and to set the stage by discussing general properties of nanoobjects and in particular of semiconductor quantum dots (QDs). Furthermore, basic properties of Si NPs and various preparation methods are discussed and the contents of the thesis outlined.

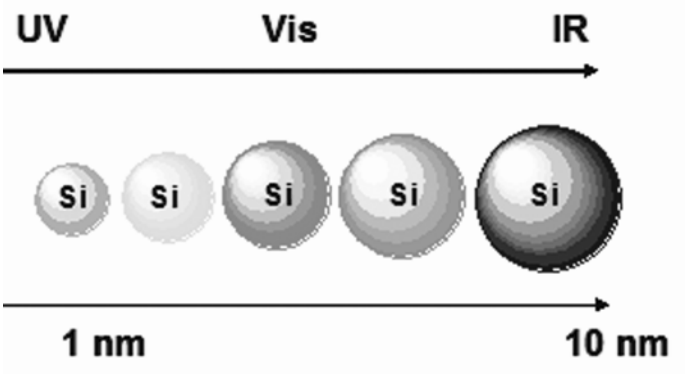

1.1 Introduction

> *"Nanotechnology will change the world. It will affect almost any aspect of our lives: medicines we use, power of our computers, the energy supplies we require, the food we eat, the cars we drive, the buildings we live in and the clothes we wear."*
> *P. Holister*

Nanotechnology is a relatively new and very promising interdisciplinary field which involves biological, chemical, physical and engineering studies of the nano-sized objects (1-100 nm). One of the most exciting and challenging aspects of the nanoscale world is the role that quantum mechanics plays in it, next to classical physics.[1,2] Quantum phenomena are, of course, the ultimate basis of atoms and molecules, but are largely hidden behind classical behavior in macroscopic matter and structures.[2] Although the awareness of the importance of nanoobjects and their possible application was present since early 1959,[3] the real breakthrough point in nanoscience was the invention of the Scanning Tunneling Microscope (STM).[4,5] This invention allowed an entrance in the nanoworld by direct observation of nanostructures.[6] Since then, this field is blossoming: knowledge, creativity and futuristic visions of scientists of different profiles meet to create and study new nanoobjects, of which many of them are already applied in various fields of medicine[7-9] and technology.[10-17]

For almost two decades, research into semiconductor nanoclusters has been focused on the properties of *quantum dots (QDs)* - semiconductor fragments consisting of hundreds to thousands of atoms.[1] Quantum dots have exceptional optical and electronic properties such as: size dependent - tunable light emission wavelengths,[1,18,19] intense fluorescence,[20-23] resistance against photobleaching[24] and simultaneous excitation of multiple fluorescent colors.[25-28] All these properties make QDs superior in many respects over organic dyes and fluorescent proteins.

1.2 Quantum Confinement Effect

Luminescent QDs exist in an intermediate regime between bulk and molecular behavior. The novel properties of QDs occur due to *quantum confinement*: as the cluster size of a semiconductor decreases, the gap between valence and conduction band increases (see Figure 1.1).[29-31] This basic phenomenon can be understood by considering the relation between the electron position and the crystal momentum in both free and confined space. For an electron in the periodic potential of an extended solid, the energy or crystal momentum can be precisely defined, while the position cannot. In the case of a confined particle, the uncertainty in the electron position decreases, so that the momentum is no longer well defined. In the bulk solid, series of nearby transitions occur at slightly different

energies and in the quantum dot transitions will be compressed by quantum confinement into a single, intense transition.[31]

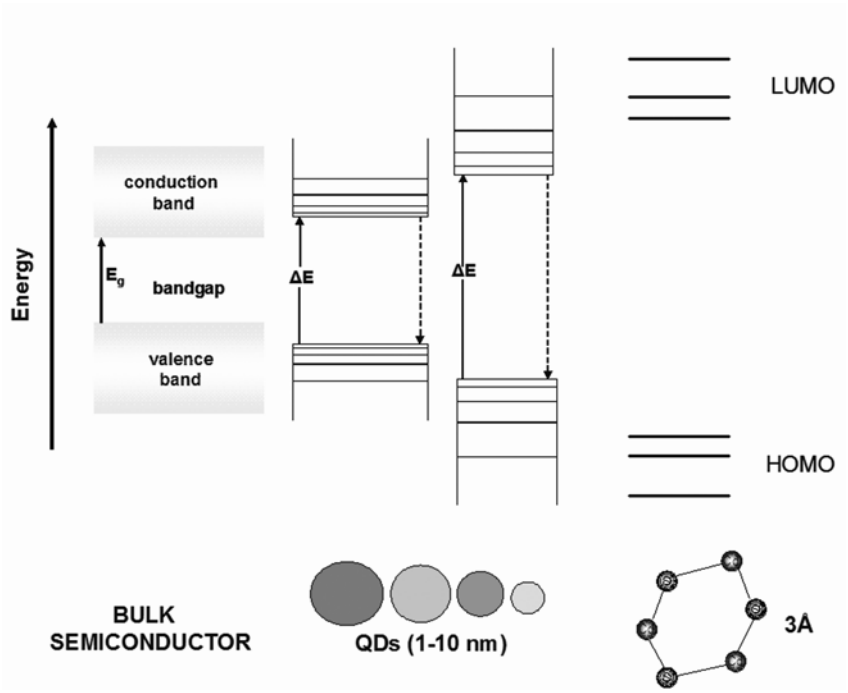

Figure 1.1. Semiconductor energy levels. (*See Appendix at the end of the thesis for the color picture)*

The absorption of a photon creates an electron-hole pair that is delocalized across the interior of the nanoparticle, confined by its finite size. Emission of a photon can occur upon recombination of the electron and hole. Efficient photoluminescence (PL) is only possible when the size of QDs is smaller than the Bohr radius of the material. This radius controls how large a crystal must be before its energy bands can be treated as continuous. Therefore, the exciton Bohr radius defines whether a crystal can be called a semiconductor quantum dot, or simply acts like a bulk semiconductor.[18, 32]

1.3 Core-shell Semiconductor Quantum Dots

Since the first directed synthesis of QDs,[33] it took 16 years until QDs entered their new role – as fluorescent probes.[34-37] The limiting factor was the development of a procedure for the synthesis of stable, high-quality QDs.

Following the initial reports,[1,24,33] extensive research has been directed towards developing a variety of II-VI SC QDs.[38] With the development of CdSe/ZnS/silane (core/shell/coat) QDs, this research has finally progressed to an advanced, commercial stage. Stable and multifunctional QDs are nowadays used for a variety of *in vivo* and *in vitro* bioimaging purposes as highly bright and stable emitters.[39-42] In the center of the nanoparticle is the

CdSe core (heart), which is responsible for the PL and which can be varied in size to tune the transition energy (color) across the visible region of spectrum.[43] The ZnS shell is a layer of high band-gap material that is needed to stabilize the PL of the core, and to provide a physical barrier with the surrounding.[44] Finally, the silane coat is a supplementary layer attached in order to mask the toxicity[45] of the semiconductor materials. At the same time it provides a hydrophilic interface for aqueous stability and subsequent functionalization (Figure 1.2).[41]

To specifically adjust the emission wavelength of QDs from UV to IR, different substitutes can be used for building core/shell/coat complex structures, like II-VI compounds (ZnSe and CdTe [46-52] or SnTe[53]) and II-V materials (InP and GaAs[54-58]).

The development of multilayered QDs has led to many novel applications in biophysics, mainly for bioimaging purposes.[59-61] Their improved photostability minimizes problems associated with photobleaching that is characteristic for organic fluorophores.[62] Their broad excitation spectra and narrow emission profiles[39,63] make QDs particularly well-suited for use in multicolor imaging[64-67] and cross-correlation spectroscopy.[68-70]

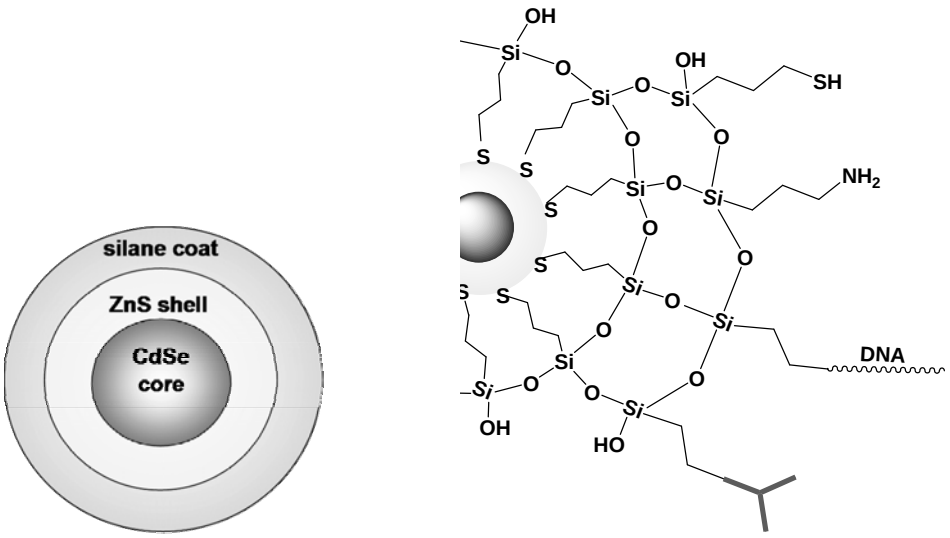

Figure 1.2. Sketch of core/shell/coat quantum dot and some possible functionalizations.
(*See Appendix at the end of the thesis for the color picture)*

Besides all the mentioned advantages, core/shell/coat QDs have a few downsides that considerably limit their potential application range:

1. Large overall size
2. High intrinsic elemental toxicity

In the best case, core-shell nanostructures have a minimal size between 10 and 20 nm,[41] which is significantly larger than most biomolecules. This restricts their use in cellular applications, as the internalization (cellular uptake) of small NPs is much more efficient.

Besides, intracellular localization of larger NPs is very limited.[42] Although it would be possible to make smaller core/shell QDs, there is a definite minimally obtainable size of at least several nm, which is incompatible with most applications in molecular scale dynamics.

The intrinsic toxicity of II-VI semiconductors is a major concern for application in any biological system.[45,71] Silane coatings help to reduce this problem, but the porosity thereof is hard to control. In addition, long-term toxicity of waste materials after the use of such QDs is also a concern. Since these complex structures are decoupled from the environment due to shielding, they are outperformed by organic fluorophores in regard of luminescent probes of the local surroundings, e.g. of specific sensitivity towards the pH in solutions.[32,72]

Another often used method for coating of core/shell QDs is the use of various polymers. In this case further specific functionalization is not trivial as required reaction conditions may interfere with the stability of the polymer coating, but such stabilized QDs are still highly useful for novel solar cell and light-emitting diode applications.[73-75]

Taking into account above described limiting factors, there is undoubtedly a great opportunity (and huge commercial interest) for the development of a smaller, more versatile, and less toxic class of luminescent QDs for use in biological and many other applications.

1.4 Silicon Nanoparticles (Si NPs)

1.4.1 The Origin of Fluorescence and (In-)direct Bandgap

Si is a bioinert semiconductor that is electronically very stable.[76,77] In contrast to all II-VI nanoparticle types, Si exhibits a low inherent toxicity.[78] As a semiconductor material, it would be more natural to also name Si nanoparticles “quantum dots”, but in the wide body of literature they are named silicon nanoparticles (Si NPs) and this is how it will be referred to them in this thesis.

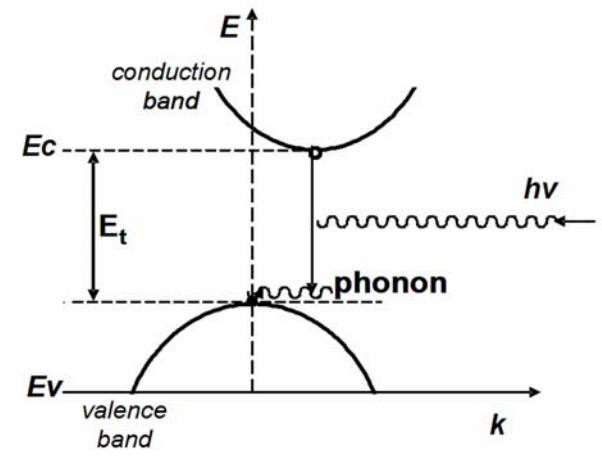

Figure 1.3. Indirect band-gap diagram; k – wave vector of Si lattice vibration, E – energy, E_t – the energy difference between maximal energy of the valence band (E_v) and minimal energy of the conduction band (E_c).

While most of the II-VI QDs are known to have a direct band-gap transition, bulk Si is an indirect band-gap semiconductor. In this case the transition from the bottom of the conduction band to the top of the valence band violates conservation of momentum and is electronically forbidden.[79,80]

The transition does occur, but only with phonon (a quantum of lattice vibration) assistance.[81-85] That means that the absorption and emission of photon require the additional change in lattice vibration mode. This is an indirect process with a low probability, and for this reason, in contrast to its extensive use in electronic devices bulk Si has only found limited optical applications. Based on this, it might be anticipated that Si NPs would tend to have a long PL lifetime (at least microseconds) and low PL efficiencies when compared to direct band-gap semiconductors.[86]

However, as the size of Si NPs gets smaller (less than a few nm), the concepts of crystallinity, periodic structure and crystal momentum, from which the relevant selection criteria are derived, gradually lose their meaning as the behavior of nanoparticles shifts from the regime of bulk semiconductor physics to molecular physics.[87] It has been shown experimentally by us[88] (Chapter 2) and Korgel *et al.*[89] that PL lifetimes of Si NPs smaller than 2 nm are on the nanosecond time scale, which is much more rapid than would be anticipated if the transition remained indirect in origin. Therefore, it is concluded that electronic transitions in this case must have direct-like character.

1.4.2. Surface Reconstruction and Termination

Besides quantum confinement effects, PL mechanisms in Si NPs are also dependent on *surface reconstruction*[90-92] and *surface termination*[93] of Si NPs.

The result of *surface reconstruction* phenomenon is that Si atoms on the surface of the nanoparticle adopt a significantly different geometry than the bulk lattice structure. These alternations can have a major impact on NPs properties, particularly in ultrasmall Si NPs (1 - 2 nm), where the surface atoms must reconstruct their bonding geometry to accommodate the high curvature of the interface.[91]

Surface termination also has a big effect on final photophysical properties of Si NPs. In the case of a dihydride termination, each Si atom on the surface forms two “back-bonds” with neighboring Si atoms and two terminal bonds with H atoms. In a monohydride termination, each surface atom has three Si-Si “back-bonds” and one Si-H bond, which gives a different set of bonding constrains. This can significantly change PL properties of the NPs. On the basis of theoretical studies of the lattice of Si NPs, it is predicted that substantial reconstruction occurs on the dihydride surface of ultrasmall Si NPs, creating novel Si-Si dimer bonds that may serve as the primary location of PL transitions.[81,94]

Beside the mentioned phenomena, the sensitivity of hydrogen-terminated Si NPs to oxidation plays a major role in defining their photophysical characteristics,[95-97] especially for the ultrasmall Si NPs. Upon the (partial) oxidation of Si NPs, a significant red shift in absorption and emission occurs.[86,95] Hydrogen-terminated Si NPs have optically allowed, direct bandgap transitions. However, if the Si NPs surface is passivated by oxygen, a stabilized electronic state (or even a trapped exciton) may be formed centered around the Si–O covalent bond. Depending on the size of the Si NPs, the influence of oxidation will vary. For bigger Si NPs (3-5 nm), (partial) oxidation yields no red-shift independent of whether the Si NPs are hydrogen- or oxygen-terminated: although the Si–O surface state may have a relatively low energy, it has no influence on the optical properties since the LUMO is still lower in energy. In the case of ultrasmall Si NPs, there is a large red shift when the surface is exposed to oxygen.[86] Also, upon the formation of Si–O bonds on ultrasmall Si NPs, the remaining Si–Si bonds are destabilized and electron density of the HOMO and LUMO is drawn from the silicon core to the Si-O shell. It is calculated that the oxide passivation (with one Si=O bond) lowers the band gap to a significant extent: by ~1.5 eV for 0.8 nm cores and ~0.9 eV for 1.5 nm Si NPs.[86,95] These theoretical results are in good agreement with experimental data.[86]

1.5 Functionalization of Si NPs

Well developed methods for tailoring silicon surfaces involve the formation of stable covalent bonds (Si–C) that prevent surface oxidation. On planar or porous silicon surfaces, the hydrosilylation reaction - which involves addition of silicon and hydrogen on an unsaturated carbon-carbon bond - can be initiated thermally,[98-100] photochemically (with UV[101] or visible light[102-104]) or by a radical initiator[101,105] and alkyl- or aryl-carbanions.[106]

The main difference between Si NPs and well-defined silicon surfaces (100, 111, etc.) is that different surface orientations can be distinguished on the surface of a Si NP.[107,108] The starting point of functionalization of Si NPs are halogen-[109,110] or hydrogen-terminated[111-114] Si NPs. Due to the low stability of Si–H and Si–X (X = Cl, Br) bonds,[115] these types of NPs are extremely prone to oxidation in air. Further stabilization is a necessity and is usually performed by reaction with alkyl-lithium salts[110] or terminal alkenes,[116] to provide very stable Si-C linkages. The reaction with terminal alkenes is performed by using light,[111] heat,[117] or a variety of platinum-[118] and triphenylcarbenium-based catalysts.[119]

The advantage of hydrosilylation reactions is that they occur without breaking Si-Si bonds.[120,121] This fact is particularly important for the functionalization of ultrasmall Si NPs (which consist of about 100 - 200 Si atoms). Indeed, any route leading to Si-Si bond cleavage could have an adverse impact on Si NPs optical properties, potentially even dissolving particles completely.[117] Such an effect was observed in the case of the reaction

with alcohols, where the alkoxylation results in the cleavage of Si-Si bonds and the formation of Si-H and Si-O-C species.[122] Alkylation with Grignard or alkyl lithium reagents occurs through nucleophilic attack by a carbanion on an electron-deficient Si atom, cleaving Si-Si bonds to form Si-C bonds and silyl anion (Si^-) species.[120,121]

Applying the previously described functionalization reactions, a very broad range of compounds can be used to cap the core of Si NPs, and to provide the desired functionality and solubility. It has, for example, been demonstrated that attaching terminating –COOH[117] or $–NH_2$ groups[123,124] (Chapter 3) makes the NPs water soluble, while using nonpolar groups at the end of the alkyl chain makes them soluble in nonpolar solvents (Chapter 2).[88] Basically, just by slightly changing the polarity of the terminal group, it is possible to tune and adjust the solubility of NPs in a wide variety of solvents for specific applications.

Besides chemical stability towards oxidation and Ostwald ripening (the growth of larger NPs by merging not-well passivated smaller ones), passivation of the Si NPs surfaces also ties down defect states at surfaces caused by dangling bonds.[125] Moreover, the effective band gap of alkyl-passivated Si NPs is relatively unperturbed by the presence of Si-C bonds at the surface.[126]

1.6 Synthetic Strategies for Si NPs

To date, a lot of work on obtaining stable, defined and monodisperse Si NPs with reproducible surface chemistry, sizes, shapes and optical properties has been reported. An ideal method would effectively address all these requirements while also producing large amounts of pure Si NPs in a very short time, using low-cost, non-hazardous precursors.

The first synthesis of Si NPs was reported by Heath *et al*. in 1992,[127] and was based on the simultaneous reduction of $SiCl_4$ and $RSiCl_3$ (R = H, n-octyl) by sodium in a nonpolar organic solvent (pentane or hexane). The reaction was performed in a high pressure (> 100 atm) bomb reactor at 658 K for one week. The resulting Si NPs were hexagonally-shaped in 2-9 nm size range, exhibiting strong Si-Cl, Si-H and Si-O bands in FTIR spectra, indicating a high degree of oxidation.

Nowadays, Si NPs synthesis methods can be categorized in two classes:

1. Bulk reduction methods (Top-down)
2. Assembly methods (Bottom-up)

In bulk reduction methods, Si NPs are produced from crystalline Si by applying an etching procedure to reduce the bulk Si to nanometer-sized NPs. In assembly methods, Si NPs are constructed one Si atom at a time, through routes such as solution-phase oxidation-reduction reactions, thermal decomposition of silane precursors in supercritical fluids and synthesis in reverse micelles. Each of the individual methods has its own advantages and disadvantages

with respect of control of monodispersity, surface chemistry, shape, stability and optical properties, and will be further described in detail.

1.6.1. Bulk Reduction Methods

Ultrasonication of silicon wafers

Initially, researchers focussed on cutting larger silicon wafers into as small as possible pieces. Sailor and co-workers[128] used ultrasonication of anodically etched porous silicon and obtained a polydisperse colloidal solution of Si NPs with sizes ranging from less than 1 nm to several µm. Nayfeh and co-workers used this method to produce Si NPs with a very broad range of sizes that can not be well controlled.[129]

Electrochemical dispersion

More recently, Rogozhina used an electrochemical dispersion of crystalline Si wafers to produce carboxylic- and methylester-terminated Si NPs with diameters between 1 nm and 1.5 nm. Hydrogen-terminated Si NPs were formed through HF/H_2O_2 anodization and ultrasonic fractionation of crystalline Si wafers. The functionalization of thus formed Si NPs was subsequently performed through thermal hydrosilylation with methyl 4-pentenoate.[130]

Annealing of SiO powders

Finally, a relatively new method has been described by Liu, Kimura and co-workers.[131,132] They annealed SiO powders at 1000°C under ambient atmosphere, etched the annealed powders with 10% HF and functionalized the etched particles by common hydrosilylation. The resulting Si NPs (5 mg/h) are rather polydisperse (5.1 ± 1.9 nm) and still have a significant amount of oxygen on their surface. The advantage of this method is its low cost.

1.6.2. Assembly Methods

Synthesis in supercritical fluids

Among others Korgel and co-workers have used the decomposition of organosilanes (e.g. diphenylsilane) in solvents heated and pressurized above their critical points to build Si NPs.[89,133-135] Arrested precipitation of Si is performed in a continuous flow reactor, in octanol at 500 °C and at approximately 250 bar.[136] Relatively monodisperse Si NPs can be obtained with an average diameter of 1.5 nm, but the chemical composition was not easily controlled, since the obtained NPs were 50% alkoxy-terminated.[89] Particle growth is initiated by the thermally induced decomposition of a Si-containing precursor. Growing nanoclusters are

stabilized by octoxy groups [Si-O$(CH_2)_7CH_3$], which are produced when adding octanol to the reaction mixture. The size of the NPs can be increased by adding hexane as a cosolvent, thereby reducing the Si/octanol ratio. The same synthesis principle can be used to produce more polydisperse Si NPs with a diameter of 4.7 ± 1.4 nm.[134] The drawback of the decomposition method is the lack of control of the functionalization of the NPs. The same synthetic approach can be employed to produce Si nanowires.[133,137,138]

Laser-driven pyrolysis

Swihart and co-workers have fine-tuned a method in which silane is pyrolyzed (thermally dissociated) by a CO_2 laser beam.[139] A flow of H_2/He gas is used to confine the reaction zone in the laser beam and to further increase the temperature. Particle nucleation occurs from a certain temperature onwards (at least 850 °C), and by controlling the flow rates and the laser power the NP sizes can be controlled to a certain extent. After formation the NPs are etched with HF/HNO_3 in water to reduce the NP size. The obtained NPs (up to 20 - 200 mg/h) have an average diameter of 5 nm with a mixture of hydrogen- and oxygen-terminated Si atoms at the surface. The photoluminescence from these particles is not stable, mainly because of the significant degree of oxidation and the irregularity of the surface.[140] After additional treatment with 5% HF and hydrosilylation, various alkyl- and ester-terminated Si NPs can be produced,[141,142] which show a much more stable photoluminescence.

Solution phase oxidation-reduction methods

Various solution phase oxidation–reduction reactions have been developed and extensively studied by Kauzlarich and co-workers. Precursor Si-containing compounds are combined in solution for NP nucleation and growth under atmospheric conditions.[116] A variety of different routes have been investigated: reduction of $SiCl_4$ with NaSi,[143] oxidation of Mg_2Si with Br_2,[144,145] reduction of $SiCl_4$ with Na-naphthalenide[146] to give stable Si NPs.

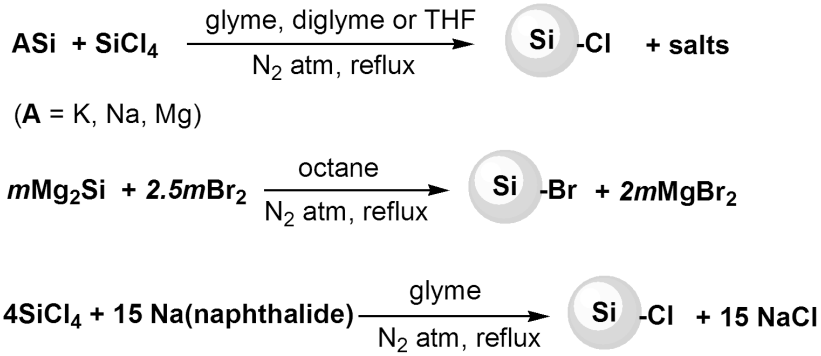

Figure 1.4. Examples of some solution-based reactions.

The size of Si NPs can be varied by changing the balance between growth and nucleation speeds through the control of the reaction temperature, concentration of precursors and choice of surface ligands. The same synthesis principle can be used to produce Ge NPs (size of 2 nm).[147]

The main advantage of these methods is definitely their versatility; they can also be employed to produce doped Si NPs (with Mn[148] or P[149]) or mixed Si-Ge NPs.[150] Obtained Si NPs are initially terminated with halogen atoms (Cl or Br) that allow a lot of possible options for further functionalization/stabilization, for example by using alkyllithium (R-Li) compounds,[143,144] alkoxy groups (via reaction with alcohols),[146,151] or hydrogen atoms by reduction with $LiAlH_4$.[145]

These methods are some of a few that can claim to provide partial control over the NP shape. Particularly sodium naphthalenide has been proven useful for preparing free standing Si NPs of various sizes and surface chemistry.[152] The major drawbacks of this synthesis approach are: the polydispersity of the obtained material (1 - 20 nm, and in the best case 3 - 6 nm), the labor- and time-consuming reaction conditions (~72 h per reaction), and the requirement of an extensive purification. FTIR analysis of isolated NPs shows, besides characteristic C-H bands, also a significant degree of oxidation which subsequently leads to red-tailed broad emission features.

Synthesis in reverse micelles

Homogeneous solution reactions have also found application in preparing free-standing Si NPs. The reduction of $SiCl_4$ by $LiAlH_4$ has long been known to yield pyrophoric silane,[153] which can be employed as a main precursor for Si NP synthesis. Nucleation and growth of the nanoclusters can be performed in nanoreactors, nanosized surfactant aggregates (inverse micelles). In this approach, an anhydrous compound (e.g. SiX_4; X = Cl, Br or I) is dissolved in the hydrophilic interior of a solution of micelles and nucleation and growth of Si NPs are restricted to the micelle interior. Control of cluster size can be achieved by variation of the micelles size, intermicellar interactions and reaction chemistry.[154] The reaction is performed under inert atmosphere in order to prevent the oxidation of Si NPs. Wilcoxon *et al*. found that the reaction also yielded polydisperse (d = 2 - 10 nm) Si NPs,[155] which exhibit a highly structured optical absorption and photoluminescence across the visible range of the spectrum. It was assumed that the resulting NP surfaces were hydride terminated, however, no experimental evidence was provided. HRTEM and selected-area electron diffraction of small samples were consistent with diamond lattice Si.

Tilley et al. later used a variation of such solution reduction to prepare very small quantities of small, relatively monodisperse, free-standing Si NPs (d = 1.8 ± 0.2 nm). While the surface

chemistry of Si NPs that are obtained directly from the reaction of $SiCl_4$ with $LiAlH_4$ was not presented, the reactivity of these NPs suggests hydride surface termination.[123]

1.7 Model of Si NPs

A model of hydrogen-terminated Si NP (~1.5 nm) is shown in Figure 1.5 (left). The surface-bound Si sites correspond to 28 SiH sites and 21 SiH_2 sites, and thus have a ratio of H-bound (surface) Si atoms to "core" Si atoms of 49/81 = 0.60, giving the molecular formula - $Si_{81}H_{70}$. At some places, two hydrogen atoms are relatively close together, indicating that it might be difficult to functionalize both surface sites by alkene molecules. The majority of the Si atoms resides at the surface and carries one or two H atoms that can be replaced by alkyl chains. For clarity, the alkylation was modeled by attachment of n-butyl chains corresponding to the insertion of 1-butene into the Si-H bonds

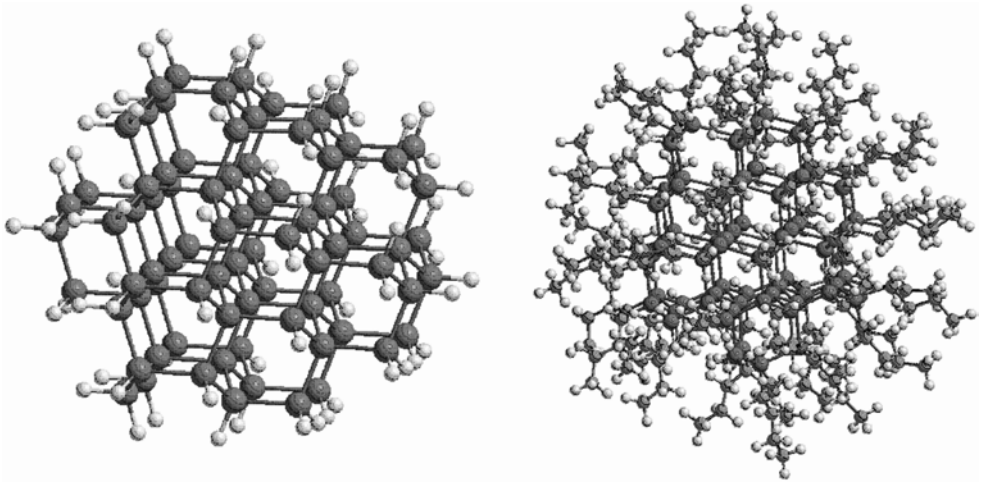

Figure 1.5. (left) $Si_{81}H_{70}$ nanoparticle as optimized with the MMFF94 force field. (right) $Si_{81}H_{21}(C_4H_9)_{49}$ nanoparticle, as optimized with the MMFF94 force field.

The $Si_{81}H_{70}$ model NP has a surface area of roughly 7 nm^2, giving an area of 0.1 nm^2 per surface site. Comparing this value to the area that an alkyl tail occupies in a closely packed monolayer on the Si(111) face - 0.16 nm^2, it is impossible to functionalize all sites on the surface of a Si NP.[156] Functionalized silicon NPs are in that respect similar to closely packed monolayers on flat silicon: the silicon surfaces can be covered to a maximum of 60%, because the area per surface site is also 0.1 nm^2. The remaining 40% of the sites remains hydrogen-terminated. The surface coverage of Si NPs by alkyl-chains has been estimated to 55%,[89] although the real surface coverage might be even higher for a strongly curved surface.

1.8 Scope of This Thesis

This thesis deals with the development and optimization of method for the preparation of stable and monodisperse Si NPs, and with their photophysical characterization. In addition, it displays possible applications of Si NPs, specifically in the realm of bioimaging.

Chapter 1 gives a general introduction about semiconductor quantum dots and Si NPs, in particular. It gives an overview about variety of methods published so far, that are used for production of Si NPs and the description of the origin of Si NPs luminescence.

Chapter 2, 3, 4, 5 and 6 are experimental chapters.

Chapter 2 describes the first gram–scale preparation of monodisperse alkyl-terminated Si NPs. Both steady-state and time-resolved absorption and emission techniques, as well as FTIR (Fourier Transform InfraRed Spectroscopy) and XPS (X-ray Photoelectron Spectroscopy) measurements are used to study their photophysical properties and chemical composition in detail. For the first time, the extinction coefficient of alkyl-terminated Si NPs is determined.

In *Chapter 3* is described the preparation of water-soluble amine-terminated Si NPs, with different alkyl-chain lengths between the amine group and the surface of the NP. A highly improved synthesis method is presented, and the photophysical characterization of alkyl-amine coated Si NPs including steady-state and time resolved fluorescence and STS (Scanning Tunnelling Spectroscopy) measurements are outlined and discussed. The topography of amine-terminated Si NPs is examined using transmission electron and scanning tunnelling microscopy techniques. Also, possible application of these Si NPs for bioimaging purposes is studied by using BV2 nerve cells. It is shown that amine-terminated Si NPs can be successfully used for staining multiple cell generations.

Chapter 4 deals with the use of Si NPs for energy transfer purposes. Towards that aim, a ruthenium-containing dye was attached to Si NPs, while the alkyl-spacer chain length between possible donor and acceptor was varied. It was shown that Si NPs can act as very efficient energy donor, with energy transfer efficiencies up to 55%. In all the cases the energy transfer rates were determined from both reduction in the emission intensities and lifetime, derived from for time-resolved fluorescence studies.

Chapter 5 deals with the production of stable azide-terminated Si NPs and their detailed photophysical and chemical characterization. Azide-terminated Si NPs are further functionalized by using “click” chemistry with a number of functional moieties: undec-10-yn-1-ol, propargyl amine, undec-10-ynoic acid, undec-10-ynyl hepta-O-acetyl lactoside and rhodamine-labeled lactoside. Furthermore, the uptake of Si NPs by yeast cells (*Rhodotorula glutinis)* is successfully demonstrated, by allowing cells to *actually grow in the presence of* Si NPs.

To conclude this thesis, *Chapter 6* consists of the outlook and the most significant overall conclusions. Moreover, some personal views and recommendations for further research are given.

1.9 References

(1) Alivisatos, A. P. *Science* **1996**, *271*, 933-937.

(2) Whitesides, G. M. *Small* **2005**, *1*, 172-179.

(3) Feynman, R. *"There's plenty of room at the bottom"* **1959**, *seminar talk*.

(4) Baratoff, A.; Binnig, G.; Rohrer, H. *J. Vac. Sci. Tech. B* **1983**, *1*, 703-704.

(5) Binnig, G.; Rohrer, H. *Helv. Phys. Acta* **1982**, *55*, 726-735.

(6) Hey, T.; Walters, P. *The New Quantum Universe*; Cambridge University Press: Cambridge, 2003.

(7) Wang, X.; Yang, L. L.; Chen, Z.; Shin, D. M. *Canc. J. Clin.* **2008**, *58*, 97-110.

(8) Nazem, A.; Mansoori, G. A. *J. Alzheimers Disease* **2008**, *13*, 199-223.

(9) Iverson, N.; Plourde, N.; Chnari, E.; Nackman, G. B.; Moghe, P. V. *Biodrugs* **2008**, *22*, 1-10.

(10) Chesser, D. *Food Australia* **2007**, *59*, 235-235.

(11) Moraru, C. I.; Panchapakesan, C. P.; Huang, Q. R.; Takhistov, P.; Liu, S.; Kokini, J. L. *Food Technology* **2003**, *57*, 24-29.

(12) Tarver, T. *Food Tech.* **2006**, *60*, 22-26.

(13) Weiss, J.; McClements, J.; Takhistov, P. *Food Australia* **2007**, *59*, 274-275.

(14) Chapman, P. *Expert Opin. Therap. Pat.* **2005**, *15*, 249-251.

(15) Kaounides, L.; Yu, H.; Harper, T. *Mater. Techn.* **2007**, *22*, 209-237.

(16) Wegner, T.; Jones, P. *Wood Fib. Sci.* **2005**, *37*, 549-551.

(17) Wu, Y. H.; Chong, T. C. *J. Nanosci. Nanotech.* **2007**, *7*,1-12.

(18) Kastner, M. A. *Physics Today* **1993**, *46*, 24-31.

(19) Brus, L. *J. Phys. Chem. Solids* **1998**, *59*, 459-465.

(20) Guyot-Sionnest, P.; Hines, M. A. *A. Phys. Lett.* **1998**, *72*, 686-688.

(21) Hines, M. A.; Guyot-Sionnest, P. *J. Phys. Chem.B* **1998**, *102*, 3655-3657.

(22) Eychmuller, A. *J. Phys. Chem. B* **2000**, *104*, 6514-6528.

(23) Willard, D. M.; Carillo, L. L.; Jung, J.; Van Orden, A. *Nano Lett.* **2001**, *1*, 469-474.

(24) Chan, W. C. W.; Nie, S. M. *Science* **1998**, *281*, 2016-2018.

(25) Chan, W. C. W.; Maxwell, D. J.; Gao, X. H.; Bailey, R. E.; Han, M. Y.; Nie, S. M. *Curr. Opin. Biotech.* **2002**, *13*, 40-46.

(26) Chu, M. Q.; Sun, Y.; Liu, G. J. *Mat. Sci. Tech.* **2006**, *22*, 1240-1244.

(27) Gao, X. H.; Chan, W. C. W.; Nie, S. M. *J. Biomed. Optics* **2002**, *7*, 532-537.

(28) Gao, X. H.; Dave, S. R. *Bio-Applic. Nanoparticles* **2007**, *620*, 57-73.
(29) Krishna, M. V. R.; Friesner, R. A. *J. Chem. Phys.* **1991**, *95*, 8309-8322.
(30) Zorman, B.; Ramakrishna, M. V.; Friesner, R. A. *J. Phys. Chem.* **1995**, *99*, 7649-7653.
(31) Nirmal, M.; Brus, L. *Acc. Chem. Res.* **1999**, *32*, 407-414.
(32) Eckhoff, D. A., PhD Thesis, Optical characterization of ultrasmall hydrogen-terminated and carboxyl-functionalized silicon nanoparticles in aqueous envoroments, 2006.
(33) Murray, C. B.; Norris, D. J.; Bawendi, M. G. *J. Am. Chem. Soc.* **1993**, *115*, 8706-8715.
(34) Hoshino, A.; Fujioka, K.; Oku, T.; Nakamura, S.; Suga, M.; Yamaguchi, Y.; Suzuki, K.; Yasuhara, M.; Yamamoto, K. *Microbiol. Immunol.* **2004**, *48*, 985-994.
(35) Santra, S.; Xu, J. S.; Wang, K. M.; Tan, W. H. *J. Nanosci. Nanotech.* **2004**, *4*, 590-599.
(36) Sharrna, P.; Brown, S.; Walter, G.; Santra, S.; Moudgil, B. *Adv. Colloid. Interfac. Sci.* **2006**, *123*, 471-485.
(37) Wang, Y. *J. Nanosci. Nanotech.* **2008**, *8*, 1068-1091.
(38) Liu, W. H.; Choi, H. S.; Zimmer, J. P.; Tanaka, E.; Frangioni, J. V.; Bawendi, M. *J. Am. Chem. Soc.* **2007**, *129*, 14530-14537.
(39) Michalet, X.; Pinaud, F.; Lacoste, T. D.; Dahan, M.; Bruchez, M. P.; Alivisatos, A. P.; Weiss, S. *Single Molecules* **2001**, *2*, 261-276.
(40) Pinaud, F.; Michalet, X.; Bentolila, L. A.; Tsay, J. M.; Doose, S.; Li, J. J.; Iyer, G.; Weiss, S. *Biomater.* **2006**, *27*, 1679-1687.
(41) Gerion, D.; Pinaud, F.; Williams, S. C.; Parak, W. J.; Zanchet, D.; Weiss, S.; Alivisatos, A. P. *J. Phys. Chem. B* **2001**, *105*, 8861-8871.
(42) Bruchez, M.; Moronne, M.; Gin, P.; Weiss, S.; Alivisatos, A. P. *Science* **1998**, *281*, 2013-2016.
(43) Dabbousi, B. O.; RodriguezViejo, J.; Mikulec, F. V.; Heine, J. R.; Mattoussi, H.; Ober, R.; Jensen, K. F.; Bawendi, M. G. *J. Phys. Chem. B* **1997**, *101*, 9463-9475.
(44) Little, R. B.; El-Sayed, M. A.; Bryant, G. W.; Burke, S. *J. Chem. Phys.* **2001**, *114*, 1813-1822.
(45) Kirchner, C.; Liedl, T.; Kudera, S.; Pellegrino, T.; Javier, A. M.; Gaub, H. E.; Stolzle, S.; Fertig, N.; Parak, W. J. *Nano Lett.* **2005**, *5*, 331-338.
(46) Ando, M.; Li, C. L.; Yang, P.; Murase, N. *J. Biomed. Biotech.* **2007**, 52971-52978.
(47) Lee, H. S.; Park, H. L.; Kim, T. W. *J. Cryst. Growth* **2006**, *291*, 442-447.
(48) Li, C. L.; Nishikawa, K.; Ando, M.; Enomoto, H.; Murase, N. *Coll. Surf.-Physchem. Engineer. Asp.* **2007**, *294*, 33-39.
(49) Liu, F. C.; Cheng, T. L.; Shen, C. C.; Tseng, W. L.; Chiang, M. Y. *Langmuir* **2008**, *24*, 2162-2167.

(50) Thuy, U. T. D.; Liem, N. Q.; Thanh, D. X.; Protiere, M.; Reiss, P. *Appl. Phys. Lett.* **2007**, *91, 241908-241916*

(51) Yang, C. S.; Wang, J. S.; Lai, Y. J.; Luo, C. W.; Chen, D. S.; Shih, Y. T.; Jian, S. R.; Chou, W. C. *Nanotech.* **2007**, *18*, 385602-385610.

(52) Zheng, Y. G.; Yang, Z. C.; Ying, J. Y. *Adva. Mat.* **2007**, *19*, 1475-1479.

(53) Kovalenko, M. V.; Heiss, W.; Shevchenko, E. V.; Lee, J. S.; Schwinghammer, H.; Alivisatos, A. P.; Talapin, D. V. *J. Am. Chem. Soc.* **2007**, *129*, 11354-11360.

(54) Anantathanasarn, S.; Barbarin, Y.; Cade, N. I.; van Veldhoven, P. J.; Bente, E. A. J. M.; Oei, Y. S.; Kamada, H.; Smit, M. K.; Notzel, R. *Mater. Sci. Engineer. B* **2008**, *147*, 124-130.

(55) Gong, M.; Duan, K. M.; Li, C. F.; Magri, R.; Narvaez, G. A.; He, L. X. *Phys. Rev. B* **2008**, *77*, 045326-045334.

(56) Ulloa, J. M.; Anantathanasarn, S.; van Veldhoven, P. J.; Koenraad, P. M.; Notzel, R. *Appl. Phys. Lett.* **2008**, *92*,083103-083111.

(57) Veloso, A. B.; Nakaema, M. K. K.; de Godoy, M. P. F.; Lopes, J. M. J.; Iikawa, F.; Brasil, M. J. S. P.; Bortoleto, J. R. R.; Cotta, M. A.; Fichtner, P. F. P.; Morschbacher, M.; Madureira, J. R. *Appl. Phys. Lett.* **2007**, *91*,121917-121914.

(58) Yin, Z.; Tang, X.; Zhang, J.; Deny, S.; Teng, J.; Du, A.; Chin, M. K. *Nanotech.* **2008**, *19*, 085603-085609.

(59) Fu, A. H.; Gu, W. W.; Boussert, B.; Koski, K.; Gerion, D.; Manna, L.; Le Gros, M.; Larabell, C. A.; Alivisatos, A. P. *Nano Lett.* **2007**, *7*, 179-182.

(60) Alivisatos, P. *Nature Biotechn.* **2004**, *22*, 47-52.

(61) Liu, W.; Howarth, M.; Greytak, A. B.; Zheng, Y.; Nocera, D. G.; Ting, A. Y.; Bawendi, M. G. *J. Am. Chem. Soc.* **2008**, *130*, 1274-1284.

(62) Larson, D. R.; Zipfel, W. R.; Williams, R. M.; Clark, S. W.; Bruchez, M. P.; Wise, F. W.; Webb, W. W. *Science* **2003**, *300*, 1434-1436.

(63) Lacoste, T. D.; Michalet, X.; Pinaud, F. F.; Chemla, D. S.; Alivisatos, A. P.; Weiss, S. *Biophys. J.* **2000**, *78*, 402a-402a.

(64) Agrawal, A.; Deo, R.; Wang, G. D.; Wang, M. D.; Nie, S. M. *PNAS* **2008**, *105*, 3298-3303.

(65) Choi, J. H.; Burns, A. A.; Williams, R. M.; Zhou, Z. X.; Flesken-Nikitin, A.; Zipfel, W. R.; Wiesner, U.; Nikitin, A. Y. *J. Biom. Opt.* **2007**, *12*, 064007-064014.

(66) Kobayashi, H.; Hama, Y.; Koyama, Y.; Barrett, T.; Regino, C. A. S.; Urano, Y.; Choyke, P. L. *Nano Lett.* **2007**, *7*, 1711-1716.

(67) Smith, A. M.; Dave, S.; Nie, S. M.; True, L.; Gao, X. H. *Expert Rev. Molec. Diagn.* **2006**, *6*, 231-244.

(68) Pu, S. C.; Yang, M. J.; Hsu, C. C.; Lai, C. W.; Hsieh, C. C.; Lin, S. H.; Cheng, Y. M.;

Chou, P. T. *Small* **2006**, *2*, 1308-1313.

(69) Fujii, F.; Kinjo, M. *ChemBioChem* **2007**, *8*, 2199-2203.

(70) Ouattara, L.; Ulloa, J. M.; Mikkelsen, A.; Lundgren, E.; Koenraad, P. M.; Borgstrom, M.; Samuelson, L.; Seifert, W. *Nanotechnology,* **2007**, *18*, 145403-145409.

(71) Derfus, A. M.; Chan, W. C. W.; Bhatia, S. N. *Nano Lett.* **2004**, *4*, 11-18.

(72) Eckhoff, D. A.; Sutin, J. D. B.; Clegg, R. M.; Gratton, E.; Rogozhina, E. V.; Braun, P. V. *J. Phys. Chem. B* **2005**, *109*, 19786-19797.

(73) Chaudhary, S.; Ozkan, M.; Chan, W. C. W. *Appl. Phys. Lett.* **2004**, *84*, 2925-2927.

(74) Li, F.; Son, D. I.; Seo, S. M.; Cha, H. M.; Kim, H. J.; Kim, B. J.; Jung, J. H.; Kim, T. W. *App. Phys. Lett.* **2007**, *91*, 122111-122120.

(75) Li, Y. Q.; Rizzo, A.; Cingolani, R.; Gigli, G. *Microchim. Act.* **2007**, *159*, 207-215.

(76) Canham, L. *New Scientist* **1993**, *138*, 23-27.

(77) Brus, L. *Nature* **1991**, *353*, 301-302.

(78) Mayne, A. H.; Bayliss, S. C.; Barr, P.; Tobin, M.; Buckberry, L. D. *Phys. Stat. Solidi A* **2000**, *182*, 505-513.

(79) Kovalev, D.; Diener, J.; Heckler, H.; Polisski, G.; Kunzner, N.; Koch, F. *Phys. Rev. B* **2000**, *61*, 4485-4487.

(80) Kovalev, D.; Heckler, H.; Polisski, G.; Koch, F. *Phys. Stat. Sol. B* **1999**, *215*, 871-932.

(81) Allan, G.; Delerue, C.; Lannoo, M. *J. Luminesc.* **1993**, *57*, 239-242.

(82) Allan, G.; Delerue, C.; Lannoo, M. *Phys. Rev. Lett.* **1996**, *76*, 2961-2964.

(83) Delerue, C.; Allan, G.; Lannoo, M. *J. Luminesc.* **1998**, *80*, 65-73.

(84) Delerue, C.; Martin, E.; Lampin, J. F.; Allan, G.; Lannoo, M. *J. Phys. Iv* **1993**, *3*, 359-362.

(85) Lannoo, M.; Delerue, C.; Allan, G.; Martin, E. *Annal. Phys.* **1995**, *20*, 271-276.

(86) Wolkin, M. V.; Jorne, J.; Fauchet, P. M.; Allan, G.; Delerue, C. *Phys. Rev. Lett.* **1999**, *82*, 197-200.

(87) van Buuren, T.; Dinh, L. N.; Chase, L. L.; Siekhaus, W. J.; Terminello, L. J. *Phys. Rev. Lett.* **1998**, *80*, 3803-3806.

(88) Rosso-Vasic, M.; Spruijt, E.; van Lagen, B.; de Cola, L.; Zuilhof, H. *Small*, **2008**, in press.

(89) Holmes, J. D.; Ziegler, K. J.; Doty, R. C.; Pell, L. E.; Johnston, K. P.; Korgel, B. A. *J. Am. Chem. Soc.* **2001**, *123*, 3743-3748.

(90) Puzder, A.; Williamson, A. J.; Reboredo, F. A.; Galli, G. *Phys. Rev. Lett.* **2003**, *91*, 1574051-1574054.

(91) Mitas, L.; Therrien, J.; Twesten, R.; Belomoin, G.; Nayfeh, M. H. *Appl. Phys. Lett.* **2001**, *78*, 1918-1920.

(92) Vasiliev, I.; Martin, R. M. *Phys. Stat. Sol. B* **2002**, *233*, 5-9.

(93) Belomoin, G.; Rogozhina, E.; Therrien, J.; Braun, P. V.; Abuhassan, L.; Nayfeh, M. H.; Wagner, L.; Mitas, L. *Phys. Rev. B* **2002**, *65*, 193406-189416.

(94) Nayfeh, M. H.; Rigakis, N.; Yamani, Z. *Phys. Rev. B* **1997**, *56*, 2079-2084.

(95) Zhou, Z. Y.; Brus, L.; Friesner, R. *Nano Lett.* **2003**, *3*, 163-167.

(96) Zhou, Z. Y.; Friesner, R. A.; Brus, L. *J. Am. Chem. Soc.* **2003**, *125*, 15599-15607.

(97) Vasiliev, I.; Chelikowsky, J. R.; Martin, R. M. *Phys. Rev. B* **2002**, *65*,121302-121308.

(98) Sieval, A. B.; Vleeming, V.; Zuilhof, H.; Sudholter, E. J. R. *Langmuir* **1999**, *15*, 8288-8291.

(99) Sieval, A. B.; Demirel, A. L.; Nissink, J. W. M.; Linford, M. R.; van der Maas, J. H.; de Jeu, W. H.; Zuilhof, H.; Sudholter, E. J. R. *Langmuir* **1998**, *14*, 1759-1768.

(100) Scheres, L.; Arafat, A.; Zuilhof, H. *Langmuir* **2007**, *23*, 8343-8346.

(101) Linford, M. R.; Fenter, P.; Eisenberger, P. M.; Chidsey, C., E.D.; *J.Am.Chem.Soc.* **1995**, *117*, 3145-3155.

(102) de Smet, L. C. P. M.; Pukin, A. V.; Sun, Q. Y.; Eves, B. J.; Lopinski, G. P.; Visser, G. M.; Zuilhof, H.; Sudholter, E. J. R. *Appl. Surf. Sci.* **2005**, *252*, 24-30.

(103) Sun, Q. Y.; de Smet, L. C. P. M.; van Lagen, B.; Giesbers, M.; Thune, P. C.; van Engelenburg, J.; de Wolf, F. A.; Zuilhof, H.; Sudholter, E. J. R. *J. Am. Chem. Soc.* **2005**, *127*, 2514-2523.

(104) Stewart, M. P.; Buriak, J. M. *J. Am. Chem. Soc.* **2001**, *123*, 7821-7830.

(105) de Smet, L. C. P. M.; Zuilhof, H.; Sudholter, E. J. R.; Lie, L. H.; Houlton, A.; Horrocks, B. R. *J. Phys. Chem. B* **2005**, *109*, 12020-12031.

(106) Buriak, J. M. *Chem. Rev.* **2002**, *102*, 1271-1308.

(107) Holmes, J. D.; Ziegler, K. J.; Doty, R. C.; Pell, L. E.; Johnston, K. P.; Korgel, B. A. *J. Am. Chem. Soc.* **2001**, *123*, 3743-3748.

(108) Zou, J.; Baldwin, R. K.; Pettigrew, K. A.; Kauzlarich, S. M. *Nano Lett.* **2004**, *4*, 1181-1186.

(109) Mayeri, D.; Phillips, B. L.; Augustine, M. P.; Kauzlarich, S. M. *Chem. Mater.* **2001**, *13*, 765-770.

(110) Pettigrew, K. A.; Liu, Q.; Power, P. P.; Kauzlarich, S. M. *Chem. Mater.* **2003**, *15*, 4005-4011.

(111) Hua, F. J.; Swihart, M. T.; Ruckenstein, E. *Langmuir* **2005**, *21*, 6054-6062.

(112) Rogozhina, E. V.; Eckhoff, D. A.; Gratton, E.; Braun, P. V. *J. Mater. Chem.* **2006**, *16*, 1421-1430.

(113) Sato, S.; Swihart, M. T. *Chem. Mater.* **2006**, *18*, 4083-4088.

(114) Hua, F. J.; Erogbogbo, F.; Swihart, M. T.; Ruckenstein, E. *Langmuir* **2006**, *22*, 4363-4370.

(115) David R. Lide, *Handbook of Chemistry and Physics*; 81 ed., 2000.

(116) Veinot, J. G. C. *Chem. Comm.* **2006**, 4160-4168.

(117) Rogozhina, E. V.; Eckhoff, D. A.; Gratton, E.; Braun, P. V. *J. Mat. Chem.* **2006**, *16*, 1421-1430.

(118) Warner, J. H.; Hoshino, A.; Yamamoto, K.; Tilley, R. D. *Angew. Chem. Int. Ed.* **2005**, *44*, 4550-4554.

(119) Nelles, J.; Sendor, D.; Ebbers, A.; Petrat, F. M.; Wiggers, H.; Schulz, C.; Simon, U. *Colloid Polymer Sci.* **2007**, *285*, 729-736.

(120) Buriak, J. M. *Adva. Mat.***1999**, *11*, 265-267.

(121) Stewart, M. P.; Buriak, J. M. *Comm. Inorg. Chem.***2002**, *23*, 179-203.

(122) Sweryda-Krawiec, B.; Cassagneau, T.; Fendler, J. H. *J. Phys.Chem.B* **1999**, *103*, 9524-9529.

(123) Warner, J. H.; Hoshino, A.; Yamamoto, K.; Tilley, R. D. *Angew. Chem. Int. Ed.* **2005**, *44*, 4550-4554.

(124) Rosso-Vasic, M.; Spruijt, E.; Popovic, Z.; Overgaag, K.; Van Lagen, B.; Grandidier, B.; Vanmackelenbergh, D.; De Cola, L.; Zuilhof, H. *submitted*.

(125) Heintz, A. S.; Fink, M. J.; Mitchell, B. S. *Adva. Mater.* **2007**, *19*, 3984-3990.

(126) Reboredo, F. A.; Galli, G. *J. Phys. Chem. B* **2005**, *109*, 1072-1078.

(127) Heath, J. R. *Science* **1992**, *258*, 1131-1133.

(128) Heinrich, J. L.; Curtis, C. L.; Credo, G. M.; Kavanagh, K. L.; Sailor, M. J. *Science* **1992**, *255*, 66-68.

(129) Yamani, Z.; Ashhab, S.; Nayfeh, M. H. *J. Appl. Phys.* **1998**, *83*, 3929-3931.

(130) Rogozhina, E. V.; Eckhoff, D. A.; Gratton, E.; Braun, P. V. *J. Mater. Chem.* **2006**, *16*, 1421-1430.

(131) Liu, S.; Sato, S.; Kimura, K. *Langmuir* **2005**, *21*, 6324-6329.

(132) Liu, S.; Yang, Y.; Sato, S.; Kimura, K. *Chem. Mater.* **2006**, *18*, 637-642.

(133) Shah, P. S.; Hanrath, T.; Johnston, K. P.; Korgel, B. A. *J. Phys. Chem. B* **2004**, *108*, 9574-9587.

(134) English, D. S.; Pell, L. E.; Yu, Z. H.; Barbara, P. F.; Korgel, B. A. *Nano Lett.* **2002**, *2*, 681-685.

(135) Ding, Z. F.; Quinn, B. M.; Haram, S. K.; Pell, L. E.; Korgel, B. A.; Bard, A. J. *Science* **2002**, *296*, 1293-1297.

(136) Johnston, K. P.; Shah, P. S.; Doty, R. C.; Ziegler, K. J.; Korgel, B. A.; Holmes, J. D. *J. Am. Chem. Soc.* **2001**, *221*, 625-631.

(137) Lee, D. C.; Hanrath, T.; Korgel, B. A. *Angew. Chem. Int. Ed.* **2005**, *44*, 3573-3577.

(138) Holmes, J. D.; Johnston, K. P.; Doty, R. C.; Korgel, B. A. *Science* **2000**, *287*, 1471-1473.

(139) Li, X. G.; He, Y. Q.; Talukdar, S. S.; Swihart, M. T. *Langmuir* **2003**, *19*, 8490-8496.

(140) Li, X.; He, Y.; Talukdar, S. S.; Swihart, M. T. *Langmuir* **2003**, *19*, 8490-8496.

(141) Li, X.; He, Y.; Swihart, M. T. *Langmuir* **2004**, *20*, 4720-4727.

(142) Hua, F.; Swihart, M. T.; Ruckenstein, E. *Langmuir* **2005**, *21*, 6054-6062.

(143) Mayeri, D.; Phillips, B. L.; Augustine, M. P.; Kauzlarich, S. M. *Chem. Mater.* **2001**, *13*, 765-770.

(144) Pettigrew, K. A.; Liu, Q.; Power, P. P.; Kauzlarich, S. M. *Chem. Mater.* **2003**, *15*, 4005-4011.

(145) Liu, Q.; Kauzlarich, S. M. *Mater. Sci. Engineer. B* **2002**, *96*, 72-75.

(146) Baldwin, R. K.; Pettigrew, K. A.; Ratai, E.; Augustine, M. P.; Kauzlarich, S. M. *Chem. Comm.* **2002**, 1822-1823.

(147) Tanke, R. S.; Kauzlarich, S. M.; Patten, T. E.; Pettigrew, K. A.; Murphy, D. L.; Thompson, M. E.; Lee, H. W. H. *Chem. Mater.* **2003**, *15*, 1682-1689.

(148) Zhang, X.; Brynda, M.; Britt, R. D.; Carroll, E. C.; Larsen, D. S.; Louie, A. Y.; Kauzarich, S. M. *J. Am. Chem. Soc.* **2007**, *129*, 10668-10674.

(149) Baldwin, R. K.; Zou, J.; Pettigrew, K. A.; Yeagle, G. J.; Britt, R. D.; Kauzlarich, S. M. *Chem. Comm.* **2006**, 658-660.

(150) Yang, C. S.; Kauzlarich, S. M.; Wang, Y. C. *Chem. Mater.* **1999**, *11*, 3666-3670.

(151) Zou, J.; Baldwin, R. K.; Pettigrew, K. A.; Kauzlarich, S. M. *Nano Lett.* **2004**, *4*, 1181-1186.

(152) Baldwin, R. K.; Pettigrew, K. A.; Garno, J. C.; Power, P. P.; Liu, G. Y.; Kauzlarich, S. M. *J. Am. Chem. Soc.* **2002**, *124*, 1150-1151.

(153) Finholt, A. E.; Bond, A. C.; Schlesinger, H. I. *J. Am. Chem. Soc.* **1947**, *69*, 1199-1203.

(154) Wilcoxon, J. P.; Samara, G. A.; Provencio, P. N. *Phys. Rev. B* **1999**, *60*, 2704-2714.

(155) Wilcoxon, J. P.; Samara, G. A. *Appl. Phys. Lett.* **1999**, *74*, 3164-3166.

(156) Hurley, P. T.; Nemanick, E. J.; Brunschwig, B. S.; Lewis, N. S. *J. Am. Chem. Soc.* **2006**, *128*, 9990-9991.

Chapter 2

Alkyl-functionalized oxide-free Silicon Nanoparticles: Synthesis and Optical Properties.

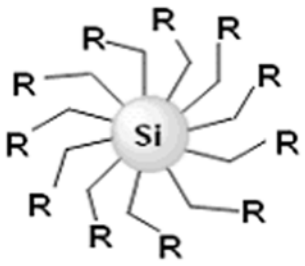

This chapter is published as:

"Alkyl-functionalized oxide-free Silicon Nanoparticles: Synthesis and Optical Properties ", Milena Rosso-Vasic, Evan Spruijt, Barend van Lagen, Luisa De Cola and Han Zuilhof , *Small*, **2008**,10, 1835-1841.

Abstract – Highly monodisperse silicon nanoparticles (Si NPs; 1.57 ± 0.21 nm) were synthesized with a covalently attached alkyl monolayer on a gram-scale. Infrared spectroscopy shows that these Si NPs contain maximally only a few oxygen atoms per nanoparticle. XPS spectra clearly show the presence of Si and attached alkyl chains. Due to the relatively efficient synthesis the molar extinction coefficient ε can be measured; ε_{max} = 9.4 x 10^3 $M^{-1}cm^{-1}$, only a factor 7 lower than that of CdS and CdSe NPs of that size. The quantum yield of emission ranges from 0.12 ($C_{10}H_{21}$-capping) to 0.23 ($C_{16}H_{33}$-capping). UV-Vis absorption and emission spectroscopy displays narrow spectra (FWHM = 32-39 nm), which support the monodispersity observed by TEM. This was also confirmed by time-resolved fluorescence anisotropy measurements, which display a strictly monoexponential decay that can only be indicative of monodisperse, ball-shaped nanoparticles.

2.1. Introduction

Free-standing silicon nanoparticles (Si NPs) have attracted an increasing amount of attention over the last decade, as they combine size-dependent optical properties with the richness and stability of silicon surface chemistry.[1] Since quantum confinement effects for Si NPs are expected for particles smaller than ~5 nm, the controlled synthesis of well-defined and monodisperse Si NPs in the 1-5 nm range is of interest for a variety of optoelectronic applications. Such Si NPs are very prone to oxidation, and the incorporation of oxygen atoms has been shown, both experimentally[2, 3] and from theory,[4] to influence the optical properties of these quite extensively. Therefore the synthesis of stable, oxide-free Si NPs would open up a new venue for their study and possible applications.

An attractive way to obtain the Si NPs is via the use of hydrogen-terminated ones which can then react with terminal alkenes to provide Si-C linkages, in analogy to the reactivity of planar hydrogen-terminated Si surfaces.[5] Several routes for such functionalized nanoparticles have been reported, which hinge on the formation of hydrogen-terminated Si NPs. The methods for NP functionalization are usually similar to those developed for planar[6] or porous[7] silicon, and also allow the functionalization of Si NPs with e.g. carboxylic acids.[8, 9] Methods to produce H-terminated Si NPs include annealing of SiO_x powders at high temperatures followed by etching with HF,[10] electrochemical HF-mediated etching of crystalline Si wafers,[11] plasma synthesis,[12] reduction of $SiCl_4$ with alkali naphthalide[13] or Zintl salts,[14] or the metathesis reaction between sodium silicide and NH_4Br.[15, 16] Probably the method yielding currently the best defined functionalized Si NPs is that of Tilley et al., who reported on the synthesis of alkyl- (1.8 ± 0.2 nm),[17] and aminoalkyl-terminated[18] Si NPs (1.4 ± 0.3 nm) via the use of micelles in apolar solvents. This method typically yields on the order of 20 mL of 1 μM solution of alkyl-capped Si NPs,[17] i.e. tens of micrograms of functionalized Si NPs, which displayed only small Si-O vibrational features in the infrared spectrum. Both the influence of the amino-functionalization on the optical properties of Si NPs,[19] and the amount of material produced, however, hamper their possible use in applications and even a detailed photophysical study of these NPs. In addition, to more strongly define the influence of Si-O bonds on the optical properties of Si NPs, it is of interest to produce Si NPs that are – as far as can be detected– free of Si-O bonds. To these aims we report in this paper the gram-scale synthesis of stable, alkyl-functionalized and oxide-free Si NPs, their characterization using TEM and IR spectroscopy, and an extensive study of their photophysical properties using absorption spectroscopy, steady-state and time-resolved emission spectroscopy, and - for the first time - time-resolved anisotropy measurements to determine the shape of the Si NP.

2.2. Experimental Section

All chemicals used were purchased from Sigma-Aldrich and employed without further purification unless specified differently. Toluene ((H_2O ≤ 0.005%), ≥ 99.7 % (GC)) was dried over Na wire overnight prior to use. 1-alkenes were freshly doubly distilled at reduced pressures and deairated before reaction. Methanol was distilled and stored on anhydrous $MgSO_4$.

2.2.1. Synthesis and purification of Si NPs.

Alkyl-capped Si NPs were made according to the following procedure (summarized in Figure 1): Dry toluene (165 mL) was made oxygen-free prior to use by 3 freeze-pump-thaw cycles, and put under argon (using the Schlenk-line) during the whole synthesis. Tetraoctylammonium bromide (≥ 99.0 %, 63 g, 118 mmol) was dispersed in the toluene by 20 min of sonication. $SiCl_4$ (99.998 %, 6.3 mL, 55.6 mmol) was added via a gas-tight syringe, followed by 20 min of sonication. Subsequently, a 1 M $LiAlH_4$-solution in THF was added (110 mL, 110 mmol), followed by 30 min of sonication in order to form hydrogen-terminated Si NPs in the TOAB micelles. Excess $LiAlH_4$ was oxidized with dry methanol (1 L, 25 mol), and the reaction mixture was sonicated for another 30 min. Alkyl-terminated Si NPs were obtained by adding degassed and dry 1-dodecene (220 mL; 1 mol) and a catalytic amount of a 0.05 M H_2PtCl_6 solution in methanol (~1 mL) to the reaction mixture. Sonication was continued for 60 min.

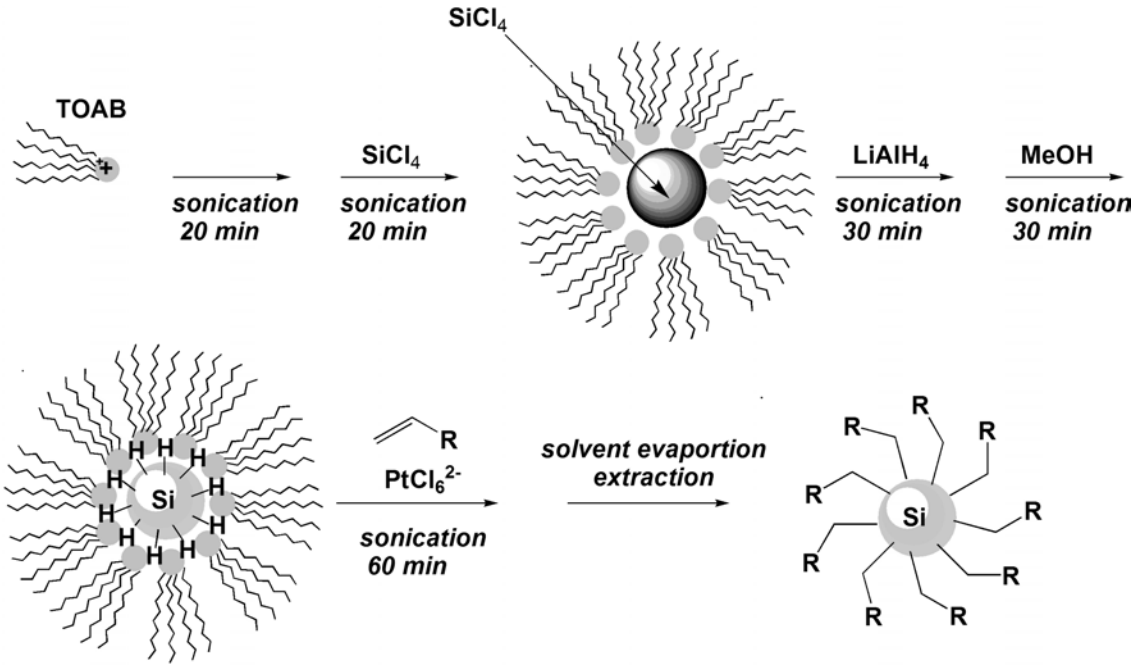

Figure 2.1. Gram-scale synthesis of alkyl capped oxide-free Si NPs.

The resulting Si NPs were purified by evaporation of all solvent under reduced pressure, dissolved in hexane, filtrated through hydrophilic 450 nm PVDF membrane filters (MILLEX-HV, Millipore) in order to remove surfactant and dialyzed against hexane (MWCO 7000, SERVA, Membra-Cel dialysis tubing, diameter 22 mm) to remove residuals of unreacted alkene, to finally yield 0.85 g of $C_{12}H_{25}$-capped Si NPs. This amounts to a 100-fold increase in yield compared to previous reports. 1-decene, 1-tetradecene and 1-hexadecene were attached to hydrogen-terminated Si NPs using the same synthesis procedure.

2.2.2. Optical measurements.

All measurements were performed at standard pressure and room temperature, unless stated differently. Electronic absorption spectra were recorded in a quartz cuvette (1 cm, Hellma), using a Cary 1 UV-Vis double-beam spectrophotometer and were corrected for the solvent absorption. The scan range was 200-500 nm with a 600 nm/min rate. Absorption spectra are corrected for toluene absorption, by subtracting the contribution from toluene from the recorded spectrum.

Steady-state and time-resolved measurements were performed on a Time-Correlating Single Photon Counting F900 spectrometer (Edinburgh Instruments), with an instrument response function for time-resolved measurements of 87 ps. All steady-state spectra are corrected for the wavelength-dependent sensitivity of the detector and the source by recording reference data simultaneously. Additionally, emission spectra have been corrected for Raman scattering using the solvent emission spectrum.

Using a comparative method, as described by Williams *et al.*,[31] the quantum yields of fluorescence in hexane were determined in optically dilute solutions (optical density ~0.1), employing naphthalene in cyclohexane (ϕ_{em} = 0.23 ± 0.02) as a reference emitter.

Time-resolved fluorescence and anisotropy measurements (at room temperature) were performed with the exact same solution as was used for steady-state spectra (absorption was always adjusted to be ≤ 0.5). A pulsed light-emitting diode ($\lambda_{excitation}$ = 283 nm) was used as excitation source, and photons were collected up to 100 ns (4096 channels) until a maximum of 10^4 counts.

2.2.3. FTIR, TEM and XPS measurements

Fourier Transform Infrared Spectroscopy (FTIR). FTIR measurements (Bruker, Vector 22 FTIR spectrometer), thin films of particle solutions in CCl_4 were made between NaCl crystals and corrected for the background signal, by collecting 32 scans for each measurement.

High-Resolution Transmission Electron Microscopy (TEM) The TEM studies were performed with a LIBRA 200 FE (200 kV) microscope. TEM samples were prepared by

dipping a carbon-coated 300-mesh copper grid into a sonicated and filtered silicon nanoparticles solution in hexane. The solvent was evaporated in air and TEM micrographs were typically taken at five different spots of each grid. Olympus Soft Imaging iTEM Solution and iTEM Solution EMaker were used to view and analyze the micrographs, respectively.

X-ray Photoelectron Spectroscopy (XPS). The XPS analysis was performed using a JPS-9200 Photoelectron Spectrometer (JEOL, Japan). The high-resolution spectra were obtained under UHV conditions using monochromatic Al Kα X-ray radiation at 12 kV and 25 mA, with an analyzer pass energy of 10 eV. Gold surfaces were cleaned for 20 min in piranha solution, rinsed with water and ethanol and dried with nitrogen. Si NPs dissolved in CCl_4 were dropped on a gold surface and dried in vacuum.

2.3. Results and Discussion

2.3.1. Size and Dispersity

Grams-scale amounts of alkyl-capped silicon nanoparticles – up to 0.85 g per batch – were obtained without compromising the monodispersity. This scale, now for the first time, allows many detailed investigations into the composition of the NPs and their electronic properties. As was determined by measuring the size of 1725 randomly chosen NPs with transmission electron microscopy these NPs have a mean diameter of 1.57 ± 0.21 nm (Figure 2.2). It should be noticed that the observed dispersity of these particles (0.21 nm) corresponds very closely to the lattice spacing in silicon crystals,[17] confirming the high definition of these NPs. Given the electron density of the alkyl chains, it is likely that only the silicon core of the NP will be visible by TEM.

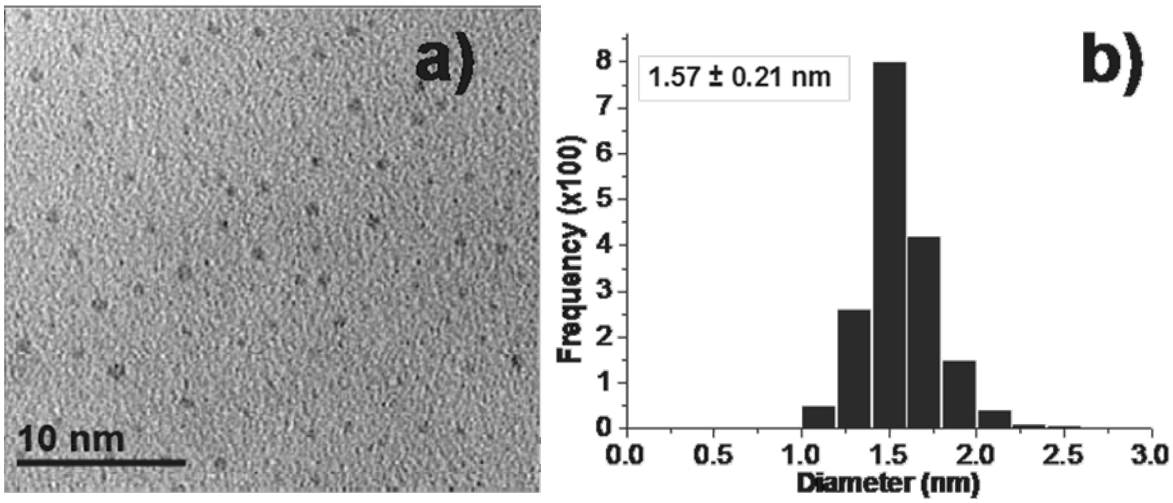

Figure 2.2. (a) TEM image of Si-$C_{10}H_{21}$ NPs, (b) Size distribution of 1725 randomly chosen Si NPs.

2.3.2. FTIR and XPS spectra

These alkylated Si NPs were further characterized by FTIR spectroscopy (Figure 2.3), which reveals clear C-H stretching signals, with the symmetric CH_2 antisymmetric CH_2 and asymmetric CH_3 stretching vibrations at 2856, 2928 and 2958 cm^{-1}, respectively. Scissoring and stretching vibration bands of Si−C bonds (1466 and 1259 cm^{-1}, respectively) also show the covalent attachment of 1-alkene molecules to the surface of the H-terminated Si NPs. Interestingly, while the $C_{10}H_{21}$-coated Si NP still displays features from Si-O bonds at 1015 and 1098 cm^{-1},[20] as e.g. observed by Tilley,[18] these features are absent in the spectra from the NPs with monolayers of $C_{12}H_{25}$, $C_{14}H_{29}$ and $C_{16}H_{33}$. This indicates the presence of only a very small number of Si-O bonds per nanoparticle, as these are easily visible due to the polarity of the Si-O bond.

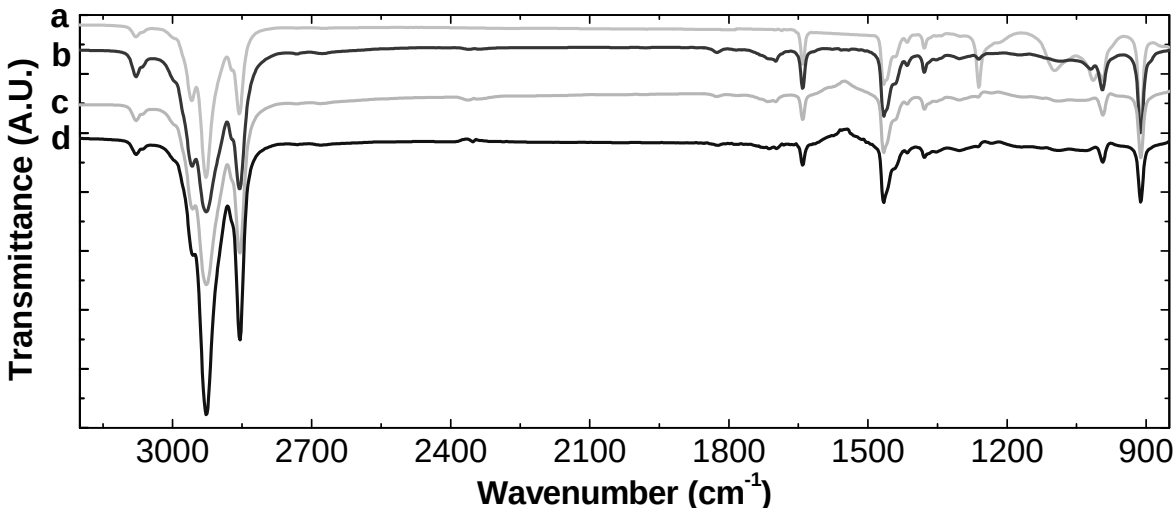

Figure 2.3. FTIR spectra of alkyl-terminated Si NPs: (a) Si-$C_{10}H_{21}$, (b) Si-$C_{12}H_{25}$, (c) Si-$C_{14}H_{29}$, (d) Si-$C_{16}H_{33}$.

These data are in stark contrast with observations by Nelles *et al*., who found extensive Si-O formation for Pt-catalyzed hydrosilylation of silicon nanoparticles,[21] which we attribute to differences in reaction conditions rather than to specifics in the nature of the alkylation reaction. In addition, Figure 2.3 displays no bands characteristic for Si-H stretching around 2100-2200 cm^{-1}. This is in line with the significant broadening of these peaks that is usually observed for planar hydrosilylated Si surfaces.[22]

XPS data confirm the presence of non-oxidized Si and C atoms in the material. Even in the case of the shortest alkyl chain attached (Figure 2.4), no peak of oxidized silicon is observed above 102 eV as was observed in oxidized Si NPs,[23] which confirms the high degree of passivation. In the case of Si-$C_{10}H_{21}$ NPs, after integration and correction for the carbon content in a reference sample (= clean gold surface), a Si/C

ratio of 39.8 : 60.2 was obtained. Assuming that Si NPs contain 81 Si atoms (derived from the average diameter of the TEM measurements), this means that there are approximately 28 alkyl chains attached per nanoparticle. For ball-shaped Si NPs of this size, there would approximately be 50 surface sites. This implies that there is a coverage with alkyl chains of ~50%, which is close to what has been observed for planar silicon surfaces.[24]

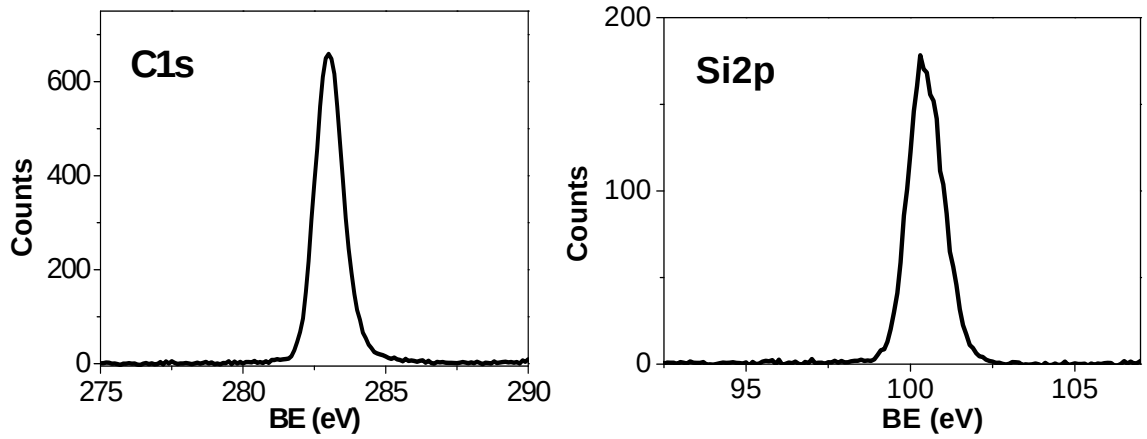

Figure 2.4. XPS spectra of Si-$C_{10}H_{21}$ NPs.

2.3.3. Optical Properties

The UV/Vis absorption and emission spectra of these alkyl-capped Si NPs (Figure 2.5) display a strong optical transition in the 240-320 nm range.[25] The narrow emission and absorption spectra observed for all four alkyl-capped Si NPs at room temperature indicate two things: 1) a high monodispersity of these NPs, as otherwise the variation in NP size would have implied a broadening of the optical transitions; 2) an unparalleled reproducibility of the size and monodispersity (e.g. Tilley reports mean diameters of 1.8 ± 0.2 nm[17] and 1.4 ± 0.3 nm,[18] for Si NPs made in the same way), which is significant in combination with the significantly increased yields of the synthesis.

Since these NPs can now be made in macroscopic quantities, their molar extinction coefficients can be determined. This is of significant practical importance, as their efficient light absorption makes it possible to work with very small amounts, for which it may be hard to determine the exact concentration by gravimetric methods while it is trivial to do via the measurement of a UV-Vis absorption spectrum. For the $C_{16}H_{33}$-capped Si NPs these values are given in Figure 2.5 at the right y-axis. The most reliable values are obtained for $\lambda \geq 280$ nm, as at these wavelengths remaining traces of toluene do not display any absorption. For the shoulder at 280 nm ε corresponds to 9.4×10^3 $M^{-1}cm^{-1}$.

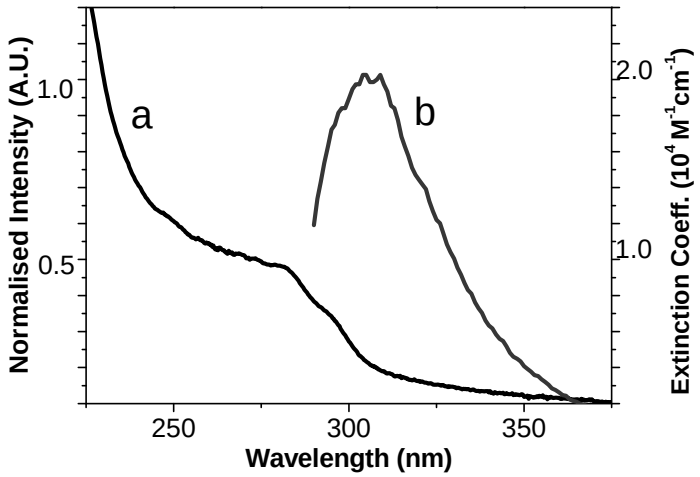

Figure 2.5. Absorption (a) and emission (b) (λ_{exc} = 280 nm) spectra of Si-$C_{16}H_{33}$ (0.5×10^{-4} M) in n-hexane. Note: the right-hand y-axis of the left figure (UV-Vis absorption spectra) denotes the extinction coefficient

This extinction coefficient is comparable to that of organic molecules with extended π-systems, and only slightly smaller than the values obtained for 1.5 nm NPs of II-VI semiconductors such as CdS, and CdSe, for which values of ~7×10^4 $M^{-1}cm^{-1}$ have been reported.[26] Yet, in comparison to the indirect bandgap transition in bulk Si, the optical transition is very efficient. The distinction between direct and indirect bandgaps seems therefore to be blurred in the nm-scale regime.

Table 2.1. Emission properties of alkyl-capped Si NPs in n-hexane (λ_{exc} = 280 nm; room temperature).

Alkyl coating	**Fluorescence maxima λ_{em} (nm)**	**FWHM (nm)**	**QY (%)**	**Lifetimes**	
				τ_1 (ns) (B1 (%))	**τ_2 (ns) (B2 (%))**
$C_{10}H_{21}$ [a)]	309	33	13.2 ± 1.2	0.69 ± 0.03 (31.0)	3.78 ± 0.05 (69.0)
$C_{12}H_{25}$	310	32	14.2 ± 1.2	0.76 ± 0.03 (12.7)	4.80 ± 0.05 (87.3)
$C_{14}H_{29}$	322	39	-	0.82 ± 0.03 (13.6)	4.45 ± 0.05 (86.4)
$C_{16}H_{33}$	308	38	22.9 ± 1.2	0.71 ± 0.03 (34.2)	3.29 ± 0.05 (65.8)

Note: a) The data for Si-$C_{10}H_{21}$ NPs are the average of four independent samples.

Fluorescence quantum yields increase monotonously from 0.13 for $C_{10}H_{21}$ to 0.23 for $C_{16}H_{33}$. The latter value starts to approach the highest reported quantum yield for solution-made alkyl-coated oxide-free Si NPs (0.28, for octyl-coated Si NPs with an additional polymer coating around it).[16] Apparently, the interaction of the silicon core with the solvent plays an important role in quenching the fluorescence, and an improved shielding of this core from the solvent by the coating is then reflected in higher fluorescence quantum yields.

As is clear from the fluorescence spectra (Figure 2.6.) the fluorescence is very narrow, in fact to the best of our knowledge for our $C_{12}H_{25}$–coated NPs narrower (FWHM = 32 nm) than ever reported before for Si NPs.[27] This again reflects the monodispersity of the samples under study. A slight red-shift in the emission is observed when exciting Si NPs with higher wavelengths. For λ_{exc} > 300 nm the emission peaks are of very small intensity, which points to a small fraction of slightly bigger Si NPs, as also indicated by TEM (Figure 2.2.b).

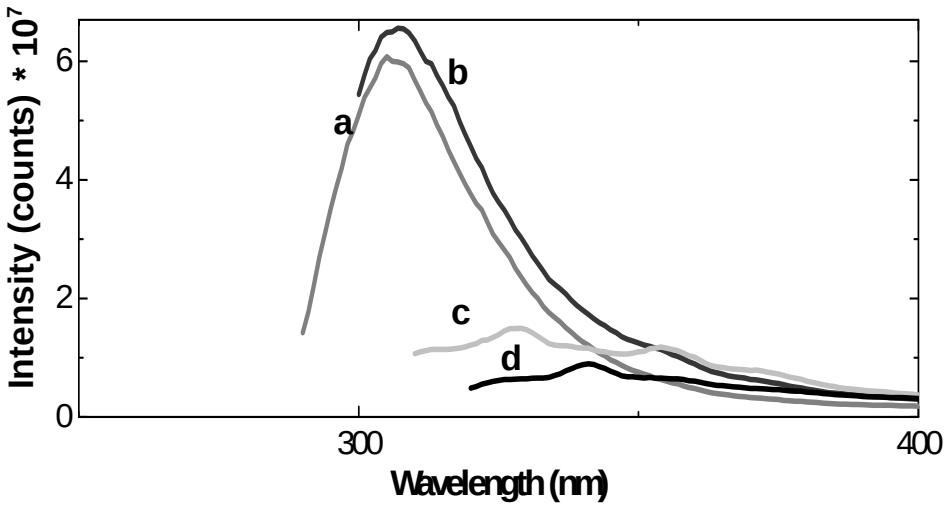

Figure. 2.6. Emission map of Si-$C_{10}H_{21}$ NPs (1.2×10^{-4} M in n-hexane); a) λ_{exc}=280 nm; b) λ_{exc}=290 nm; c) λ_{exc}=300 nm; d) λ_{exc}=310 nm.

Picosecond time-correlated single photon counting (TCSPC) measurements (instrument response time ~87 ps) indicates a rapid relaxation of electronically excited Si NPs to the ground state. It should be noticed that the fluorescence follow a bi-exponential decay curve. The longer component of 4.0 ± 1.0 ns is near-identical to what has been reported for amino-terminated Si NPs by Tilley *et al.*[18] However, a distinct shorter component of 0.75 ± 0.15 ns can also be observed for all four compounds. This fast component substantiates a direct bandgap transition. Interestingly, these TCSPC measurements also allow us to discern the shape of the Si NPs in solution: Time-resolved anisotropy measurements reveal that the fluorescence anisotropy decays strictly according to a mono-exponential curve (Figure 2.7).

This can only be the case if all three perpendicular axes around which the NP can rotate are the same, i.e. if the Si NPs are ball-shaped as also observed by TEM (Figure 2.2a).[28]

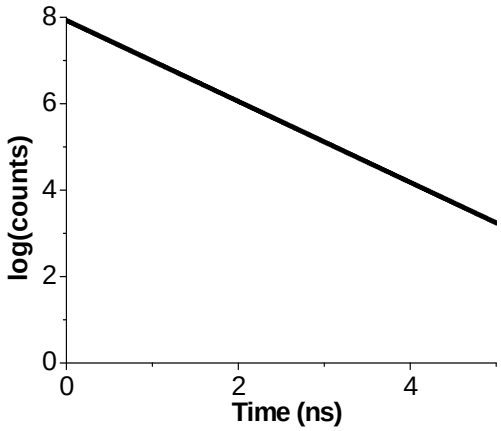

Figure 2.7. Anisotropy decay in logarithmic scale of Si-$C_{12}H_{25}$ NPs in hexane (fitted line totally overlaps with data points).

In addition, the strict linearity of logarithmic representations of these data confirm the high monodispersity of the species under study, as a wide size-distribution would yield straight decays with different slopes for each size, and thus a highly curved overall decay.

2.4. Conclusions

In summary, using inverse micelles it was shown to be easily possible to produce well-defined (1.57 ± 0.21 nm), nearly oxide-free alkylated Si nanoparticles on a gram scale. This easy and highly reproducible 100-fold increase in synthetic yield opens up the way for more systematic studies and for (bio-)applications of these NPs.

The exact composition of synthesized particles, confirmed by XPS measurements, gave information about the surface coverage which is comparable to those of planar Si surfaces. The extinction coefficient of these Si nanoparticles was determined to be 9.4×10^3 $M^{-1}cm^{-1}$, which is only a factor of 7 smaller than that of CdS and CdSe nanoparticles of the same size, which points to the quasi-direct bandgap transition in these nanoparticles. This clearly contrasts with the indirect bandgap transition observed in bulk silicon.

Photophysical studies reveal the high monodispersity by display of narrow fluorescence spectra at room temperature.

Finally, from both TEM data and time-resolved anisotropy measurements, these Si NPs were shown to be both highly monodisperse and ball-shaped.

2.5. References

(1) Veinot, J. G. C., *Chem. Comm*. **2006**, 4160-4168.

(2) Hua, F.; Erogbogbo, F.; Swihart, M. T.; Ruckenstein, E., *Langmuir* **2006**, 22, 4363-4370.

(3) (a) Chao, Y. H., A.; Horrocks, B. R.; Hunt, M. R. C.; Poolton, N. R. J.; Yang, J.; Šiller, L. *Appl.Phys. Lett* .**2006**, 88, 263119-263121 . (b) Chao, Y.; Krisnamurthy, S.; Montalti, M.; Lie, L. H.; Houlton, A.; Horrocks, B. R.; Kjeldgaard, L.; Dhanak, V. R.; Hunt, M. R. C.; Šiller, L. *J. Appl.Phys.* **2005**, 98, 044316 (8pp).

(4) Zhou, Z. Y.; Brus, L.; Friesner, R., *Nano Lett.* **2003**, 3, 163-167.

(5) See for reviews: (a) Sieval, A. B. L., R.; Zuilhof, H.; Sudholter, E. J. R. *Adv. Mat.* **2000**, 12, 1457-1460. (b) Wayner, D.D.M.; Wolkow R.A., *J. Chem Soc. Perkin* 2 **2002**, 1, 23-34; (c) Buriak, *J. M. Chem. Rev*. **2002**, 102, 1271-1308.; (d) Shirahata, N.; Hozumi, A.; Yonezawa, T. *Chem. Rec*. **2005**, 5, 145-159.; (e) Boukherroub, R. *Curr. Op. Sol. St. & Mat. Sci.* **2006**, 9, 66-72.

(6) (a) photochemical: Sun, Q.-Y. D. S., L. C. P. M.; Van Lagen, B.; Giesbers, M.; Thuene, P. C.; Van Engelenburg, J.; De Wolf, F. A.; Zuilhof, H.; Sudhoelter, E. J. R. *J. Am. Chem. Soc.* **2005**, 127, 2514-2523. ; (b) thermal: Sieval, A. B.; Vleeming, V.; Zuilhof, H.; Sudholter, E. J. R. *Langmuir* **1999**, 15, 8288-8291.

(7) (a) Stewart, M. P. R., E. G.; Geders, T. W.; Allen, M. J.; Choi, H. C.; Buriak, J. M. *Phys. Stat. Sol. A:* **2000**, 182, 109-115.; (b) Buriak, J. M.; Stewart, M. P.; Geders, T. W.; Allen, M. J.; Choi, H. C.; Smith, J.; Raftery, D.; Canham, L. T. *J. Am. Chem. Soc.* **1999**, 121, 11491-11502. (c) Buriak, J. M. Adv. Mat. 1999, 11, 265-267.

(8) Rogozhina, E. V.; Eckhoff, D. A.; Gratton, E.; Braun, P. V., *J. Mat. Chem*. **2006**, 16, 1421-1430.

(9) Sato, S.; Swihart, M. T., *Chem. Mater*. **2006**, 18, 4083-4088.

(10) Liu, S.-M.; Yang, Y.; Sato, S.; Kimura, K., *Chem. Mater.* **2006**, 18, 637-642.

(11) Carter, R. S.; Harley, S. J.; Power, P. P.; Augustine, M. P., *Chem. Mater.* **2005,** 17, 2932-2939.

(12) (a) Jurbergs, D.; Rogojina, E.; Mangolini, L.; Kortshagen, U., *Appl. Phys. Lett.* **2006**, 88, 2331161-2331163. (b) Kortshagen, U.; Mangolini, L.; Bapat, A. *J. Nanoparticle Res*. **2007**, 9, 39-52.

(13) Zou, J.; Sanelle, P.; Pettigrew, K. A.; Kauzlarich, S. M., *J. Clust. Sci.* **2006**, 17, 565-578.

(14) Bley, R. A.; Kauzlarich, S. M., *J. Am. Chem.Soc.* **1996**, 118, 12461-12462.

(15) Neiner, D.; Chiu, H. W.; Kauzlarich, S. M., *J. Am. Chem. Soc.* **2006**, 128, 11016-11017.

(16) Zhang, X. M.; Neiner, D.; Wang, S. Z.; Louie, A. Y.; Kauzlarich, S. M., *Nanotechnology* **2007**, 18, 095601 (6pp).

(17) See e.g.: Tilley, R. D. W., J. H.; Yamamoto, K.; Matsui, I.; Fujimori, H. *Chem. Comm*.

2005, 1833-1835. .

(18) Warner, J. H.; Hoshino, A.; Yamamoto, K.; Tilley, R. D., *Angew. Chem. Int. Ed.* **2005**, 44, 4550-4554.

(19) Wang, X. Zhang, R.Q.; Niehaus, T.A.; Frauenheim, Th. *J. Phys. Chem. C* **2006**, 111, 2394-2400.

(20) Wang, J. P.; Song, L.; Zou, B. S.; El-Sayed, M. A., *Phys. Rev. B* **1999**, 59, 5026- 5031.

(21) Nelles, J.; Sendor, D.; Ebbers, A.; Petrat, F. M.; Wiggers, H.; Schulz, C.; Simon, U., *Colloid Polym. Sci.* **2007**, 285, 729-736.

(22) Boukherroub, R.; Morin, S.; Sharpe, P.; Wayner, D. D. M.; Allongue, P., *Langmuir* **2000**, 16, 7429-7434.

(23) Holmes, J. D. Z., Doty, R. C.; Pell, L. E.; Johnston, K. P.; Korgel, B. A. *J. Am. Chem. Soc.* **2001**, *123*, 3743.

(24) Sieval, A. B.; van der Hout, B.; Zuilhof, H.; Sudhoelter, E. J. R., *Langmuir* **2000**, *16*, 2987

(25) Spectra shown are for the $C_{16}H_{33}$-capped Si NPs. The shape of the peaks and intensity of the transitions is hardly affected by the nature of the alkyl coating.

(26) Yu, W. W.; Qu, L. H.; Guo, W. Z.; Peng, X. G., *Chem. Mat.* **2003**, 15, 2854-2860.

(27) (a) Pettigrew, K. A. L., Q.; Power, P. P.; Kauzlarich, S. M. *Chem. Mater.* **2003**, 15, 4005- 4011; (b) Li, X. G.; He, Y. Q.; Swihart, M. T. *Langmuir* **2004**, 20, 4720-4727; (c) Liu, S.-M.; Yang, Y.; Sato, S.; Kimura, K. *Chem. Mat.* **2006**, 18, 637-642.

(28) Lakowicz, J. R., *Principles of Fluorescence Spectroscopy*. 3rd ed.; Springer: Singapore, **2006**.

Chapter 3

Amine-terminated Silicon Nanoparticles: Synthesis, Optical Properties and their Use in Bioimaging

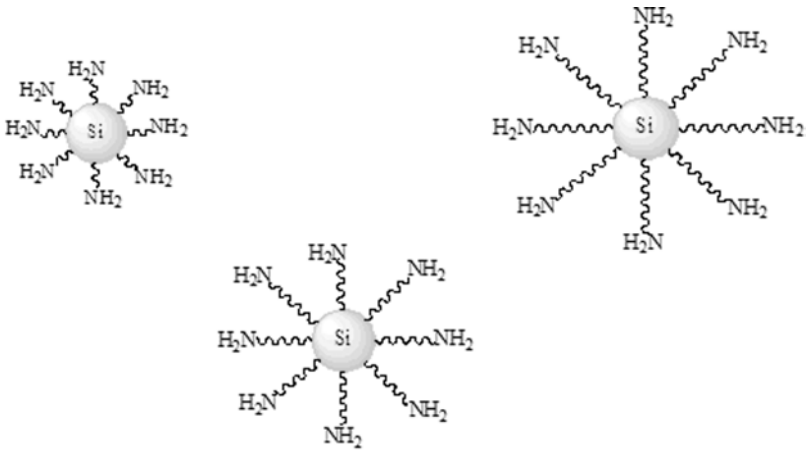

This chapter is submitted for publication as:

"Amine-terminated Silicon Nanoparticles: Synthesis, Optical Properties and their Use in Bioimaging", Milena Rosso-Vasic, Evan Spruijt, Zoran Popović, Karin Overgaag, Barend van Lagen, Bruno Grandidier, Daniel Vanmaeckelbergh, Luisa De Cola and Han Zuilhof

Abstract – Very stable and bright amine-terminated Si nanoparticles (NPs) with different alkyl-chain lengths between the Si core and amine end-group are synthesized. The obtained NPs have a spherical shape and homogeneous size distribution (1.57 ± 0.24 nm). Their emission can be tuned from the UV to the blue spectral region, in a controllable fashion, by only changing the alkyl spacer length. The emission quantum yields are ~12 % for all synthesized Si NPs. Excited-state lifetimes are in the ns range and point to a direct band-gap excitation. NH_2-terminated Si NPs exhibit an exceptional stability over a wide pH range (1-13) and high temperatures (120 °C). Diffusion coefficient of prepared Si NPs is determined by Fluorescence Correlation Spectroscopy (FCS) - $3.3 \cdot 10^{-10}$ $m^2 s^{-1}$. Derived size of Si NPs from mobility corresponds to 1.4 nm which is in a good agreament with the size obtained by Transmission Electron Microscopy (TEM). NH_2-terminated are shown to be highly suitable for bio-imaging studies as they are readily taken up by BV2 cells. Si NPs are located in the cells cytosol. Proliferation of stained BV2 cells is observed and showed that newly formed cells are also stained with Si NPs, indicating their minimal toxicity. By using Si NPs it is possible to stain multiple cell generations by only staining mother cells.

3.1. Introduction

Over the last few years silicon nanoparticles (Si NPs) have attracted a lot of interest because of their exceptional optical properties, such as size-dependent tunable light emission,[1-3] high brightness,[4] and their great stability against photo-bleaching compared to organic dye molecules.[5,6] Moreover, Si exhibits a low inherent toxicity[7] in comparison with the heavy elements of several other types of semiconductor quantum dots.[8-10] The combination of these properties opens up a new venue of applications of Si NPs for optoelectronic[11] and bioimaging purposes.[12,13]

Free-standing luminescent Si NPs of 1-8 nm size have been produced using a variety of techniques such as: ultrasonic dispersion of electrochemically etched silicon,[14] laser-driven pyrolysis of silane,[15-18] synthesis in supercritical fluids[2,19] and wet chemistry techniques - reduction of Zintl salts in inert organic solvents[20-24] and in micelles using SiX_4 (X = Cl, Br or I) as a silicon source.[5,25-27] The obtained NPs were halogen-terminated[21,28] or hydrogen-terminated[15,16,29,30] and very prone to oxidation.[31] Therefore, further stabilization is desirable, e.g. by reaction with alkyl-lithium salts[21] or terminal alkenes[32] to provide Si-C linkages. These passivation methods were similar to those developed for planar[33] or porous[34] silicon, for which the attachment can be initiated thermally,[35,36] or photochemically with UV[37] or visible light.[38-40] Hydrosilylation of Si NPs was also successfully performed by using a variety of platinum-based[5,41] or triphenylcarbenium-based catalysts.[42]

The light emission of Si nanocrystals has been attributed to the decay of quantum-confined excitons[43] as well as to decay mechanisms mediated by surface atoms.[44,45] The exciton can be self-trapped or luminescence can occur via an energy level located in the bandgap.[46] Quantum confinement is controlled by the size of the core of the NPs, but full control over the surface properties is also important in order to achieve desirable emission characteristics, which itself requires improved methods for producing well-defined NPs. Indeed, changing the capping group of Si NPs can significantly shift the emission energy. A direct comparison of the emissions of alkyl- and amine-terminated Si NPs of the same size displays a significant red shift for the amine-terminated NPs.[27] Interestingly, the emission of NH_2-terminated NPs was intense, despite of the presence of NH_2 moieties. This contrast with observations of CdSe NPs, the emission of which is strongly quenched when an amine group is present in the solvent, in the form of alkylamine.[47,48]

The ability to make NPs water soluble and to target them to specific biomolecules using proper anchors as capping groups has led to promising applications in cellular and assay labelling techniques, as well as in deep-tissue imaging.[49-52] For such purposes

core/shell/coating NPs (e.g. CdSe/ZnS/silane NPs) have been studied the most so far.[53-55] Despite their wide absorption and emission range (from UV to IR) and their exceptional brightness there are two main disadvantages that significantly limit their application: large overall size and toxicity. The minimal size of core/shell/coat NPs is 10-20 nm and while the core size is still small enough for quantum confinement phenomena, this overall size greatly restricts their use for cellular application. In addition, although the silane coating plays an important role in reducing their toxicity, the packing density and porosity of this organic monolayer is hard to control.

Water-soluble Si NPs seem to be good candidates to overcome these drawbacks. Li *et al.* already demonstrated the possibility of labeling the surface of Chinese hamster ovary (CHO) cells with red-emitting poly(acrylic acid) functionalized Si NPs.[56] More recently, Tilley *et al.* labeled Vero cells with amino-terminated Si NPs, and gave an indication that NPs were probably transfected into the cytosol.[27] However, the uptake and lifecycle of cells labeled with Si NPs has not been studied yet.

The aim of our research is twofold: to determine the influence of amine groups and linker lengths on the optical properties of alkyl-amine-functionalized Si NPs, to determine their band gap and examine their cellular uptake by determining their location inside the cell and the behavior of cells after labeling.

For that purpose we have synthesized hydrogen-terminated Si NPs in reverse micelles and functionalized them with three different amine-terminated ω-alkenes: allyl-amine, hex-5-enylamine and dodec-11-enylamine. Here we report on the synthesis and photophysics of such species, including both steady-state and time-resolved absorption and emission spectroscopy at various pH values. We have also performed In UHV cryogenic Scanning Tunneling Microscopy (STM) and Spectroscopy (STS) on Si NPs, with the aim to provide unique information on the electronic properties of the individual nanocrystals as STS can probe the complete density of states without being limited by selection rules that play a part in e.g. optical experiments.[57] addition, we have, for the first time, experimentally determined the diffusion coefficient of Si NPs, a highly relevant value to predict their mobility in the physiological media. Finally, we successfully stained a murine cell line (BV2) with Si NPs and observed the location of NPs inside the cell, and the continued proliferation of cells. This last experiment truly reveals the potential of Si NPs for bioimaging.

3.2. Experimental Section

All chemicals used were purchased from Sigma-Aldrich and employed without further purification unless specified differently. Toluene ((H_2O ≤ 0.005%), ≥99.7% (GC)) was dried over Na wire overnight prior to use. Methanol was distilled and stored on anhydrous $MgSO_4$.

3.2.1. Synthesis of alkene-amines and Si NPs

Hex-5-enylamine. 6-bromo-1-hexene (5 ml; 0.04 mol) was dissolved in 50 ml of DMF. After addition of NaN_3 (0.20 mol) mixture was stirred at 35 ^{0}C for 24 h. Cold water was added and 6-azido-hex-1-ene was extracted with petroleum ether (PE 40/60) and washed 3 times with brine. Pure 6-azido-hex-1-ene has been obtained with 75 % yield. ^{1}H NMR (300 MHz, $CDCl_3$, 293 K): δ(ppm) 5.81 (m, 1H), 4.99 (m, 2H), 3.26 (t, 2H), 2.07 (m, 2H), 1.60-1.36 (m, 6H)

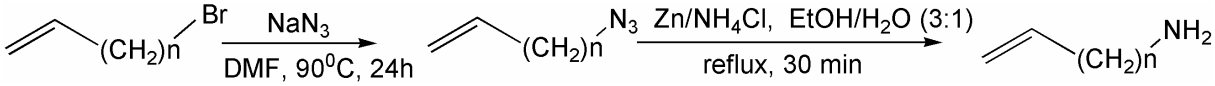

Figure 3.1. Synthesis of alkene-amines

NH_4Cl (0.09 mol, in 120 ml of ethanol/water (3:1) mixture) was added to 6-azido-hex-1-ene. Upon addition of 3.4 g of Zn powder, reaction mixture was refluxed for 30 min. The mixture was filtered and ethanol was evaporated under reduced pressure. 12 ml of aqueous ammonia solution and 120 ml of ethyl acetate were added in order to extract hex-5-enylamine. Amine solution in ethyl acetate was washed 3 times with brine and solvent was removed under reduced pressure and dried over magnesium sulfate. Pure hex-5-enylamine is obtained with 62% yield. ^{1}H NMR (300 MHz, $CDCl_3$, 293 K): δ(ppm) 5.81 (m, 1H), 4.98 (m, 2H), 2.71 (t, 2H), 1.40-1.10(m, 10H)

Dodec-11-enylamine. 11-bromo-undecene-1-ene (10 ml; 0.05 mol) was dissolved in 50 ml of DMF. After addition of NaN_3 (0.20 mol) mixture was stirred at 90 ^{0}C for 24 h. Cold water was added and 11-azido-undec-1-ene was extracted with petroleum ether (PE 40/60) and washed 3 times with brine. Pure 11-azido-undec-1-ene has been obtained with 90.3% yield. ^{1}H NMR (300 MHz, $CDCl_3$, 293 K): δ(ppm) 5.80 (m, 1H), 4.99 (m, 2H), 3.26 (t, 2H), 2.09 (m, 2H), 1.61 (m, 2H), 1.39 (m, 12H)

NH_4Cl (0.14 mol dissolved in 200 ml of ethanol/water (3:1) mixture) was added to 11-azido-undec-1-ene. Upon addition of 3.9 g of Zn powder, reaction mixture was refluxed for 30 min. The mixture was filtered and ethanol was evaporated under reduced pressure. 20 ml of aqueous ammonia solution and 200 ml of ethyl acetate were added in order to extract dodec-11-enylamine. Amine solution in ethyl acetate was washed 3 times with brine and solvent

was removed under reduced pressure and dried over magnesium sulfate. Pure dodec-11-enylamine is obtained with 85% yield. ^{1}H NMR (300 MHz, $CDCl_3$, 293 K): δ(ppm) 5.87 (m, 1H), 4.97 (m, 2H), 2.71 (t, 2H), 1.42 - 1.17 (m, 18H)

3.2.2. Synthesis of amino-terminated Si NPs

Silicon nanoparticles were prepared using a modification of a method reported by Warner *et al*. 1.5 g of tetraoctylammonium bromide was mixed with 100 ml of dry toluene and mixture was sonicated for 30 min, under flow of dry Ar. 100 µl of $Si(OCH_3)_4$ was added via a gas-tight syringe and sonication was continued for 30 min allowing entrance in micelles. Subsequently, 2.3 mL of $LiAlH_4$ (1 M in THF) was added in order to form hydrogen-terminated Si NPs. After 30 min of sonication, dry and deairated methanol (30 ml) was added to react with the excess $LiAlH_4$.

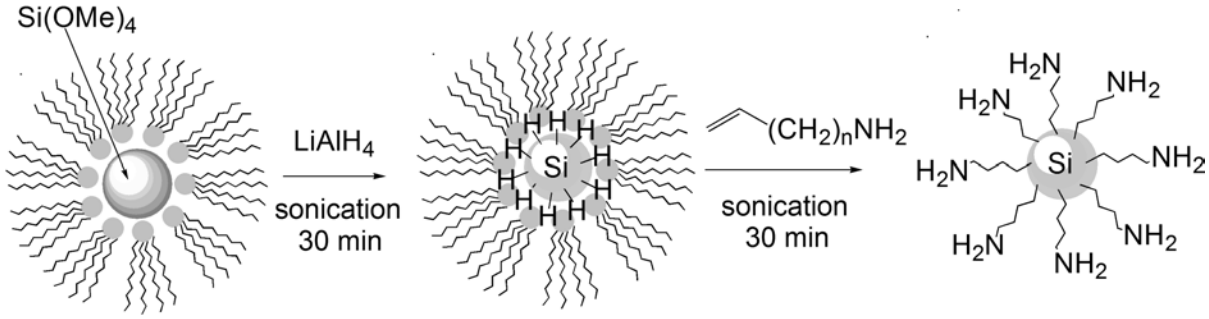

Figure 3.2. Synthesis and functionalization of Si NPs (n = 1, 4, 9).

Alkyl-amino terminated particles with three different alkyl chain-lengths were obtained in the reactions of degassed allyl-amine (2.7 g), hex-5-enylamine (2.4 g) and dodec-11-enylamine (4.4 g) to each flask with hydrogen-terminated Si NPs under Ar, in the presence of 40 µl of 0.05 M H_2PtCl_6 catalyst. After 30 min of sonication, 3-amino-propyl, 6-amino-hexyl and 11-amino-dodecyl Si NPs were extracted with water, washed with ethyl-acetate and filtrated twice through syringe membrane filters (Millex, Millipore, PVDF, 0.45 µm). The resulting Si NPs were further purified by dialysis against water (MWCO 7000, SERVA, Membra-Cel dialysis tubing, diameter 22 mm) to remove any residuals of nonreacted amino-alkene and surfactant.

3.2.3. Optical measurements

All measurements have been performed at standard pressure and room temperature, unless stated differently. Electronic absorption spectra were recorded in a quartz cuvette (1 cm, Hellma), using a Cary 1 UV-Vis double-beam spectrophotometer and were corrected for the solvent absorption. The scan range was 200-500 nm with a 600 nm/min rate.

Steady-state and time-resolved measurements were performed on a Time-Correlating Single Photon Counting F900 spectrometer (Edinburgh Instruments), with an instrument response function for time-resolved measurements of 87 ps. All steady-state spectra are corrected for the wavelength-dependent sensitivity of the detector and the source by recording reference data simultaneously. Additionally, emission spectra have been corrected for Raman scattering using the solvent emission spectrum.

Using a comparative method by Williams *et al.*,[58] luminescence quantum yields were measured in optically dilute solutions (optical density ~0.1), using 2-aminopyridine in 0.05 M aqueous solution of sulphuric acid (Φ_{em} = 0.60) as a reference emitter.

Time-resolved fluorescence measurements were performed with the exact the same solution used for steady-state spectra (absorption was always adjusted to be ≤ 0.5). A pulsed light-emitting diode ($\lambda_{excitation}$ = 372 nm) was used as excitation source, and photons were collected up to 20 ns (4096 channels) until a maximum of 10^4 counts.

pH values were set to 1.0 by adding trifluoro-acetic acid, 7.5 by adding phosphate buffer (75 mM) and pH = 13.6 with NaOH in water.

3.2.4. NMR, TEM and FCS measurements

^{1}H NMR spectra were recorded on a Bruker AC-E 400 spectrometer in $CDCl_3$ (dried over Al_2O_3).

High-Resolution Transmission Electron Microscopy (TEM). TEM studies were performed with a LIBRA 200 FE (200 kV) microscope. TEM samples were prepared by dipping a carbon-coated 300-mesh copper grid into a sonicated and filtered silicon nanoparticles solution in water. The solvent was evaporated in air and TEM micrographs were typically taken at five different spots of each grid. Olympus Soft Imaging iTEM Solution and iTEM Solution EMaker were used to view and analyse the micrographs, respectively.

Fluorescence Correlation Spectroscopy (FCS). FCS measurements were performed with a Zeiss LSM ConfoCor 2 combined microscope system (Carl Zeiss, Jena, Germany). For the excitation of the Alexa488 and Si NPs, the 457 nm line of an air-cooled argon ion laser was used. The laser power was set at 2.5 microwatts. A solution of Alexa 488 in nanopure water was used for calibration of the beam profile. The beam radius is determined from the measured diffusion time (τ_D) and known diffusion coefficient of Alexa 488 (D = 2.24 $\times 10^{-10}$

m^2s^{-1}). Samples were placed in 8-chambered plates (Nunc, Rochester, NY) with borosilicate bottom. Autocorrelation traces were acquired 10 times with 30 s periods.

3.2.5.Scanning Tunneling Microscopy (STM) and Spectroscopy (STS)

A flame-annealed Au(111) substrate is placed in a solution (chloroform) with amine-terminated Si NPs for a few min and then thoroughly rinsed before placing it in the set-up. Amine-terminated Si NPs were attached to a Au substrate by a Au-NH_2 bond. The STM-STS was performed on UHV cryogenic set-up (OMICRON). Tunneling spectra were acquired at 5 K in at low temperature STM, by placing the STM tip above the center of an isolated dot well-separated from the neighboring NPs and disconnecting the feedback loop. The tunneling current *I* is measured as a function of the tip-substrate potential difference (V_{bias}).[59] Typically, 100 spectra per STS setting were acquired above a single dot and checked for reproducibility. The spectra are acquired at low set-point currents to ensure the experiments were performed in the shell-tunneling regime.[57]

3.2.6. Cell Staining

BV2 cells (total of ~2.5 10^5, as determined by optical absorption) were suspended in PBS and mixed with NPs (15.3 mg dm^{-3}) in 1:1 ratio. The mixture was incubated at 37 ^oC for 5 min and cells were centrifuged. The formed pallet was suspended in 500 μl of PBS and analyzed under the microscope in a microwell plate. Cells were observed using a laser scanning confocal microscope Leica TCS SPE through a 100 x 1.30 NA oil immersion objective. The pinhole was set to one Airy. Si NPs were excited using a 488 nm laser. Epifluorescence was recorded with a black and white Leica DFC350FXR2 digital camera mounted to the Leica microscope. The sample was observed through an oil immersion 63X/1.4 objective.

3.3. Results and Discussion

3.3.1. Characterization of amine-terminated Si NPs

A typical TEM image of 3-amino-propyl-terminated Si NPs (Figure 3.3) displays a particle-size distribution of 1.57 ± 0.24 nm, measured on 1365 NPs from different parts of the grid. This value and distribution of the size of the Si core (the alkyl chains do not show up in TEM) was independent of the alkyl spacer length, which excludes effects of the Si NP core size on their optical properties, and also shows that the method used to make such NPs is reproducible.

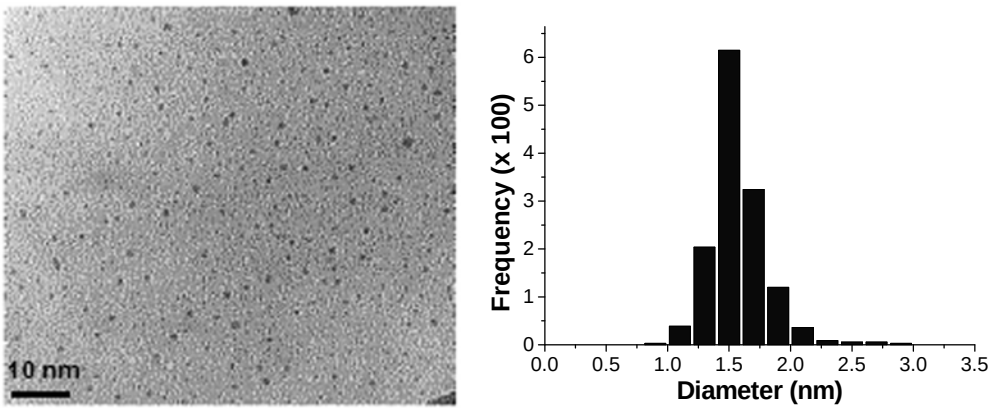

Figure 3.3. TEM image of 3-amino-propyl-terminated Si NPs and corresponding particle size distribution histogram.

The topographic STM image (Figure 3.4 a) also shows well-separated Si NPs that can be easily identified. The stable topography indicates that the Si NPs are anchored via Au-NH_2 bonds. From previous investigations performed on different types of nanocrystals[59], it was shown that the size of the particles can be measured in the height profile obtained from the topographic images. In contrast, the lateral dimensions of the nanoparticle are generally larger due to tip convolution effects. Histograms of the height of the NPs measured from the topographic images are shown in Figure 3b. The average STM height is around 1 nm which is slightly smaller than the core diameter deduced from the TEM analysis (Figure 3.3), which may reflect a combination of topology and electronic effects (i.e. different density of states on bare Au and the Si NPs). However, the shape of STM height histogram completely resembles TEM histogram.

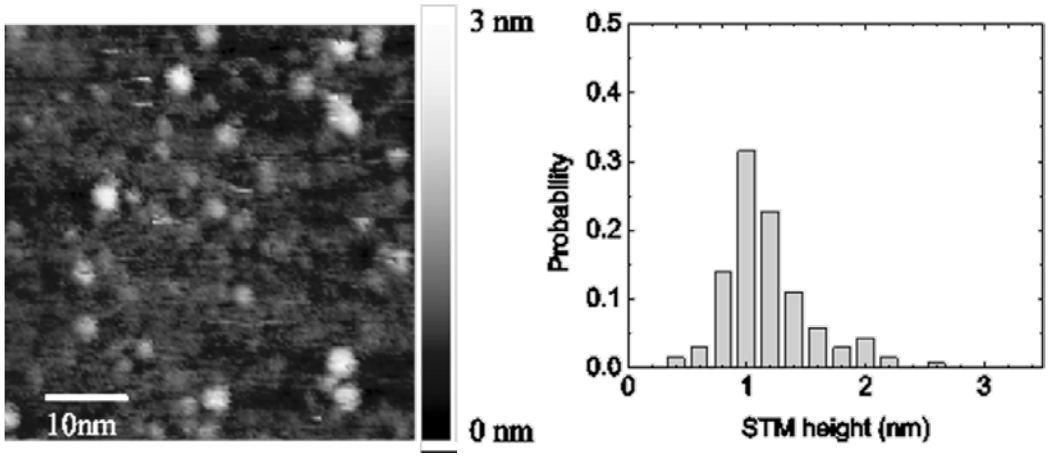

Figure 3.4. Large-scale STM image of : a) 3-amino-propyl-terminated Si NPs on a Au(111) substrate. STM parameters V_{bias}: 2.5 V, $I_{set\text{-}point}$: 10 pA. The insert shows well-separated individual NPs. b) Histogram of Si NP heights extracted from STM topography.

3.3.2. Determination of the band gap: optical absorption and scanning tunneling spectroscopy

All synthesized amine-terminated Si NPs show a broad continuous absorption between 200 - 450 nm (Figure 3.5). Comparing to alkyl-terminated Si NPs[41] (Figure 3.5, curve d), the spectra are broader. The absorption spectrum of 3-amino-propyl-terminated Si NPs has a distinctive broad peak at 300 nm and a less pronounced absorption around 265 nm. The disappearance of the most apparent peak/shoulder in the absorption spectra with increasing length of the alkyl spacer probably reflects variations in the oxygen contents at the NP surface, which has for alkyl-terminated Si NPs been shown to be linked to the length of the alkyl spacer.

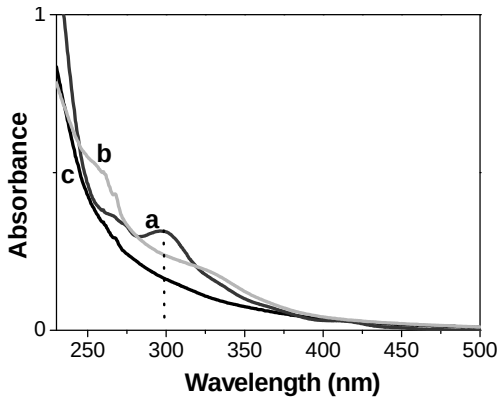

Figure 3.5. Absorption spectrum of a) Si-$C_3H_6NH_2$, b) Si-$C_6H_{12}NH_2$ and c) Si-$C_{11}H_{22}NH_2$ NPs;

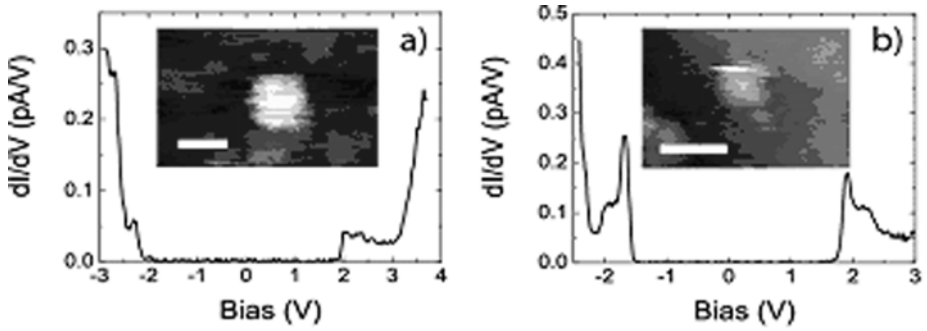

Figure 3.6. Spectroscopy on individual Si. STS settings are V_{bias}: 3.6 V, *I*set-point: 100 pA and V_{bias}: 3.0 V, $I_{set\text{-}point}$: 100 pA; 5 K. The spectra show a large zero-conductance gap in the range of 4 V with a strongly increasing LDOS at positive and negative bias. The scale represents 10 nm.

Quantum chemical calculations predict that the presence of an NH_2 group in the vicinity of Si NPs results, for small NPs as those under study, in narrowing the energy gap between the HOMO and LUMO orbitals.[60] When the length od the capping molecules is increased, the effect of narrowing of the band gap is smaller, resulting in the blue shift of

the absorption bands.

It should also be noted that with increasing alkyl chain length the obtained alkyl-terminated Si NPs are less oxidized (noticable via the Si-O bond in the IR spectra).[41] Thus, beside a distance dependence of the influence of the amine groups to the Si core, a higher degree of oxidation can also contribute to red-shifted absorption.[61]

The electronic spectra of individual Si NPs are also studied. Bandgaps of individual Si NPs were measured by scanning tunneling spectroscopy (STS), and are in the 4 – 5 eV range for 60% of the measured NPs, and 3 - 3.75 eV for the rest.[59,62] On two identically prepared samples 14 and 17 dots were investigated, respectively. Figures 3.6a and 3.6b show two measured conductance spectra on Si NPs with STM heights of 3 nm and 1 nm, respectively. The spectra show resonances at positive (conduction levels) and negative bias (valence levels) separated by a large zero-conductance gap. Here we only focused on the STS spectra showing a large STS gap. This value is close to what is theoretically calculated for Si NPs with a Si core diameter of ~1 nm.[63] Such a large bandgap has also been seen in the optical spectroscopy (Figure 3.5) and accurately corresponds to the most pronounced band at 300 nm.

3.3.3.Luminescence spectra

Emission spectra of amino-terminated Si NPs are recorded upon various excitation wavelengths, from 280 to 460 nm. All NPs under study display an intense emission in the 350 – 600 nm range. The size dispersion is revealed in the luminescence data, where excitation with different wavelenghts specifically causes the emission of Si NPs of different sizes. However, the emission spectra, and specifically the wavelength at which the maximum emission intensity is observed depends on the length of the alkyl spacer (Figure 5). With a short (-C_3H_6) spacer the maximum emission is observed in the blue at λ_{em}^{max} = 475 nm, when exciting Si NPs at 390 nm. For longer chains the maximum emission gradually shifts to the UV: for the C_6H_{12} spacer λ_{exc}^{max} = 380 nm and λ_{em}^{max} = 467 nm; for the $C_{11}H_{22}$ spacer λ_{exc}^{max} = 320 nm, while λ_{em}^{max} = 385 nm. These values can be compared to analogous features for alkyl-functionalized oxide-free Si NPs of the same size, which display λ_{exc}^{max} = 260 nm and λ_{em} = 283 nm.[41] The longer the alkyl chain between Si NPs core and amine moiety, the shorter the wavelength of maximum emission, and thus: the more the NH_2-terminated Si NPs resemble alkyl-terminated Si NP. The positions of the emission maxima are almost identical for excitation wavelengths above 360 nm for all synthesized Si NPs. However, upon excitation with light of 300-320 nm, maxima of the Si-$C_{11}H_{22}NH_2$ NPs are blue shifted by ~45 nm (~0.3 eV) compared to what is observed for Si NPs with shorter chains. With an increase of the excitation

wavelength, this difference becomes smaller until finally disappears above λ_{exc} = 350 nm. In all cases, the luminescence is very broad and between 2 and 3 eV. A large Stokes shift (~1 eV) and the broadness of the emission indicate that the observed luminescence is not a true bandgap process. As previously mentioned, the exciton can be self-trapped or luminescence can occur via an energy level bandgap.[46] These results are in line with the change in passivation; attachment of shorter chains used for passivation of Si NPs is accompanied by a more oxidized NP surface and vice versa.[41]

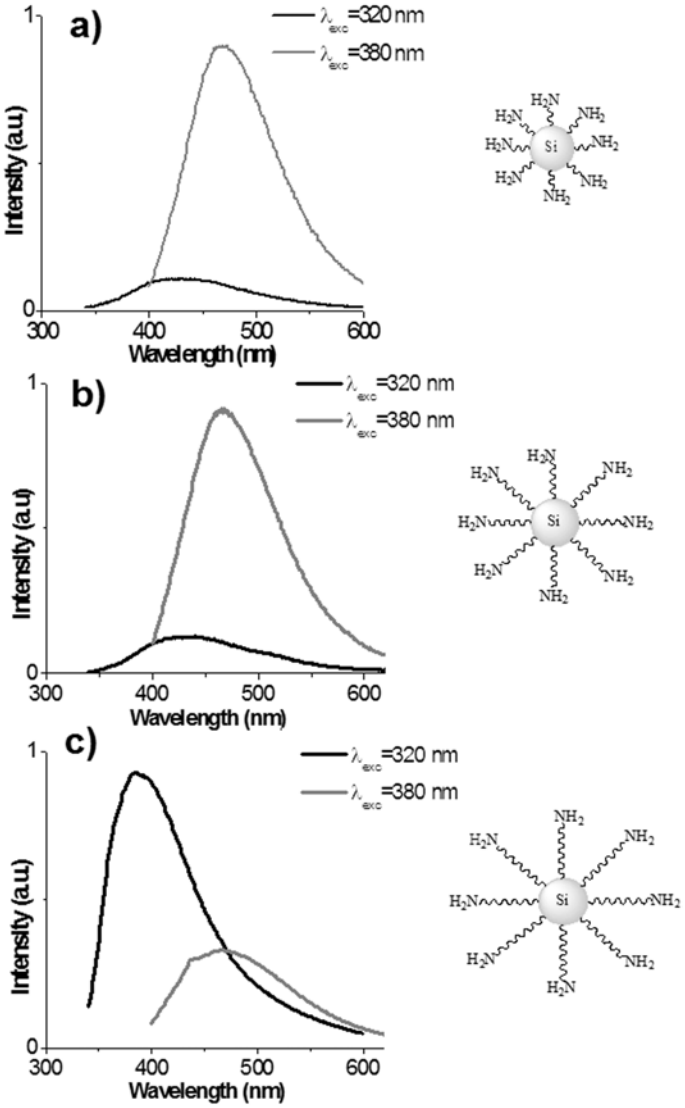

Figure 3.7. Dominant emission of 3-amino-propyl (a), 6-amino-hexyl (b) and 11-amino-undecyl (c) terminated Si NPs in water. Note: Si NP core size is identical in all cases.

Therefore it is likely that Si NPs with shorter alkyl-amine chains have more trapped states. Electron-hole recombination then occurs via carriers trapped in oxygen-related

localized states that become observable due to the widening of the bandgap induced by quantum confinement. This effect is especially pronounced for ultrasmall Si NPs (1-2 nm), while for bigger Si NPs (> 3 nm) there is no broadening or red-shift in emission, since the Si=O surface states are located outside the bandgap.[63]

The quantum yields of photoluminescence of amino-terminated Si NPs were measured in water at pH = 7.5, and are displayed in Table 3.1. The fluorescence quantum efficiency is ~12 % and is comparable to the published quantum yields for wet-chemically prepared functionalized Si NPs,[5,19] and independent of the chain length. So, while the energy of emission can be fine-tuned by the chain length, the overall efficiency is more or less independent.

Table 3.1. Optical properties of amine-terminated Si NPs

	Emission Maximum		**FWHM**		**QY**
	λ_{exc} (nm)	λ_{max} (nm)	nm	eV	**(%)**
Si-$C_3H_6NH_2$	390	475	98	0.53	13.2 ± 0.6
Si-$C_6H_{12}NH_2$	380	467	100	0.56	11.0 ± 0.5
Si-$C_{11}H_{22}NH_2$	320	385	98	0.77	12.4 ± 0.5

All three types of Si NPs show similar lifetimes at λ_{em} = 450 nm, which can be fitted as a three-exponential decay with lifetime contributions of 0.1 ns (~10%), 0.9 ns (25 – 40 %) and 4.5 ns (45 – 65%). Upon excitation of the NPs with 372 nm light, the overall decay time increases for longer emission wavelengths by an increase of the longest component from 4.2 to 4.9 ns (Figure 3.8). This is likely caused by some dispersity of the Si core size, as the relaxation rates are likely size dependent. Probing at longer emission wavelengths may, due to quantum confinement, shift the focus to larger NPs.

These short lifetimes (< 10 ns) indicate a direct band gap emission of amine-terminated Si NPs.[2] If this would not be the case, lifetimes would be in μs range.[63] Combining the obtained values for the fluorescence quantum yield and lifetimes, the overall decay rates can be calculated to be in the range of 0.6 - 4.4 $\times$ 10^9 s^{-1},[64] which is in line with a direct band gap excitation of the thus formed Si nanostructures.[2]

Since it is known that the amine moiety can strongly quench the emission of semiconductor quantum dots,[47,48] it was of interest to investigate this phenomenon with the amino-terminated Si NPs. This can be easily achieved via a variation of the pH, since this effectively transforms an $–NH_2$ moiety with a lone electron pair, available for electron donation, into an $–NH_3^+$ group that lacks this capability. With this aim, we obtained emission spectra at pH = 1.0, 7.5 and 13.3, and observed that λ_{em}^{max} is independent of

the pH, to within the experimental error of ~1 nm. This surprising result implies that the emission of NPs with protonated (non-quencher) and nonprotonated (quencher) amino groups originates from the same state. An effect of the pH on the emission intensity for Si NPs is observed (maximum changes of ~40% for C_3H_6 linker; smallest (~10%) changes for $C_{11}H_{22}$ chains): at lower pH the overall emission intensity is always higher, while – as said before – the energy of the emission maximum is unaffected.

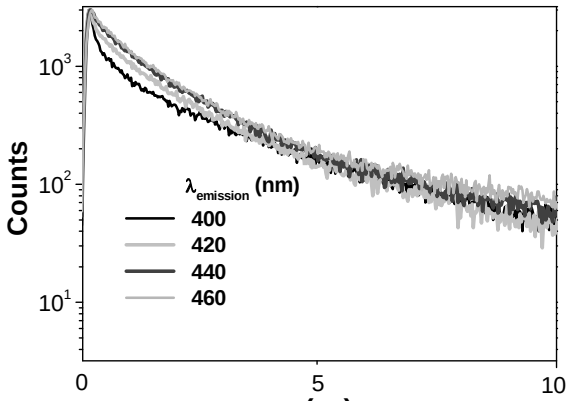

Figure 3.8. Fluorescence time-resolved decays at different emission wavelength for 3-amino-propyl terminated Si NPs in water, λ_{exc} = 372 nm. (*See Appendix at the end of the thesis for the color picture)*

Combined with the data shown in Figure 3.7 the following picture arises: Amine moieties can display some influence on the Si core, but there is only a marginal electronic coupling (i.e. delocalization of HOMO and/or LUMO onto the NH_2 groups). The excited states of the various alkylamine-terminated Si NPs are therefore more or less the same, only differing by the degree of oxidation that is slightly chain dependent. The length of the alkyl spacer influences the rate of excited state relaxation processes, which likely include electron transfer. At low pH all amino groups are protonated, and electron transfer between the amino moieties and the Si core are precluded, yielding a higher emission intensity as observed. At higher pH protonation is either incomplete or absent, which allows involvement of the nitrogen lone pair in relaxation processes and yields a reduced emission and shorter excited state lifetime.

It has to be noted that the NPs remained highly stable also in these extremely acidic or basic conditions. Upon the exposure to pH = 1 at room temperature, the NPs remained chemically and photophysically stable even after several months! Perhaps even more surprisingly is that Si NPs also display tremendous resistance to a high pH of 13.3: the emission dropped only 5 % after 10 h, and 38% after 150 h (Figure 3.9). The lifetimes (Figure 3.10) become somewhat shorter with increasing pH.

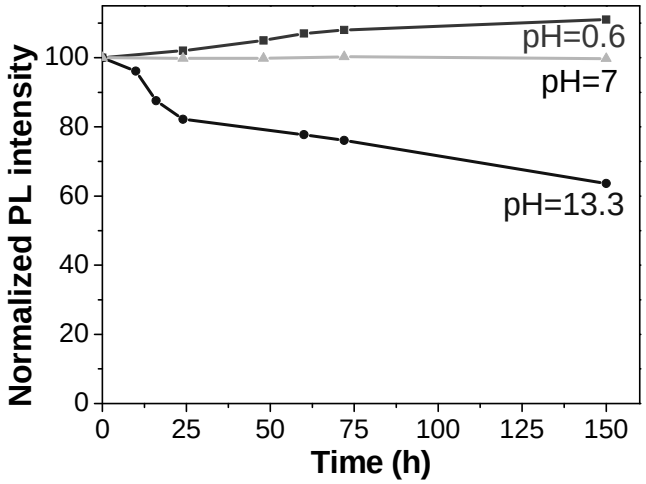

Figure 3.9. Change of 3-amino-propyl terminated-Si NPs emission intensity with time at different pH.

This is not due to a change of the three components (0.1, 0.9 and 4.5 ns, respectively), but lowering the pH increases the 0.9 ns component at the cost of the 4.5 ns component. In other words: the pH dependence on both the overall emission and lifetime point to a quenching route for excited Si NPs that involves the N lone pair, but which is not the exclusive decay path.

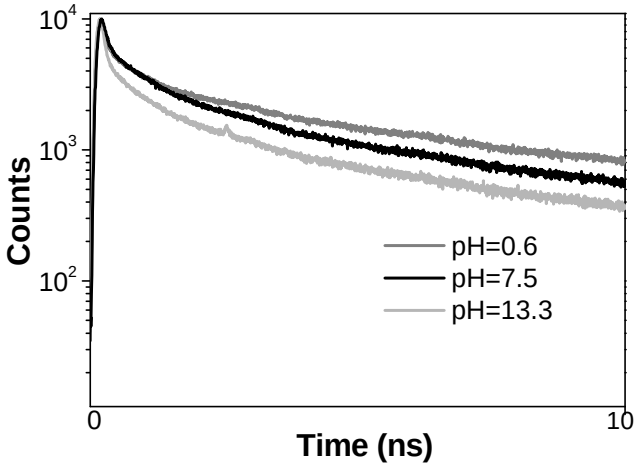

Figure 3.10. Dependence of pH of the aqueous medium on the fluorescence lifetime of 3-amino-propyl terminated-Si NPs.

Importantly, IR measurements after storing the particles at pH = 13.3 for 6 h still indicates the presence of an amino-alkyl monolayer.

These observations indicate a very high degree of surface passivation by the amino-alkyl layer, and can be placed in context by noting that a planar Si surface that is coated with a

covalently attached monolayer will typically lose that monolayer within 1 h at pH = 13. In other words: while NPs have a relatively large surface in comparison to their core, and are thus extremely prone to surface reactions – as is observed in the oxidation of H-terminated Si NPs[65] – the surface passivation of alkylamine-terminated Si NPs is good enough to withstand even these extreme conditions. Such coated NPs are also very stable under sterilization conditions (121 °C, 30 min), which is essential for any toxicology studies. The overall emission intensity remains unchanged after the exposure of the NPs to 121 ^{o}C for 30 min, while a slight peak broadening was observed (increase of FWHM by 1 - 2 nm), probably due to some oxidation. This very long stability of the fluorescence in aqueous media is, of course, also highly beneficial for bioimaging studies.

3.3.4.Shape and diffusion of Si NPs

To determine the exact shape and possible aggregation of alkylamine-coated Si NPs, fluorescence anisotropy measurements were performed in solutions of different viscosities. All anisotropy decay curves could be fitted well with one-exponential functions, which implies that these NPs are really monodisperse, and also that the shape of these NPs is spherical, as not obeying either of these conditions would have yielded multi-exponential fits.[64] In addition, it follows that aggregation of these NPs does not occur to any significant degree.

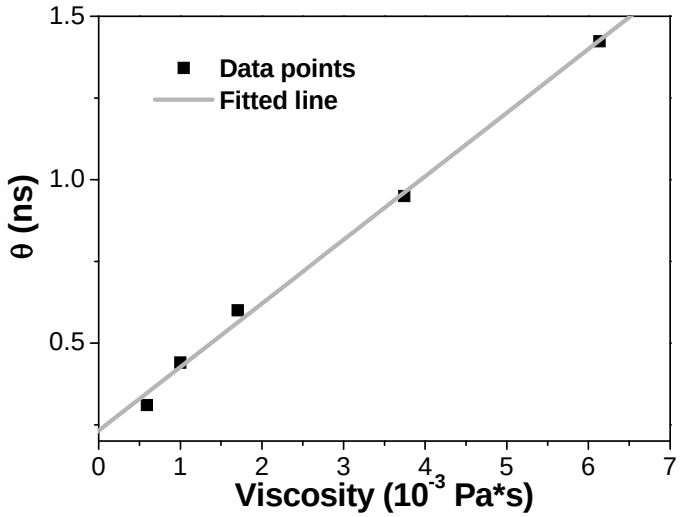

Figure 3.11. Dependence of the rotation correlation time (θ) on solvent viscosity for 3-amino-propyl Si NPs at constant temperature (298 K).

The viscosity dependence of the rotation correlation time of 3-amino-propyl Si NPs has been measured in the viscosity range of 0.6 - 6.2·10^{-3} Pa·s. For this purpose NPs were

dried and dissolved in different solvents: methanol, water and sucrose solutions in water (20 - 42%). Figure 3.11 shows that this dependence is linear in the examined viscosity range, as expected for spherical bodies,[64] further confirming the ball-shape of the NPs. From the slope of the line in Figure 3.11 the diameter of the Si NPs can be determined to be 1.6 ± 0.1 nm. This is in good agreement with the TEM data (Figure 3.3), given the short and flexible -$(CH_2)_3NH_2$ chain.

Fluorescence Correlation Spectroscopy was used to determine the mobility of Si NPs. The obtained diffusion times in water (τ_D = 13.5 μs) and in 25% sucrose solution in water (τ_D = 33.8 μs) allowed us to calculate the diffusion coefficient of Si NPs.[66] Their values are $3.13 \cdot 10^{-10}$ m^2s^{-1} in water, and $1.25 \cdot 10^{-10}$ m^2s^{-1} in 25% sucrose solution, respectively. By determining the diffusion time of Si NPs in an exactly determined tiny volume, the size of the NPs could be derived – under assumption of a ball shape – to be 1.4 ± 0.3 nm.[67] This size is in good agreement with the values obtained by TEM, STM, STS and the anisotropy decay measurements.

3.3.5.Bioimaging

Finally, to study the potential for bioimaging of these water-soluble Si NPs, a murine cell line (BV2) has been stained with an aqueous solution of Si-$C_6H_{12}NH_2$ NPs. To examine the exact distribution of these Si NPs in the cells, a second experiment was performed in which cellular nuclei were first stained with commercially available DRAQ5, a far-red fluorescent DNA-staining dye, and subsequently exposed to an aqueous solution of these Si NPs. After incubation and centrifugation, the cells were observed consecutively with 488 and 543 nm excitation light.

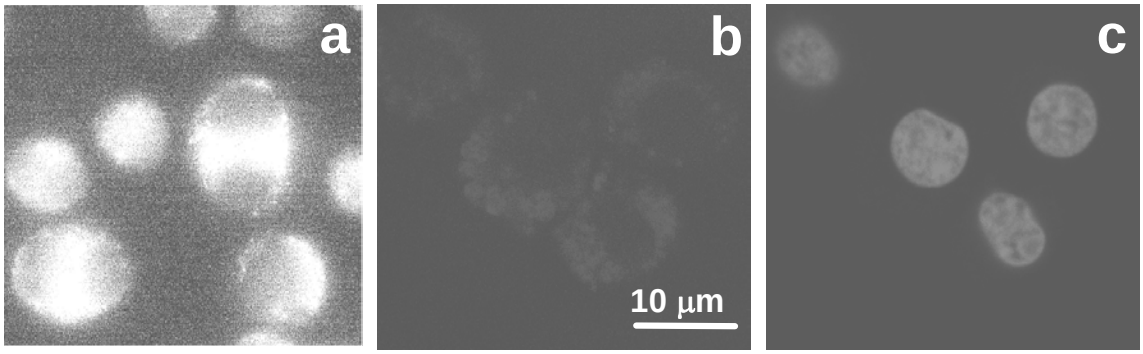

Figure 3.12. a) Epifluorescence image of mitosis of BV2 cells stained with Si NPs under blue light irradiation b) and c) Confocal images of BV2 cells simultaneously stained with Si NPs and DRAQ5. *(See Appendix at the end of the thesis for the color picture)*

From the images displayed in Figure 3.12 it is clear that these Si NPs are readily taken up by BV2 nerve cells, are selectively located in the cytosol and do not tend to relocate to the nuclei. Newly formed daughter cells are also being stained by Si NPs, and in this fashion it is possible to follow multiple generations of cells without further staining. As the cells keep on multiplying without noticable changes in the proliferation rate, this strongly indicates the fact that these Si NPs are not noticeably toxic under these conditions! This opens up a wide range of applications in biological studies.

3.4. Conclusions

In conclusion, amine-terminated Si nanoparticles (NPs) with different linker lengths between the Si core and the NH_2 moiety were successfully synthesized. The obtained NPs have a spherical shape, homogeneous size distribution and a very high mobility in water. Directly measured bandgap by STS is in line with absorption data and is ~4eV. The maximum emission of Si NPs of the same core size and functionalization can be tuned in a controllable fashion from the UV to the blue spectral region, by simply changing the distance between the Si core and the amino group. These amine-terminated Si NPs show a great chemical and photophysical stability over a very wide pH range (1-13.3). Interestingly, the lifetimes of the NPs are shorter at higher pH (at which N lone pair is available to interact with Si core), but the maximum of the emission is unaffected by the pH.

Si NPs are shown to be suitable candidates for *in vivo* labelling. Unchanged proliferation of stained BV2 cells was observed, which suggests a minimal toxicity under the conditions used. Daughter cells were still clearly stained with Si NPs, which makes it possible to follow stained multiple cell generations by simply staining the first generation of cells. Determination of the maximum concentration of Si NPs that can be used for multi-generation staining and detailed studies of the effects on different cell types are currently ongoing in our labs.

3.5. References

(1) Belomoin, G.; Therrien, J.; Smith, A.; Rao, S.; Twesten, R.; Chaieb, S.; Nayfeh, M. H.; Wagner, L.; Mitas, L. *Appl. Phys. Lett.* **2002**, *80*, 841-843.

(2) English, D. S.; Pell, L. E.; Yu, Z. H.; Barbara, P. F.; Korgel, B. A. *Nano Lett.* **2002**, *2*, 681-685.

(3) Schuppler, S.; Friedman, S. L.; Marcus, M. A.; Adler, D. L.; Xie, Y. H.; Ross, F. M.; Chabal, Y. J.; Harris, T. D.; Brus, L. E.; Brown, W. L.; Chaban, E. E.; Szajowski, P. F.; Christman, S. B.;Citrin, P. H. *Phys. Rev. B* **1995**, *52*, 4910-4925.

(4) Rogozhina, E.; Belomoin, G.; Smith, A.; Abuhassan, L.; Barry, N.; Akcakir, O.; Braun, P. V.; Nayfeh, M. H. *Appl. Phys. Lett.* **2001**, *78*, 3711-3713.

(5) Warner, J. H.; Hoshino, A.; Yamamoto, K.; Tilley, R. D. *Angew. Chem. Int. Ed.* **2005**, *44*, 4550-4554.

(6) Zou, J.; Baldwin, R. K.; Pettigrew, K. A.; Kauzlarich, S. M. *Nano Lett.* **2004**, *4*, 1181-1186.

(7) Mayne, A. H.; Bayliss, S. C.; Barr, P.; Tobin, M.; Buckberry, L. D. *Phys. Stat. Solidi A* **2000**, *182*, 505-513.

(8) Kirchner, C.; Liedl, T.; Kudera, S.; Pellegrino, T.; Javier, A. M.; Gaub, H. E.; Stolzle, S.; Fertig, N.; Parak, W. J. *Nano Lett.* **2005**, *5*, 331-338.

(9) Nilsson, J. R. *Acta Protozool.* **2003**, *42*, 19-29.

(10) Zhang, Y. B.; Chen, W.; Zhang, J.; Liu, J.; Chen, G. P.; Pope, C. *J. Nanosci. Nanotech.* **2007**, *7*, 497-503.

(11) Miller, D. A. B. *Nature* **1995**, *378*, 238-238.

(12) Zhang, H. L.; Liu, T. C.; Wang, J. H.; Huang, Z. L.; Zhao, Y. D.; Luo, Q. M. *Chin. J. Analyt. Chem.* **2006**, *34*, 1491-1495.

(13) Zhong, Y.; Kaji, N.; Tokeshi, M.; Baba, Y. *Exp. Rev. Proteom.***2007**, *4*, 565-572.

(14) Heinrich, J. L.; Curtis, C. L.; Credo, G. M.; Kavanagh, K. L.; Sailor, M. J. *Science* **1992**, *255*, 66-68.

(15) Hua, F. J.; Erogbogbo, F.; Swihart, M. T.; Ruckenstein, E. *Langmuir* **2006**, *22*, 4363-4370.

(16) Hua, F. J.; Swihart, M. T.; Ruckenstein, E. *Langmuir* **2005**, *21*, 6054-6062.

(17) Li, X.; He, Y.; Swihart, M. T. *Langmuir* **2004**, *20*, 4720-4727.

(18) Li, X.; He, Y.; Talukdar, S. S.; Swihart, M. T. *Langmuir* **2003**, *19*, 8490-8496.

(19) Holmes, J. D.; Ziegler, K. J.; Doty, R. C.; Pell, L. E.; Johnston, K. P.; Korgel, B. A. *J. Am. Chem. Soc.* **2001**, *123*, 3743-3748.

(20) Liu, Q.; Kauzlarich, S. M. *Mater. Sci. & Eng. B:* **2002**, *B96*, 72-75.

(21) Pettigrew, K. A.; Liu, Q.; Power, P. P.; Kauzlarich, S. M. *Chem. Mater.* **2003**, *15*,

4005-4011.

(22) Zhang, X.; Neiner, D.; Wang, S.; Louie, A. Y.; Kauzlarich, S. M. *Nanotechnology* **2007**, *18*, 095601-095606.

(23) Neiner, D.; Chiu, H. W.; Kauzlarich, S. M. *J. Am. Chem. Soc.* **2006**, *128*, 11016-11017.

(24) Zou, J.; Sanelle, P.; Pettigrew, K. A.; Kauzlarich, S. M. *J. Cluster Sci.* **2006**, *17*, 565-578.

(25) Wilcoxon, J. P.; Samara, G. A. *Appl. Phys. Lett.* **1999**, *74*, 3164-3166.

(26) Wilcoxon, J. P.; Samara, G. A.; Provencio, P. N. *Phys. Rev. B* **1999**, *60*, 2704-2714.

(27) Tilley, R. D.; Warner, J. H.; Yamamoto, K.; Matsui, I.; Fujimori, H. *Chem. Comm.* **2005**, 1833-1835.

(28) Mayeri, D.; Phillips, B. L.; Augustine, M. P.; Kauzlarich, S. M. *Chem. Mater.* **2001**, *13*, 765- 770.

(29) Rogozhina, E. V.; Eckhoff, D. A.; Gratton, E.; Braun, P. V. *J. Mater. Chem.* **2006**, *16*, 1421-1430.

(30) Sato, S.; Swihart, M. T. *Chem. Mater.* **2006**, *18*, 4083-4088.

(31) Saár, A.; Reichman, Y.; Dovrat, M.; Krapf, D.; Jedrzejewski, J.; Balberg, I. *Nano Lett.* **2005**, *5*, 2443-2447.

(32) Veinot, J. G. C. *Chem. Comm.* **2006**, 4160-4168.

(33) (a) photochemical: Sun, Q.-Y. D. S., L. C. P. M.; Van Lagen, B.; Giesbers, M.; Thuene, P. C.; Van Engelenburg, J.; De Wolf, F. A.; Zuilhof, H.; Sudhoelter, E. J. R. *J. Am. Chem. Soc.* **2005**, 127, 2514-2523. ; (b) thermal: Sieval, A. B.; Vleeming, V.; Zuilhof, H.; Sudholter, E. J. R. *Langmuir* **1999**, 15, 8288-8291.

(34) (a) Stewart, M. P. R., E. G.; Geders, T. W.; Allen, M. J.; Choi, H. C.; Buriak, J. M. *Phys. Stat. Sol. A: Appl. Research* **2000**, 182, 109-115.; (b) Buriak, J. M.; Stewart, M. P.; Geders, T. W.; Allen, M. J.; Choi, H. C.; Smith, J.; Raftery, D.; Canham, L. T. *J. Am. Chem. Soc.* **1999**, 121, 11491-11502. (c) Buriak, J. M. *Adv. Mat*. **1999**, 11, 265-267.

(35) Scheres, L.; Arafat, A.; Zuilhof, H. *Langmuir* **2007**, *23*, 8343-8346.

(36) Sieval, A. B.; Demirel, A. L.; Nissink, J. W. M.; Linford, M. R.; van der Maas, J. H.; de Jeu, W. H.; Zuilhof, H.; Sudhoelter, E. J. R. *Langmuir* **1998**, *14*, 1759-1768.

(37) Buriak, J. M. *Chem. Rev.* **2002**, *102*, 1271-1308.

(38) de Smet, L. C. P. M.; Pukin, A. V.; Sun, Q. Y.; Eves, B. J.; Lopinski, G. P.; Visser, G. M.; Zuilhof, H.; Sudholter, E. J. R. *Appl. Surface Sci.* **2005**, *252*, 24-30.

(39) Sun, Q. Y.; de Smet, L. C. P. M.; van Lagen, B.; Giesbers, M.; Thune, P. C.; van Engelenburg, J.; de Wolf, F. A.; Zuilhof, H.; Sudholter, E. J. R. *J. Am. Chem. Soc.* **2005**, *127*, 2514-2523.

(40) Sun, Q.-Y.; de Smet, L. C. P. M.; van Lagen, B.; Wright, A.; Zuilhof, H.; Sudhoelter, E. J. R. *Angew. Chem. Int. Ed.* **2004**, *43*, 1352-1355.

(41) Rosso-Vasic, M.; Spruijt, E.; van Lagen, B.; de Cola, L.; Zuilhof, H. *Small*, **2008**, 10. 1835-1841..

(42) Nelles, J.; Sendor, D.; Ebbers, A.; Petrat, F. M.; Wiggers, H.; Schulz, C.; Simon, U. *Colloid Polym. Sci.***2007**, *285*, 729-736.

(43) Canham, L. T. *Appl. Phys. Lett.* **1990**, *57*, 1046-1048.

(44) Matsumoto, K.; Inada, M.; Umezu, I.; Sugimura, A. *Japan.J. Appl. Phys.* **2005**, *44*, 8742-8746.

(45) Bisero, D.; Comi, F.; Nobili, C.; Tonini, R.; Ottaviani, G.; Mazzoleni, C.; Pavesi, L. *Appl. Phys.Lett.* **1995**, *67*, 3447-3449.

(46) Godefroo, S.; Hayne, M.; Jivanescu, M.; Stesmans, A.; Zacharias, M.; Lebedev, O. I.; Van Tendeloo, G.; Moshchalkov, V. V. *Nature Nanotech.* **2008**, *3*, 174-178.

(47) Landes, C.; Burda, C.; Braun, M.; El-Sayed, M. A. *J. Phys. Chem. B* **2001**, *105*, 2981-2986.

(48) Landes, C. F.; Braun, M.; El-Sayed, M. A. *J. Phys. Chem. B* **2001**, *105*, 10554-10558.

(49) Bruchez, M.; Moronne, M.; Gin, P.; Weiss, S.; Alivisatos, A. P. *Science* **1998**, *281*, 2013-2016.

(50) Michalet, X.; Pinaud, F. F.; Bentolila, L. A.; Tsay, J. M.; Doose, S.; Li, J. J.; Sundaresan, G.; Wu, A. M.; Gambhir, S. S.; Weiss, S. *Science* **2005**, *307*, 538-544.

(51) Pinaud, F.; Michalet, X.; Bentolila, L. A.; Tsay, J. M.; Doose, S.; Li, J. J.; Iyer, G.; Weiss, S. *Biomatter.* **2006**, *27*, 1679-1687.

(52) Alivisatos, P. *Nature Biotech.* **2004**, *22*, 47-52.

(53) Michalet, X.; Pinaud, F.; Lacoste, T. D.; Dahan, M.; Bruchez, M. P.; Alivisatos, A. P.; Weiss, S. *Single Mol.,* **2001**, *2*, 261-276.

(54) Gerion, D.; Pinaud, F.; Williams, S. C.; Parak, W. J.; Zanchet, D.; Weiss, S.; Alivisatos, A. P. *J. Phys. Chem. B* **2001**, *105*, 8861-8871.

(55) Dabbousi, B. O.; RodriguezViejo, J.; Mikulec, F. V.; Heine, J. R.; Mattoussi, H.; Ober, R.; Jensen, K. F.; Bawendi, M. G. *J. Phys. Chem. B* **1997**, *101*, 9463-9475.

(56) Li, Z. F.; Ruckenstein, E. *Nano Lett.* **2004**, *4*, 1463-1467.

(57) Jdira, L.; Liljeroth, P.; Stoffels, E.; Vanmaekelbergh, D.; Speller, S. *Phys. Rev. B* **2006**, *73*, 115305-115311.

(58) Williams, A. T. R.; Winfield, S. A.; Miller, J. N. *Analyst* **1983**, *108*, 1067-71.

(59) Liljeroth, P.; van Emmichoven, P. A. Z.; Hickey, S. G.; Weller, H.; Grandidier, B.; Allan, G.; Vanmaekelbergh, D. *Phys., Rev. Lett.* **2005**, *95*, 086801-086807.

(60) Wang, X.; Zhang, R. Q.; Niehaus, T. A.; Frauenheim, T. *J. Phys. Chem. C* **2007**,

111, 2394-2400.

(61) Zhou, Z. Y.; Brus, L.; Friesner, R. *Nano Lett.* **2003**, *3*, 163-167.

(62) Franceschetti, A.; Zunger, A. *Physical Review B* **2000**, *62*, 2614-2623.

(63) Wolkin, M. V.; Jorne, J.; Fauchet, P. M.; Allan, G.; Delerue, C. *Phys. Rev.Lett.* **1999**, *82*, 197-200.

(64) Lakowicz, J. R. Principles of Fluorescence Spectroscopy; 3rd ed.; Springer, 2006.

(65) MacLaren, D. A.; Curson, N. J.; Atkinson, P.; Allison, W. *Surface Sci.* **2001**, *490*, 285-295.

(66) Vukojevic, V.; Pramanik, A.; Yakovleva, T.; Rigler, R.; Terenius, L.; Bakalkin, G. *Cell. Mol. Life Sci.* **2005**, *62*, 535-550.

(67) Zhang, P. D.; Li, L. A.; Dong, C. Q.; Qian, H. F.; Ren, J. C. *Anal. Chim. Acta* **2005**, *546*, 46-51.

Chapter 4

Efficient Energy Transfer between Silicon Nanoparticles and a Ru-polypyridine complex

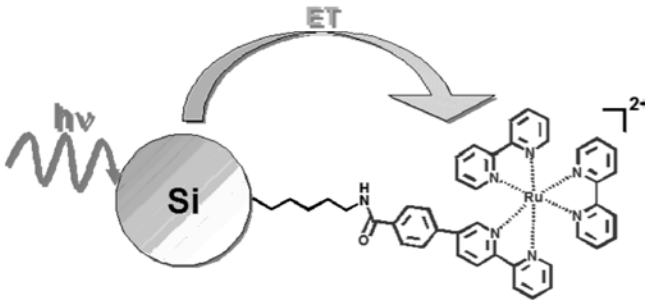

Part of this chapter is submitted for publication as:

"Efficient Energy Transfer between Silicon Nanoparticles and a Ru-polypyridine complex ", Milena Rosso-Vasic, Luisa De Cola and Han Zuilhof

Abstract – Blue-emitting amine-terminated Si nanoparticles (NPs; size: 1.57 ± 0.24 nm) are functionalized with a $Ru(bpy)_2(spb)^{2+}$ complex. The distance between the dye and Si core is controlled by different alkyl chain lengths ($-C_3H_6$, $-C_6H_{12}$ and $-C_{11}H_{22}$), and the thus formed Si NPs are two-chromophore systems that exhibit dual-emission in two separate regions: blue (~450 nm; from Si core) and red (~650 nm; from Ru dye). By measuring the Si/Ru ratio, the extinction coefficient of amino-terminated Si NPs was experimentally determined for the first time ($2.6 \cdot 10^5$ M^{-1} cm^{-1}). Energy transfer from Si NPs to acceptor molecules ($Ru(bpy)_2(spb)^{2+}$) is observed by steady-state and time-resolved fluorescence, and its distance-dependent efficiency is shown to be up to 55 % in the case of a short alkyl spacer ($-C_3H_6$). Energy transfer rates are very high for all examined cases and are in the 0.2 - $2.3 \cdot 10^9$ s^{-1} range.

4.1. Introduction

The discovery of porous silicon luminescence almost two decades ago[1] opened up a venue for possible integration of optoelectronics with traditional silicon technology. The interest for turning silicon from a purely electronic into an optoelectronic material increased even more with the synthesis of the first silicon nanoparticles (Si NPs).[2] Due to the quantum confinement effect, Si NPs have a broadly tunable size-dependent emission[3] from the UV to the IR spectral regions. The combined stability against photobleaching,[4,5] high brightness,[6] gram-scale synthesis[7] and high extinction coefficients[7] make them attractive alternatives for many organic chromophores. Furthermore, Si NPs may be highly interesting for photovoltaic applications, not in the least due to their capability for multiphoton generation.[8] In addition, Si has a very low inherent toxicity,[9] which is a great advantage in comparison to most semiconductor quantum dots (CdSe, CdS, PbS, etc.)[10-12] for various applications in biological systems.

Besides requirements for the size of Si NPs, a full control over their surface properties is particularly important to achieve desirable emission characteristics, like narrow and stable emission profiles.[13] Obtaining desirable properties requires improved methods for the production of well-defined Si NPs. Stable luminescent Si NPs of 1-8 nm diameter have been produced using a variety of techniques such as: ultrasonic dispersion of electrochemically etched silicon,[14] laser-driven pyrolysis of silane,[15-18] synthesis in supercritical fluids[3,19] and wet-chemistry techniques. This last class includes the reduction of Zintl salts in inert organic solvents[20-24] or in micelles using SiX_4 (X = Cl, Br or I) as a silicon source.[4,25-27] The obtained Si NPs are halogen- or hydrogen-terminated, and both cases are very prone to oxidation. These NPs can be further stabilized by reaction with alkyl-lithium salts[21] or terminal alkenes[28] to provide Si-C linkages. Such passivation methods are similar to those developed for planar[29] or porous[30] silicon, for which the attachment can be initiated thermally,[31,32] or photochemically with UV[33] or visible light.[29,34-36] Hydrosilylation reactions on Si NPs can also be performed by using platinum-based[4] or triphenylcarbenium-based catalysts.[37] A good surface passivation considerably increases the stability of Si NPs in a wide range of solvents and pH values and at sterilization temperatures.[38]

While the experimental study of the photophysics of alkylated Si nanoparticles is still in its infancy, it has been reported that the lifetime of the electronically excited state is in the order of nanoseconds.[3,7] Although such a lifetime makes the NPs amenable to a wide variety of energy transfer studies, no study has been undertaken concerning the interaction of electronically excited Si NPs and any energy acceptors.[39] Recently, the first report on Förster resonance energy transfer (FRET) from poly(9-vinyl carbazole) to polydisperse Si NPs (8 -

25 nm) in their composite films has been published, with an efficiency in this polydisperse material of up to 42%.[40]

Unlike Si NPs, complexes of transition metals with extended π-systems, such as pyridine and bipyridine have been studied in detail, as their long-lived excited states with tunable emission wavelengths enable their application in many light sources and detectors.[41] Those studies have led to detailed and well-understood descriptions of the photophysics of such complexes,[42] which makes them ideal chromophores for interaction studies.[43] For instance, a study of mixtures of various Ru-polypyridine complexes and CdSe quantum dots shows that photoinduced charge transfer occurs between these two photoactive species.[44] In the particular case of Si NPs, the possibility of a well-defined surface functionalization[4,38] allows the covalent coupling of Ru-containing chromophores. The defined linker lengths and the high monodispersity of Si NPs permits detailed photophysical studies.

This chapter describes the synthesis of $Ru(bpy)_2(spb)^{2+}$-labeled Si NPs with three different alkyl linkers between the Ru dye and the Si core (C_3H_6, C_6H_{12} and $C_{11}H_{22;}$ see Figure 4.1), starting from amine-terminated Si NPs with 3 different alkyl-chain lengths and the red-emitting $[Ru(bpy)_2(spb)]Cl_2$ complex (**1**). Subsequently, the energy transfer between the Si core and the Ru complex is investigated, specifically the distance dependence thereof, using both steady-state and time-resolved optical absorption and emission studies. Finally, for the first time the extinction coefficient of amine-terminated Si NPs is determined from a combination of absorption measurements and inductively coupled plasma-mass spectrometry (ICP-MS).

4.2. Experimental Section

All chemicals used were purchased from Sigma-Aldrich and employed without further purification unless specified differently. $[Ru(bpy)_2(spb)]Cl_2$ (bpy = 2, 2'-bipyridine; spb = 4-(p-N-succinimidylcarboxyphenyl)-2,2'-bipyridine) was synthesized from $RuCl_2$ and the respective ligands (details to be published elsewhere).[45]

4.2.1. Functionalization of amine-terminated Si NPs with $Ru(bpy)_2(spb)^{2+}$

Amine-terminated Si NPs with 3 different chain lengths ($–C_3H_6NH_2$, $-C_6H_{12}NH_2$ and $–C_{11}H_{22}NH_2$) were synthesized in reverse micelles and characterized in detail with respect to their photophysics.[38] After the purification of Si NPs, the $Ru(bpy)_2(spb)^{2+}$-complex was attached to peripheral amine groups, using standard amine - N-hydroxysuccinimidyl ester coupling reaction conditions (Figure 4.1).[46]

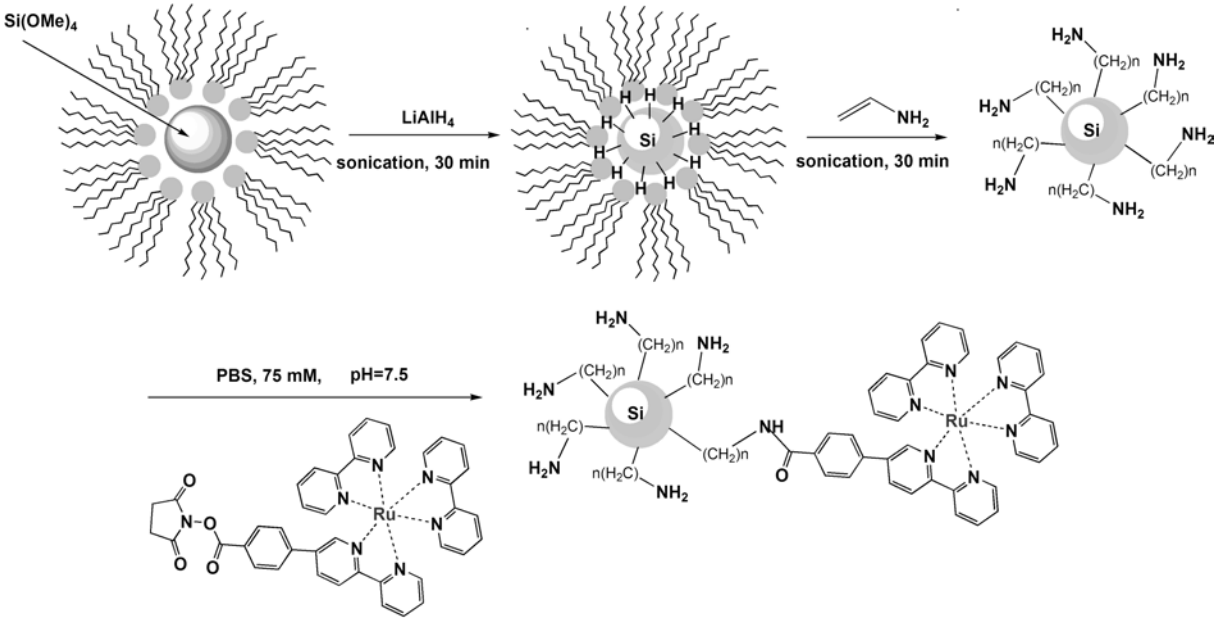

Figure 4.1. Functionalization of amine-terminated Si with $Ru(bpy)_2(spb)$.

10 mM Phosphate buffer was added to 1 ml of amino-terminated nanoparticle solution (2 mg/ml) until the pH reached 7.5, followed by addition of 2 ml of $3 \cdot 10^{-3}$ M of $Ru(bpy)_2(spb)^{2+}$ in water. The mixture was stirred for 2 h at r.t. and unreacted material was removed by dialysis (MWCO 7000, SERVA, Membra-Cel dialysis tubing, diameter 22 mm) until the solvent did not contained any $Ru(bpy)_2(spb)^{2+}$ (checked by fluorescence emission). Dialysis was typically repeated 6-8 times in 10 h cycles. Dialyzed Ru-functionalized Si NPs were filtered through membrane syringe filters (Millex, Millipore, PVDF, 0.45 μm) and used for further measurements.

4.2.2. Optical measurements.

All measurements have been performed at standard pressure and room temperature. Electronic absorption spectra were recorded in a quartz cuvette (1 cm, Hellma), using a Cary 1 UV-Vis double-beam spectrophotometer, and were corrected for the solvent absorption, using the 200 - 500 nm scan range and a 600 nm/min scan rate. Steady-state and time-resolved measurements were performed on a Time-Correlating Single Photon Counting F900 spectrometer (Edinburgh Instruments). All steady-state spectra are corrected for the wavelength-dependent sensitivity of both the detector and the source by recording reference data simultaneously. Additionally, emission spectra have been corrected for Raman scattering using the solvent emission spectrum. Time-resolved fluorescence measurements were performed with the exact same solution as used for steady-state spectra (absorption was always adjusted to be ≤ 0.5). A laser (λ_{exc} = 372 nm; IRF = 30 ps) was used as an

excitation source, and photons were collected up to 100 ns (4096 channels) until a maximum of 10^4 counts.

4.2.3. ICP-MS measurements

Inductively Coupled Plasma-Mass Spectrometry (ICP-MS) measurements were performed on Perkin Elmer Elan 6100 DRC and Optima 4300 DV spectrometers. 1 – 1.5 mL of an aqueous solution of the Si NPs was weighted into a clean polyethylene tube. Subsequently a small amount of 0.1 M NaOH or HCl was added, after which the samples were further diluted to a known volume. Then the amounts of Si and Ru were determined using ICP-MS. During ICP analysis, the solution was fed through a nebulizer. This produces an aerosol, which was led into ionizing argon plasma that produced free ions, which were introduced into a mass spectrometer. The analyses were performed in duplicate. The maximum inaccuracy in the amounts of Si and Ru is estimated to be < 5%.

4.3. Results and Discussion

4.3.1. Optical properties of $[Ru(bpy)_2(spb)]Cl_2$

The absorption spectrum of $[Ru(bpy)_2(spb)]Cl_2$ in water (see Figure 4.2, solid line a) exhibits the characteristic bands found in ruthenium complexes (e.g. $Ru(bpy)_3^{2+}$).[41,47] The intense band at 301 nm encompasses the ligand-centered $\pi \rightarrow \pi^*$ transition and the lowest-energy absorption band at 450 nm is attributed to a d(Ru*)* $\rightarrow \pi^*$(bipyridine) metal-to-ligand charge transfer (MLCT) transition.[47] The emission spectrum of complex **1** (Figure 4.2, dotted line b) displays a broad and structureless emission band centered around 625 nm that is attributed to ^{3}MLCT transitions involving the bipyridine ligands.[42]

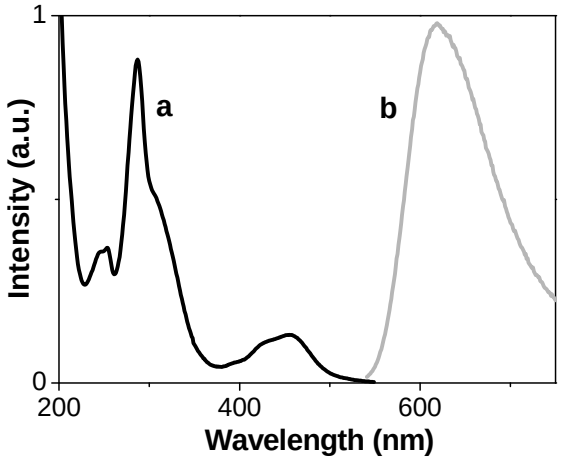

Figure 4.2. a) Absorption and b) Emission of $[Ru(bpy)_2(spb)]Cl_2$ in water (λ_{exc}=450 nm).

4.3.2. UV-Vis absorption spectra of $Ru(bpy)_2(spb)$-functionalized Si NPs

$Ru(bpy)_2(spb)^{2+}$-functionalized Si NPs exhibit an additive absorption of both constituents: the Si NPs[38] and the attached Ru complex (Figure 4.3 - 4.5). There are no signs of any additional absorption bands formed, ruling out the possibility of any strong ground-state interaction. This allows a straight-forward determination of the extinction coefficient of amine-terminated Si NPs, which to the best of our knowledge has not been reported up to now.

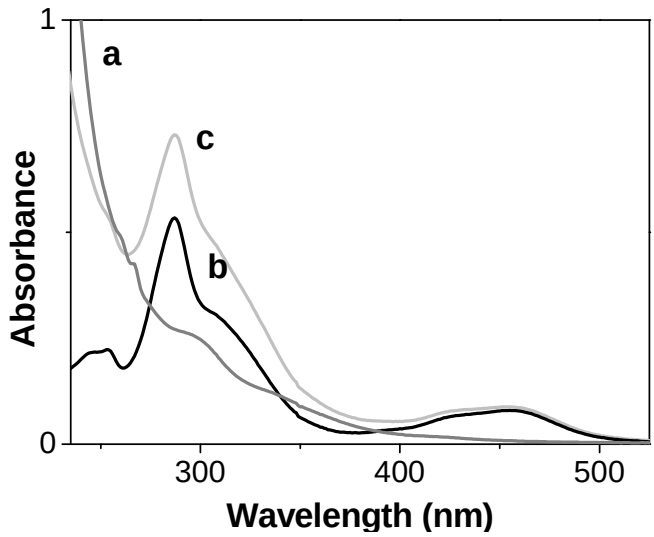

Figure 4.3. The absorption spectra of a) Si-$C_3H_6NH_2$ NPs; b) $Ru(bpy)_2(spb)^{2+}$ and c) $Ru(bpy)_2(spb)^{2+}$-functionalized Si NPs in water.

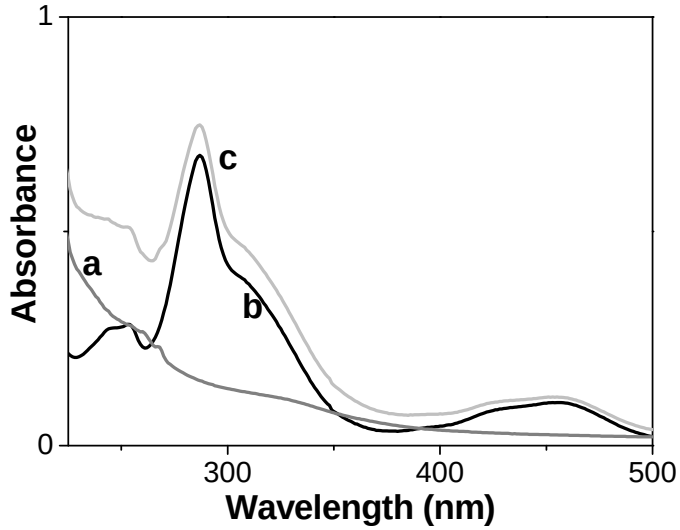

Figure 4.4. The absorption spectra of a) Si-$C_6H_{12}NH_2$ NPs; b) $Ru(bpy)_2(spb)^{2+}$ and c) $Ru(bpy)_2(spb)^{2+}$-functionalized Si-$C_6H_{12}NH_2$ NPs in water.

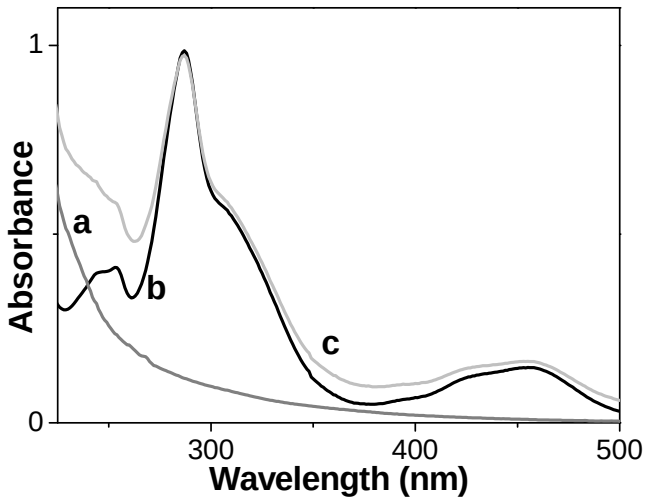

Figure 4.5. The absorption spectra of a) Si-$C_{11}H_{22}NH_2$ NPs; b) $Ru(bpy)_2(spb)^{2+}$ and c) $Ru(bpy)_2(spb)^{2+}$-functionalized Si-$C_{11}H_{22}NH_2$ NPs in water.

4.3.3. Determination of the extinction coefficient of amine-terminated Si NPs

The extinction coefficient is calculated by combining ICP-MS, TEM[38] and UV-Vis spectroscopy data.[48] The Si/Ru mass ratio of thus functionalized Ru-dye containing Si NPs was determined by ICP-MS measurements to be 7.5 : 1. From the Si NPs size distribution (1.57 ± 0.24 nm)[38] the average number of Si atoms per NP is estimated to be 115. Using this estimate, it was thus determined that there are on average 4 molecules of Ru-dye per Si-$C_3H_6NH_2$ NP. Given the extinction coefficient ε_{max} for $Ru(bpy)_2(spb)^{2+}$in water at 450 nm ($1.24 \cdot 10^4$ $M^{-1}cm^{-1}$), the extinction coefficient ε_{max} of amino-terminated Si NPs at 260 nm could be determined to be 2.6 ($\pm$ 1.0)$\cdot 10^5$ $M^{-1}cm^{-1}$.

This value is 10 times higher then determined for alkyl-terminated Si NPs of the same size[7] and 5 times higher than values reported for CdS and CdSe NPs of this size.[49] It has been shown that the presence of the capping amino group on small (< 2 nm) Si NPs has a large effect on the excitation,[38] e.g by narrowing the HOMO-LUMO gap as expected from theory,[50] and/or by the adventitious introduction of traces of oxygen. Besides this effect, the much higher extinction coefficient observed in this study indicates that the transition dipole moment is also noticeably influenced by this substitution.

4.3.4. Excitation spectra of $Ru(bpy)_2(spb)$-functionalized Si NPs

The comparison of Ru excitation spectra (λ_{em} = 630 nm) with and without Si NPs, show an additional proof that Ru-dye is attached to the surface of Si NPs. For all three Si NPs types, extra bands appear in excitation spectra of Ru-functionalized Si NPs at ~310 nm (Figure 4.6).

These bands have a different intensity for the different Si NP types, as the amount of Ru per NP is not the same in each case.

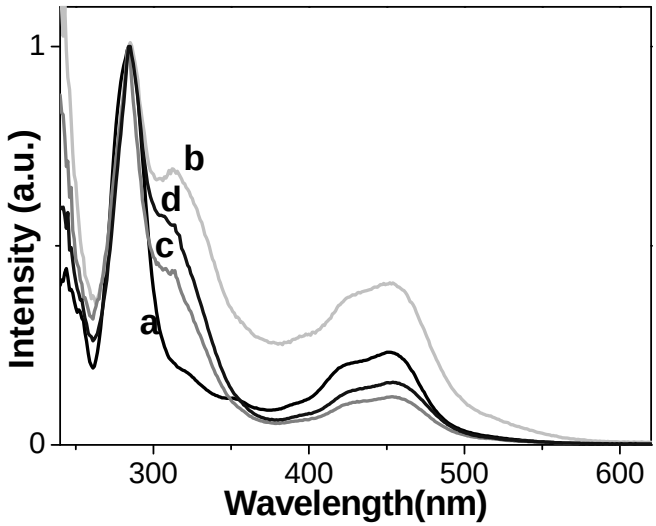

Figure 4.6. Excitation spectra at λ_{em} = 630 nm of a) $Ru(bpy)_2(spb)^{2+}$; $Ru(bpy)_2(spb)^{2+}$-functionalized b) Si-$C_3H_6NH_2$; c) Si-$C_6H_{12}NH_2$ and d) Si-$C_{11}H_{22}NH_2$ NPs in water.

4.3.5. Determination of the energy transfer efficiencies by steady-state and time-resolved fluorescence measurements

The emission spectra of $Ru(bpy)_2(spb)^{2+}$-functionalized Si NPs consist of two distinct peaks: one in the blue part (centered ~460 nm) and one in the red part of the optical spectrum (~630 nm). It accurately represents a sum of both Si NPs and Ru complex emissions. As can be clearly seen, the relative intensity of the Si NP emission and the emission of the Ru complex varies significantly over this series.

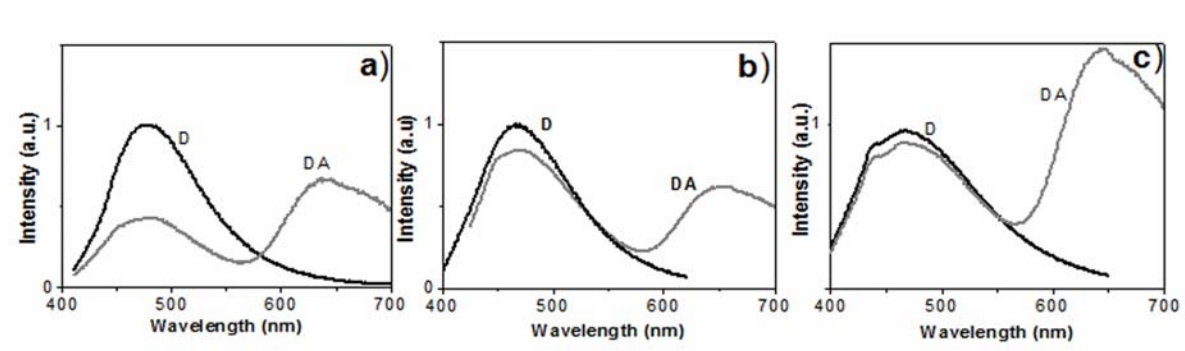

Figure 4.7. Emission spectra of Si-$C_3H_6NH_2$ (a), Si-$C_6H_{12}NH_2$ (b) and Si-$C_{11}H_{22}NH_2$ (c) NPs without Ru complex (curve D) and with Ru complex attached (curve DA) (λ_{exc} = 380 nm). Emission maxima of Si NPs are normalized to 1.

[Note: The concentration of NPs was near-identical in curves D and DA per graph, although different concentrations were used for (a), (b) and (c).]

The emission of the amine-terminated Si NPs around 460 nm is quenched to a greater degree when the distance between the Si NP and the Ru dye is shorter (compare Fig 4.7a with 4.7b and 4.7c). A detailed comparison of the emission intensities of identical amounts of Si NPs with and without attached $Ru(bpy)_2(spb)^{2+}$ provides the first indication that energy transfer occurs. Emission intensities are compared by using 3 different excitation wavelengths: 360, 380 and 400 nm (see Figure 4.7 (λ_{exc}= 380 nm)).

The energy transfer efficiency E_T^{em} is given by the formula in Equation 4.1:

$$E_T^{em} = 1 - \frac{F_{AD}}{F_D} \qquad \text{Eq. [4.1]}$$

where F_D and F_{DA} designate the integrated emission intensities of donor alone and in the presence of acceptor.[51] When $Ru(bpy)_2(spb)^{2+}$ (acceptor, A) is attached to Si-$C_3H_6NH_2$ NPs (donor, D), the energy transfer efficiency is the highest: 0.55 ± 0.03. In the case of $–C_6H_{12}$ and $–C_{11}H_{22}$ spacers, E_T^{em} drops significantly, to 0.18 ± 0.02 and 0.08 ± 0.02, respectively. In addition, it was shown that the difference in the emission intensities of Si NPs with and without Ru-dye attached was not dependent on the excitation wavelengths (all data identical within 2 - 3%). Quenching of the emission of the Si NPs by the Ru dye is expected to yield an increased emission from the Ru dye. This is indeed confirmed by a comparison between Figures 4.7.a and 4.7.b: with a longer Si – Ru distance, the energy transfer towards Ru is reduced, and the emission of the Ru dye is concomitantly reduced. The trend of a further reduced quenching of the Si NP emission is observed for the C_{11} spacer, however, the emission of the Ru-complex is in that case higher as well. This is due to the fact that Si-$C_{11}H_{22}NH_2$ NPs absorb less at higher wavelengths,[38] which yields relatively seen more direct excitation of the Ru dye, and thus more Ru emission as well. This applies for all excitation wavelengths used (360, 380 and 400 nm). From the absorption spectra it can furthermore be concluded that this is not due to different amounts of Ru being attached to the NPs (see Figure 4.3 – 4.5).

In order to confirm that the decrease of the emission intensity is not related to the smaller number of unsubstituted amine groups present on the Si NPs (due to replacement of some NH_2 moieties by amide functionalities),[38] analogous emission measurements were performed on Si NPs in which amine-terminated Si NPs have been functionalized with the NHS-ester of benzoic acid instead of with $[Ru(bpy)_2(spb)]Cl_2$. In the case of benzoic amide functionalization the emission of Si NPs did not drop. This confirms that the decrease of Si NPs emission intensity does not occur due to the reaction of the amine groups at the

periphery of the NPs with N-succinimidyl ester, but due to the energy transfer from the photo-excited Si core to the Ru complex.

The occurrence of the energy transfer process, has further been confirmed by comparing the lifetimes of the amine-terminated Si NPs with and without attached $Ru(bpy)_2(spb)^{2+}$ (Figure 4.8). The lifetimes are compared at constant pH = 7.5, as the pH has a strong influence on the lifetime of amine-terminated Si NPs.[38]

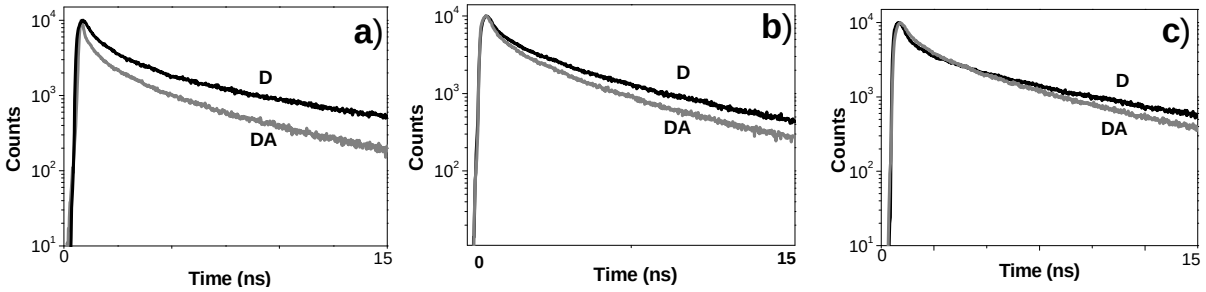

Figure 4.8. Fluorescence lifetimes of a) Si-$C_3H_6NH_2$ NPs; b) Si-$C_6H_{12}NH_2$ NPs and c) Si-$C_{11}H_{22}NH_2$ NPs without (curve D) and with attached Ru-complex (curve DA); (λ_{exc} = 372 nm; λ_{em} = 450 nm).

All the fluorescence decays were fitted as three-exponential and total lifetimes are shown in the Table 4.1, together with the lifetime-derived efficiency and rate of energy transfer (vide infra). The decay trace of each amine-terminated Si NPs type consists of ~0.1, ~0.9 and ~4.5 ns components in similar ratios (~1 : 3 : 6), giving an overall total lifetime of ~3 to 3.5 ns. Upon the attachment of the Ru-containing chromophore, the energy donor (Si NPs) lifetimes become shorter, confirming again the occurrence of the energy transfer. With the -C_3H_6 alkyl-linkers in between the Si core and the Ru-complex, the total lifetime becomes shorter by almost 2 ns. The shortest component is unchanged, while the 0.9 and 4.7 ns components drop to roughly half of the initial values (0.5 and 2.7 ns, respectively). Not only the lifetime, but also the relative abundance of these components change significantly, and the 0.5 ns component becomes dominant (ratio of three components changes from ~ 1 : 3 : 6 to 1 : 5 : 4). Upon increasing the chain length between the two photo-active species, the influence on the energy donor (Si NPs) lifetime decreases. While the 0.9 ns component in the case of a –C_6H_{12} chain still gets shorter (0.6 ns) with changing the ratios of three components in the same manner, from 1: 3 : 6 to 1 : 4 : 5, only minor changes with respect to the NH_2-terminated Si NPs are observed for the Ru-linked NPs with the -$C_{11}H_{22}$ spacer.

Table 4.1. Lifetimes of Si NPs with and without Ru-complex attached, calculated $E_T^{lifetime}$ and k_{ET}.

	τ_D^{total} (ns)	τ_{DA}^{total} (ns)	$E_T^{lifetime}$	k_{ET} ($\cdot 10^9$ s^{-1})
Si-$C_3H_6NH_2$ NPs	3.1	1.3	0.58	2.3
Si-$C_6H_{12}NH_2$ NPs	3.4	2.6	0.23	0.9
Si-$C_{11}H_{22}NH_2$ NPs	3.3	3.0	0.09	0.2

The energy transfer efficiencies can also be calculated from equation 4.2,[51] using lifetimes rather than overall intensities, where τ_{AD} and τ_D are the lifetimes of Si NPs with and without attached Ru-complex.

$$E_T^{lifetime} = 1 - \frac{\tau_{AD}}{\tau_D} \qquad \text{Eq. [4.2]}$$

For Ru-linked Si NPs with $–C_3H_6$, $–C_6H_{12}$ and $–C_{11}H_{22}$ spacers the lifetime-derived energy transfer efficiencies are 0.58, 0.23 and 0.09, respectively, which agrees very well and within experimental error with the intensity-derived efficiencies (0.55, 0.19 and 0.08, respectively). In order to exclude the possibility that energy transfer can occur when the Ru-complex is not actually attached to Si NPs, the lifetimes of amine-terminated Si NPs (with $–C_3H_6$ chain) were obtained when they are mixed with commercially available tris(2,2′-bipyridyl)dichlororuthenium(II),$[Ru(bpy)_3]Cl_2$ that is homogeneously dissolved. When the same concentration of Si NPs and $[Ru(bpy)_3]Cl_2$ was used, no change in the lifetime of the Si NPs was observed. In fact, the decay profile of photoexcited Si NPs did not change even upon a the addition of a 10× bigger amount of $Ru(bpy)_3^{2+}$. As a result it is safe to say that at the concentrations used only covalently attached Ru dyes are involved in accepting energy from the Si NP cores, and contribute to the reduced emission thereof.

Assuming a Förster-type mechanism of energy transfer,[52] and fixed distances between the Si NP core and the Ru center, the energy transfer rate, $k_{ET,}$ can be calculated from the standard Forster equations:[52]

$$k_{ET} = \frac{1}{\tau_D} \cdot \left(\frac{R_0}{R}\right)^6 \quad \text{and} \quad R_o^{\,6} = \frac{9000\,\kappa^2 \ln 10}{128\,\pi^6 n^4 N_{AV}} \cdot \Phi_D \int_0^\infty E_d(\nu)\varepsilon_a(\nu)\frac{d\nu}{\nu^4} \qquad \text{Eq. [4.3]}$$

in which τ_D = lifetime of the donor in the absence of the acceptor, R = separation distance between the donor and acceptor, R_0 = Förster critical distance, κ^2 = orientation factor that is assigned the value 2/3, N_{AV} = Avogadro's number, Φ_D = quantum yield of the donor, $E_d(\nu)$ =

normalized donor emission spectrum and $\varepsilon_a(\nu)$ = molar extinction coefficient of the acceptor.[51] As some of these quantities have appreciable uncertainties, only a fairly rough estimate of R_0 can be calculated. The overlap integral is calculated from the absorption and emission spectra given in Figures 4.2 and 4.7, with the assumption that there are only two fluorophores. In principle, the integral should be over the single particle emission,[53] and recent theoretical work has shown that the ensemble spectral overlap is determined by the inhomogeneous line broadening dictated by sample polydispersity.[54] In this case, Si NPs are rather homogeneous, but still the dispersity is ~15%, which thus adds to the uncertainty of the obtained energy transfer rates. As the quantum yield of emission of thus prepared amino-terminated Si NPs is ~0.12,[38] the calculated Förster distance R_0 is 28 ± 5 Å. Based on this value, and using the distances between the center of the NP and the Ru atom for R, the calculated energy transfer rates for $Ru(bpy)_2(spb)^{2+}$- functionalized Si-$C_3H_6NH_2$ NPs, Si-$C_6H_{12}NH_2$ and Si-$C_{11}H_{22}NH_2$ NPs are estimated to be $2.3\cdot10^9$, $0.9\cdot10^9$ and $0.2\cdot10^9$ s^{-1}, respectively.

Direct time-resolved observations suggest that the rate dependence is less steep: τ_D decreases from 3.0 to 1.3 ns, i.e. roughly 4-5 times less than expected based on the above Förster analysis. We attribute this to the actual distance between the two chromophores, which will be shorter than calculated, especially in the case of longer and flexible chains (-C_6H_{12} and -$C_{11}H_{22}$). It has been suggested that, depending on the nature of constituents, the distance dependence may vary between zeroth and negative fourth power.[55]

Our data clearly deviate from low-distance dependencies (exponent 0 or -1), and could be in line with Förster theory, but more work will be needed with stiffer spacers to more clearly indicate this relation in detail.

4.4. Conclusions

Silicon nanoparticles functionalized with red-emitting $Ru(bpy)_2(spb)^{2+}$ were successfully synthesized. This allowed the first experimental determination of the extinction coefficient of amine-terminated Si NPs ($2.6\cdot10^5$ M^{-1} cm^{-1}). This value is ~10 times higher than measured for alkyl-terminated Si NPs, indicating that transition dipole moment is significantly changed by the effects of attaching polar amine alkenes. Steady-state and time-resolved fluorescence measurements reveal that small (1.57 nm) Si NPs are excellent energy donors with $Ru(bpy)_2(spb)^{2+}$ acceptor molecules. A simple tuning of the distance between them can give desirable energy transfer efficiency. Energy transfer rates are very high for all examined cases (in the 0.2 – $2.3\cdot10^9$ s^{-1} range) and follow an approximate Förster energy transfer distance dependence.

4.5. References

(1) Canham, L. T.; Leong, W. Y.; Beale, M. I. J.; Cox, T. I.; Taylor, L. *Appl. Phys. Lett.* **1992**, *61*, 2563-2565.

(2) Heath, J. R. *Science* **1992**, *258*, 1131-1133.

(3) English, D. S.; Pell, L. E.; Yu, Z. H.; Barbara, P. F.; Korgel, B. A. *Nano Lett.* **2002**, *2*, 681-685.

(4) Warner, J. H.; Hoshino, A.; Yamamoto, K.; Tilley, R. D. *Angew. Chem. Int. Ed.* **2005**, *44*, 4550- 4554.

(5) Li, Z. F.; Ruckenstein, E. *Nano Lett.* **2004**, *4*, 1463-1467.

(6) Rogozhina, E.; Belomoin, G.; Smith, A.; Abuhassan, L.; Barry, N.; Akcakir, O.; Braun, P. V.; Nayfeh, M. H. *Appl. Phys. Lett.* **2001**, *78*, 3711-3713.

(7) Rosso-Vasic, M.; Spruijt, E.; van Lagen, B.; de Cola, L.; Zuilhof, H. *Small* **2008**, 10, 1835-1841.

(8) Timmerman, D.; Izeddin, I.; Stallinga, P.; Yassievich, N.; Gregorkiewic, T. *Nature Photonics* **2008**, *2,* 105-109.

(9) Mayne, A. H.; Bayliss, S. C.; Barr, P.; Tobin, M.; Buckberry, L. D. *Phys. Stat. Solidi A* **2000**,*182*, 505-513.

(10) Kirchner, C.; Liedl, T.; Kudera, S.; Pellegrino, T.; Javier, A. M.; Gaub, H. E.; Stolzle, S.; Fertig,N.; Parak, W. J. *Nano Lett.* **2005**, *5*, 331-338.

(11) Nilsson, J. R. *Acta Protozool.* **2003**, *42*, 19-29.

(12) Gerion, D.; Pinaud, F.; Williams, S. C.; Parak, W. J.; Zanchet, D.; Weiss, S.; Alivisatos, A. P. *J. Phys. Chem. B* **2001**, *105*, 8861-8871.

(13) Seraphin, A. A.; Ngiam, S. T.; Kolenbrander, K. D. *J. Appl. Phys.* **1996**, *80*, 6429-6433.

(14) Heinrich, J. L.; Curtis, C. L.; Credo, G. M.; Kavanagh, K. L.; Sailor, M. J. *Science*, **1992**, *255*, 66-68.

(15) Hua, F. J.; Swihart, M. T.; Ruckenstein, E. *Langmuir* **2005**, *21*, 6054-6062.

(16) Li, X.; He, Y.; Swihart, M. T. *Langmuir* **2004**, *20*, 4720-4727.

(17) Li, X.; He, Y.; Talukdar, S. S.; Swihart, M. T. *Langmuir* **2003**, *19*, 8490-8496.

(18) Hua, F. J.; Erogbogbo, F.; Swihart, M. T.; Ruckenstein, E. *Langmuir* **2006**, *22*, 4363-4370.

(19) Holmes, J. D.; Ziegler, K. J.; Doty, R. C.; Pell, L. E.; Johnston, K. P.; Korgel, B. A. *J. Am. Chem. Soc.* **2001**, *123*, 3743-3748.

(20) Liu, Q.; Kauzlarich, S. M. *Mater. Sci. & Eng.. B*, **2002**, *B96*, 72-75.

(21) Pettigrew, K. A.; Liu, Q.; Power, P. P.; Kauzlarich, S. M. *Chem. Mater.* **2003**, *15*, 4005-4011.

(22) Zhang, X.; Neiner, D.; Wang, S.; Louie, A. Y.; Kauzlarich, S. M. *Nanotechnology* **2007**, *18*, 095601-096606.

(23) Neiner, D.; Chiu, H. W.; Kauzlarich, S. M. *J. Am. Chem. Soc.* **2006**, *128*, 11016-11017.

(24) Zou, J.; Sanelle, P.; Pettigrew, K. A.; Kauzlarich, S. M. *J. Cluster Sci.* **2006**, *17*, 565-578.

(25) Wilcoxon, J. P.; Samara, G. A. *Appl. Phys. Lett.* **1999**, *74*, 3164-3166.

(26) Wilcoxon, J. P.; Samara, G. A.; Provencio, P. N. *Phys. Rev. B* **1999**, *60*, 2704-2714.

(27) Tilley, R. D.; Warner, J. H.; Yamamoto, K.; Matsui, I.; Fujimori, H. *Chem. Comm.* **2005**, 1833-1835.

(28) Veinot, J. G. C. *Chem. Comm.* **2006**, 4160-4168.

(29) (a) photochemical: Sun, Q. Y.; de Smet, L. C. P. M.; van Lagen, B.; Giesbers, M.; Thune, P. C.; van Engelenburg, J.; de Wolf, F. A.; Zuilhof, H.; Sudholter, E. J. R. *J. Am. Chem. Soc.* **2005**, *127*, 2514-2523. ; (b) thermal: Sieval, A. B.; Vleeming, V.; Zuilhof, H.; Sudholter, E. J. R. *Langmuir* **1999**, *15*, 8288-8291.

(30) (a) Stewart, M. P. R., E. G.; Geders, T. W.; Allen, M. J.; Choi, H. C.; Buriak, J. M. *Phys. Stat.Sol. A,* **2000**, *182*, 109-115.; (b) Buriak, J. M.; Stewart, M. P.; Geders, T. W.; Allen, M. J.; Choi, H. C.; Smith, J.; Raftery, D.; Canham, L. T. *J. Am. Chem. Soc.* **1999**, *121*, 11491-11502. (c) Buriak, J. M. *Adv. Mat*. **1999**, *11*, 265-267.

(31) Sieval, A. B.; Demirel, A. L.; Nissink, J. W. M.; Linford, M. R.; van der Maas, J. H.; de Jeu, W. H.; Zuilhof, H.; Sudhoelter, E. J. R. *Langmuir* **1998**, *14*, 1759-1768.

(32) Scheres, L.; Arafat, A.; Zuilhof, H. *Langmuir* **2007**, *23*, 8343-8346.

(33) Buriak, J. M. *Chem. Rev.* **2002**, *102*, 1271-1308.

(34) de Smet, L. C. P. M.; Pukin, A. V.; Sun, Q. Y.; Eves, B. J.; Lopinski, G. P.; Visser, G. M.; Zuilhof, H.; Sudholter, E. J. R. *Appl. Surface Sci.* **2005**, *252*, 24-30.

(35) Sun, Q.-Y.; de Smet, L. C. P. M.; van Lagen, B.; Wright, A.; Zuilhof, H.; Sudhoelter, E. J. R. *Angew. Chem. Int. Ed.* **2004**, *43*, 1352-1355.

(36) de Smet, L. C. P. M.; Stork, G. A.; Hurenkamp, G.H. F.; Sun, Q.Y.; Topal, H. Vronene, P.J. E.; Sieval, A. B.; Wright, A.; Visser, G. M.; Zuilhof, H.; Sudholter, E. J. R. *J. Am. Chem. Soc.* **2003**, *125*, 13916-13917.

(37) Nelles, J.; Sendor, D.; Ebbers, A.; Petrat, F. M.; Wiggers, H.; Schulz, C.; Simon, U. *Colloid. Polym. Sci.* **2007**, *285*, 729-736.

(38) Rosso-Vasic, M.; Spruijt, E.; Popovic, Z.; Van Lagen, B.; De Cola, L.; Zuilhof, H. *submitted*.

(39) Staffilani, M.; Hoss, E.; Giesen, U.; Schneider, E.; Hartl, F.; Josel, H.-P.; De Cola, L. *Inorg. Chem.* **2003**, *42*, 7789-98.

(40) Liu, N.; Chen, H. Z.; Chen, F.; Wang, M. *Chem. Phys. Lett.* **2008**, *451*.

(41) Balzani, V.; Bergamini, G.; Marchioni, F.; Ceroni, P. *Coord. Chem. Rev.* **2006**, *250*, 1254-1266.

(42) Sauvage, J. P.; Collin, J. P.; Chambron, J. C.; Guillerez, S.; Coudret, C.; Balzani, V.; Barigelletti, F.; Decola, L.; Flamigni, L. *Chem. Rev.* **1994**, *94*, 993-1019.

(43) Decola, L.; Balzani, V.; Barigelletti, F.; Flamigni, L.; Belser, P.; Vonzelewsky, A.; Frank, M.; Vogtle, F. *Inorg. Chem.* **1993**, *32*, 5228-5238.

(44) Sykora, M.; Petruska, M. A.; Alstrum-Acevedo, J.; Bezel, I.; Meyer, T. J.; Klimov, V. I. *J. Am. Chem. Soc.* **2006**, *128*, 9984-9985.

(45) Kozhevnikov, V.; De Cola, L. *unpublished results*.

(46) Sehgal, D.; Vijay, I. K. *Anal. Biochem.* **1994**, *218*, 87-91.

(47) Kalyanasundaram, K.; Zakeeruddin, S. M.; Nazeeruddin, M. K. *Coord. Chem. Rev.* **1994**, *132*, 259-64.

(48) Cademartiri, L.; Montanari, E.; Calestani, G.; Migliori, A.; Guagliardi, A.; Ozin, G. A. *J. Am. Chem. Soc.* **2006**, *128*, 10337-10346.

(49) Yu, W. W.; Qu, L. H.; Guo, W. Z.; Peng, X. G. *Chem. Mater.* **2003**, *15*, 2854-2860.

(50) Wang, X.; Zhang, R. Q.; Niehaus, T. A.; Frauenheim, T. *J. Phys. Chem. C* **2007**, *111*, 2394-2400.

(51) Lakowicz, J. R. *Principles of Fluorescence Spectroscopy*; 3rd ed.; Springer, 2006.

(52) Forster, T. *Discuss. Faraday Soc.* **1959**, *27*, 7-12.

(53) Kagan, C. R.; Murray, C. B.; Bawendi, M. G. *Phys. Rev. B* **1996**, *54*, 8633-8643.

(54) Scholes, G. D.; Andrews, D. L. *Phys. Rev. B* **2005**, *72*, 125331-125338.

(55) May, V.; Kuhn, O. *Charge and Energy Transfer Dynamics in Molecular Systems*; 2nd ed.; Willey-VCH Weinheim, 2004.

Chapter 5

Azide-terminated Silicon Nanoparticles: Functionalization using Click Chemistry & Uptake by Growing Yeast Cells

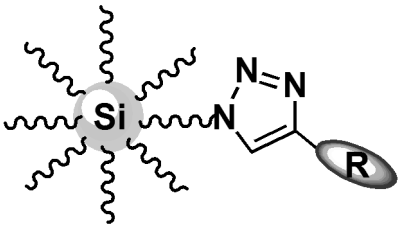

Part of this chapter is submitted for publication as:

"Azide-terminated Silicon Nanoparticles: Functionalization using Click Chemistry and Uptake by Growing Yeast Cells", Milena Rosso-Vasic, Carel Weijers, Evan Spruijt, Aliaksei Pukin, Barend van Lagen, Luisa De Cola and Han Zuilhof

Abstract – The production of stable azide-terminated Si NPs and their detailed photophysical characterization is described. These Si NPs are further functionalized by using click chemistry principles with a number of functional moieties: undec-10-yn-1-ol, propargyl amine, undec-10-ynoic acid, undec-10-ynyl hepta-O-acetyl lactose and rhodamine-labeled lactose. Subsequently, the uptake of Si NPs by yeast cells (*Rhodotorula glutinis)* is successfully demonstrated, by allowing cells to actually grow in the presence of Si NPs.

5.1. Introduction

Functionalization of Si NPs is very important from both fundamental and application points of view. Numerous methods for the synthesis of stable, free-standing Si NPs have been used successfully,[1] functionalizing them with a variety of functional groups such as: alkyl,[2,3] amino,[4] carboxyl,[5] or DNA.[6] The currently reported methods to produce stable Si NPs with specific functionalization are very time consuming, and still quite limiting in regard of the choice of capping agents, due to the high reactivity of hydrogen-[7,8] or bromine-[2] terminated Si NPs, which are general precursors for the synthesis of stable coated Si NPs.

An alternative approach is to produce stable azide-terminated Si NPs and to couple them to alkyne-terminated molecules via Cu(I)-catalyzed Huisgen-Meldal-Sharpless 1,3-dipolar cycloaddition,[9] usually known as a “click” reaction. This reaction is wide in scope, extremely selective and high yielding while utilizing very mild reaction conditions. The product of the reaction is a stable heterocyclic linker, a 1,4–disubstituted-1,2,3–triazole. Azides and alkynes are essentially inert to molecular oxygen, various solvents - including water - and common reaction conditions in organic synthesis. In fact, water is the ideal reaction solvent, providing the best yields and highest reaction rates. The Cu(I)-catalyzed reaction is mild and very efficient, requiring no protecting groups.[10] The formed triazole has similarities to the ubiquitous amide moiety found in nature and is not susceptible to cleavage. Additionally, they are nearly impossible to oxidize or reduce.[11] These advantages are particularly useful for attaching multifunctional molecules to the various surfaces[12-14] and suggest that azide-modified Si NPs would be a highly versatile platform for attachment of variety of functional molecules.[15]

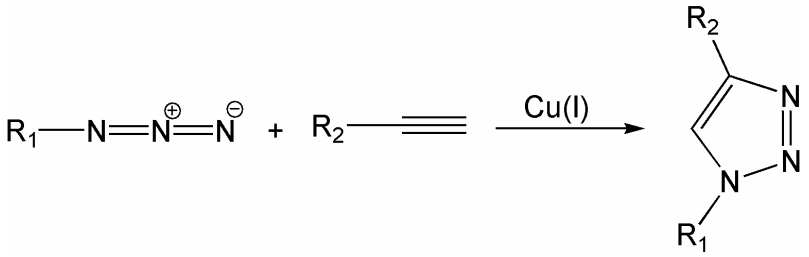

Figure 5.1. Click reaction: general reaction scheme

While click chemistry has already been used to functionalize various nanomaterials,[13-20] and to assemble nanostructures,[21] it has not been exploited yet to functionalize Si NPs. The upcoming use of NPs has logically initiated a growing interest in the effects of interaction of NPs with biological material. To study the possible biological application of NPs for biological purposes, the uptake of NPs by mammalian cells is an essential parameter. Uptake of (nano)particles by mammalian cells and other eukaryotic cells is commonly accepted to proceed by mechanisms like fagocytosis and endocytosis.[22-24] Studies on the cellular uptake

of NPs can be effectively performed by using yeast as a cell model, since yeast is a unicellar, fast growing, eukaryotic microorganism in which cellular mechanisms are highly conserved to mammals. Also, the visualization of the yeast subcellular components and possible localization of NPs is still possible by light microscopy[25] and yeasts display endocytosis-mediated uptake of extracellular material.[26-28] Furthermore, yeast cells are surrounded by a cell wall which justifies the extending of findings in particle internalization to the much less shielded mammalian cells which are only covered with a cell membrane. As to date, information about the toxicity of NPs towards yeast cells is still scarce.[29,30]

In this chapter, we describe the production of functionalized Si NPs obtained by using click chemistry with azide-terminated Si NPs and a number of functional moieties of interest. Further we demonstrate the cellular uptake of rhodamine B-labeled Si NPs (RhB Si NPs) by yeast cells - *Rhodotorula glutinis*, and note that these yeast cells were not only stained with Si NPs, but in fact grown in their presence.

5.2. Experimental Section

5.2.1. Synthesis and purification of azido-1-alkenes.

Azido-1-alkenes were synthesized from their n-bromo-1-alkene derivatives. 50 mmol of n-bromo-1-alkene was dissolved in 50 mL DMF and a five-fold excess (15 g, 0.23 mol) of NaN_3 was added. The reaction mixture was stirred and refluxed for 24 h at 90 °C. Subsequently, 50 mL of cold water was added to the reaction mixture and the n-alkenyl-azide was extracted with 50 mL of PE 40-60. The extract was washed three times with 30 mL brine. After evaporation of PE 40-60 at 40 °C and 600 mbar pure n-azido-1-alkenes were obtained.

3-azido-1-propene: ^{1}H NMR (ppm, $CDCl_3$): δ = 5.77 (m, H_2C=C**H**-R), δ = 5.16 (m, **H_2**C=CH-R), δ = 4.12 (m, C=CH-C**H_2**-N_3).

6-azido-1-hexene: ^{1}H NMR (ppm, $CDCl_3$): δ = 5.71 (m, H_2C=C**H**-R), δ = 4.90 (m, H_2C=C**H**-R), δ = 3.19 (t, R'-C**H_2**-N_3), δ = 1.99 (q, CH_2, H_2C=CH-C**H_2**-R''), δ = 1.52 (m, CH_2), δ = 1.40 (m, CH_2).

11-azido-1-undecene: ^{1}H NMR (ppm, $CDCl_3$): δ = 5.76 (m, H_2C=C**H**-R), δ = 4.95 (m, H_2C=C**H**-R), δ = 3.26 (t, R'-C**H_2**-N_3), δ = 2.05 (q, CH_2, H_2C=CH-C**H_2**-R''), δ = 1.61 (m, CH_2), δ = 1.30 (m, b, 6x CH_2).

5.2.2. Synthesis and purification of azide-terminated Si NPs.

1.5 g of tetraoctylammonium bromide was mixed with 100 ml of dry toluene and mixture was sonicated for 15 min, under flow of dry Ar. 100 µl of $SiCl_4$ was added via a gas-tight syringe and sonication was continued for 30 min equal distribution of Si source in monodisperse reverse micelles. Subsequently, 2.3 mL of $LiAlH_4$ (1M in THF) was added in

order to form hydrogen-terminated Si NPs. After 30 min of sonication, dry methanol (30 ml) was added to react with the excess $LiAlH_4$.

Azide-amino terminated particles were obtained in the reactions of degassed 0.013 mol of 11-azido-undec-1-ene, 6-azido-hex-1-ene and 3-azidoprop-1-ene and hydrogen-terminated Si NPs under Ar, in the presence of 40 μl of 0.05 M H_2PtCl_6 catalyst. After 30 min of continuous sonication azide-terminated Si NPs were extracted with hexane and filtrated twice. The filtration of synthesized Si NPs was performed through hydrophilic 450 nm PVDF (Polyvinylidene Fluoride) membrane filters (MILLEX-HV, Millipore) in order to remove surfactant, and dialyzed against hexane (MWCO 7000, SERVA, Membra-Cel dialysis tubing, diameter 22 mm) to remove residuals of nonreacted alkene.

5.2.3. Click reaction on azide-terminated Si NPs

Click reactions were performed with purified 11-azido-undecyne-functionalized Si NPs and several functional alkynes: undec-10-yn-1-ol, propargyl amine, undec-10-ynoic acid, undec-10-ynyl hepta-O-acetyl lactose and rhodamine-labeled lactose.

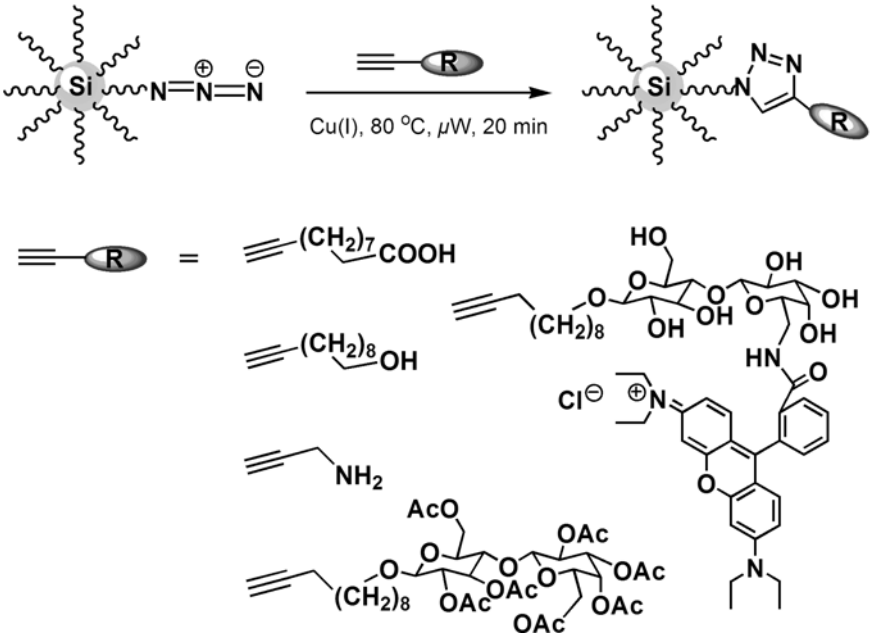

Figure 5.2. Functionalization of Si NPs using click chemistry.

Typically, the reactions were carried out in 2% water in DMF, using $CuSO_4$ and Na-ascorbate, over 20 min only, at 80 °C under microwave irradiation. After reaction, functionalized Si NPs were purified by dialysis against DMF (MWCO 10000, SERVA, Membra-Cel dialysis tubing, diameter 22 mm) for 72 h, in 8-10 h cycles.

5.2.4. Optical measurements.

All measurements were performed at standard pressure and room temperature, unless stated differently. Electronic absorption spectra were recorded in a quartz cuvette (1 cm, Hellma), using a Cary 1 UV-Vis double-beam spectrophotometer and were corrected for the solvent and toluene absorption. The scan range was 200 - 500 nm with a 600 nm/min rate.

Steady-state and time-resolved measurements were performed on a Time-Correlating Single Photon Counting F900 spectrometer (Edinburgh Instruments). All steady-state spectra are corrected for the wavelength-dependent sensitivity of the detector and the source by recording reference data simultaneously. Additionally, emission spectra have been corrected for Raman scattering using the solvent emission spectra.

Using a comparative method, as described by Williams *et al.*,[31] the quantum yields of fluorescence in hexane were determined in optically dilute solutions (optical density ~0.1), employing naphthalene in cyclohexane (Φ_{em} = 0.23 ± 0.02) as a reference emitter.

Time-resolved fluorescence measurements were performed with the exact the same solution used for steady-state spectra (absorption was always adjusted to be ≤ 0.5). A pulsed light-emitting diode ($\lambda_{excitation}$ = 283 nm) was used as excitation source, and photons were collected up to 100 ns (4096 channels) until a maximum of 10^4 counts.

5.2.5. FTIR and TEM measurements

For *FTIR measurements* (Bruker, Vector 22 FTIR spectrometer), thin films of particle solutions in CCl_4 were made between NaCl crystals and corrected for the background signal, by collecting 32 scans for each measurement.

High-Resolution Transmission Electron Microscopy (TEM) studies were performed with a LIBRA 200 FE (200 kV) microscope. TEM samples were prepared by dipping a carbon-coated 300-mesh copper grid into a sonicated and filtered silicon nanoparticles solution in hexane. The solvent was evaporated in air and TEM micrographs were typically taken at five different spots of each grid. Olympus Soft Imaging iTEM Solution and iTEM Solution EMaker were used to view and analyse the micrographs, respectively.

5.2.6. Cellular uptake

As the cellular uptake by endocytosis is a time-, temperature- and energy-dependent process, the highest endocytic activity can be expected in growing cells, with high metabolic activity. Experimental conditions for studying RhB Si NPs uptake were accordingly determined. For this, yeast *Rhodotorula glutinis*[32] was selected and cultivated the wild-type cells with glycerol as a nonfermentable carbon source in a medium supplemented with Si NPs.

As all the living cells exhibit autofluoresence which can be regarded as an unwanted interference in the detection of fluorescent labelled materials.[33,34] it is important that this possible contribution to total fluorescence of cells is reduced. This can be done by using chromophores with long emission wavelenghts (λ_{em} > 550 nm). Therefore rhodamine B-labelled Si NPs (RhB Si NPs) were selected to investigate the cellular uptake.

Cells of *Rhodotorula glutinis* were cultivated for 48 h in a mineral medium supplemented with 0.1% yeast extract, 1.0% glycerol and 2.2 µM RhB Si NPs, at 30 °C in a shaking incubator (170 rpm). The yeast cells were harvested by centrifugation at 10000 *g*, washed three times with sterile ultra pure water and resuspended to the original cell density. Cell suspensions were subsequently transferred into 8-well Lab-Tek® chamber slides for inverted confocal microscopy.

For comparison of intracellular fluorescence, yeast cell cultures were similarly prepared without addition of NPs or fluorophores, and with rhodamine B (5 µM) and rhodamine 123 (5 µM).

Possible toxicity of Si NPs was first tested towards 1.0 µM RhB-Si NPs - as determined by the fluorescence intensity of rhodamine B and absorption of Si NPs[35] - in preliminary growth experiments, but found no inhibition. For the investigation of cellular uptake, a higher concentration of 2.2 µM RhB-Si NPs was applied to increase visualization when internalized.

5.2.7. Confocal Microscopy

Yeast cells grown in the presence of RhB Si NPs and Rhodamine123 were suspended in water and dropped in the 8-well Lab-Tek chamber slides. Cells were observed using a laser scanning confocal microscope Zeiss LSM510 (Zeiss, Jena, Germany). Rhodamine B and rhodamine 123 were excited using an Ar-ion 488 nm laser. The sample was observed through an oil immersion 63X/1.4 objective.

For the quantification of the amount of RhB Si NPs taken up by the yeast cells, different rhodamine B solutions in water were prepared (in the range of 0.01-2.00 µM), transferred to 8-well Lab-Tek chamber slides and the mean emission intensity was determined by confocal microscopy. The mean fluorescence intensity was also determined for the initial solution of RhB Si NPs in water and for the supernatant of centrifuged yeast cells grown in the presence of RhB Si NPs.

5.3. Results and Discussion

5.3.1. Characterization of azide-terminated Si NPs

Synthesized azide-terminated NPs were of a high monodispersity (1.56 ± 0.22 nm), as determined with transmission electron microscopy by measuring the size of 1223 randomly chosen particles.

Optical absorption spectra of all synthesized azide-terminated Si NPs are displayed in Figure 5.3. They absorb in 220-330 nm range with the pronounced peak at 290 nm, due to the specific absorption of azide groups.[36] Si-$(CH_2)_3$-N_3 NPs differ from the other two samples, because the peak at 290 nm is not pronounced.

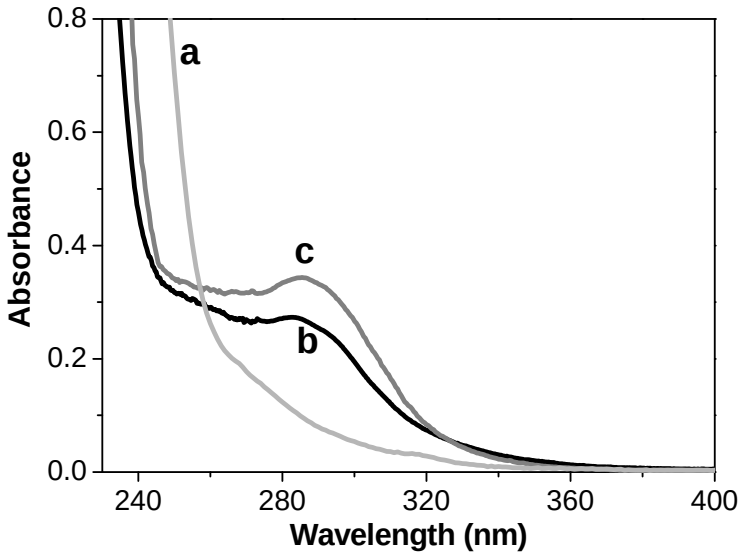

Figure 5.3. Absorption spectra of (a) Si-$(CH_2)_3$-N_3, (b) Si-$(CH_2)_6$-N_3, (c) Si-$(CH_2)_{11}$-N_3 NPs.

All types of synthesized azide-terminated Si NPs strongly fluoresce in a narrow spectral range, with the emission maxima in the range of 320 - 350 nm, depending on the excitation wavelength. Emission profiles are narrow (FWHM = 57 nm) with the emission quantum yields in the range 11-17%. Azide-terminated Si NPs with the shortest chain exhibit the highest emission quantum yield and as the chain is getting longer quantum yield drops to ~11% in the case of –C11 chain.

Fluorescence decays for azide-terminated Si NPs were fitted with three-exponential function; one exponent more than alkyl-terminated Si NPs.[35] The components are: ~0.6, ~3.6 and ~9.5 - 13 ns. Details are displayed in Table 5.1. Two of the resulting three lifetimes are nearly identical to the lifetimes for alkyl-terminated Si NPs.

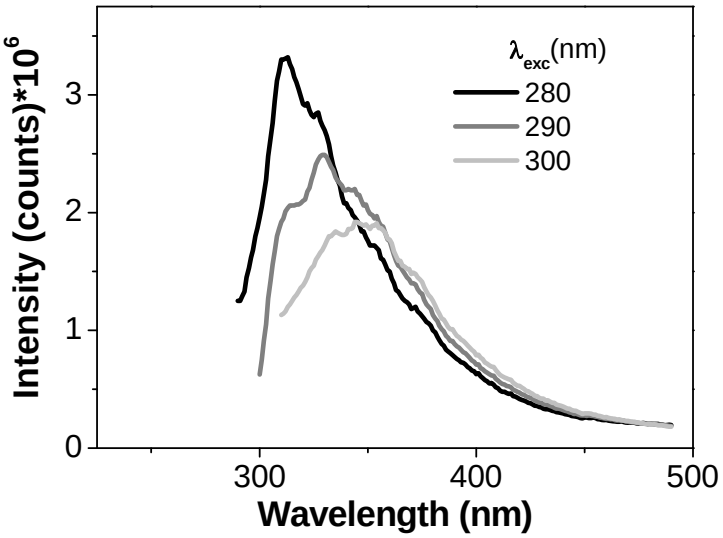

Figure 5.4. Emission map of Si-$(CH_2)_6N_3$ NPs in hexane.

While the shortest component indicates the excitation of direct band-gap,[37] resulting from the nm dimensions of the Si NP core, a very long component, is likely due to a stabilizing interaction between the azide groups and the excited electron and hole in the NP. The fraction of this lifetime corresponds then to all excited NPs that emit a photon after interaction with an azide group. For Si-$(CH_2)_{11}$-N_3 this longest lifetime component is significantly shorter, due to the weaker interaction between the azide group and the NP when the azide group is further away from the NP.

Time-resolved anisotropy measurements reveal that the fluorescence anisotropy decays strictly according to a mono-exponential curve, indicating ball-shaped Si NPs, in line with the TEM observations.

Table 5.1. Room-temperature emission properties of azide-terminated Si NPs in hexane

	Fluor. maxima					**Lifetimes**		
	λ_{exc} **(nm)**	λ_{em} **(nm)**	**Stokes shift (nm)**	**FWHM (nm)**	**QY (%)**	τ_1 **(ns)** B_1 **(%)**	τ_2 **(ns)** B_2 **(%)**	τ_3 **(ns)** B_3 **(%)**
Si-$(CH_2)_3$-N_3	280	309	41	56	17 ± 2	0.64 (14.3)	3.48 (51.5)	12.53 (34.1)
Si-$(CH_2)_6$-N_3	280	313	45	58	14 ± 1	0.57 (9.4)	4.35 (54.0)	12.75 (36.7)
Si-$(CH_2)_{11}$-N_3	280	315	47	57	12 ± 1	0.60 (10.1)	3.59 (53.5)	9.44 (36.4)

The FTIR spectra of azide-terminated Si NPs (Figure 5.5) show a very strong absorption at 2100 cm^{-1} due to the azide N=N=N antisymmetric stretch, and strong bands of antisymmetric and symmetric CH_2 stretching vibrations at 2856 and 2928 cm^{-1}, respectively. Covalent attachment of the alkyl chains to the surface is confirmed by the scissoring and stretching vibration bands of Si−C bonds (1464 and 1259 cm^{-1}, respectively).

For shorter chain lengths (-C3 and C6) peaks in the range of 1010 - 1100 cm^{-1} reveal the presence of Si-O bonds, while these peaks almost disappear in the case of -C11 alkyl-spacer (Figure 5.5), showing the high-quality passivation. This covalently attached -$(CH_2)_{11}$-N_3 monolayer allows a complete passivation, and prevents particle aggregation as confirmed by TEM data.

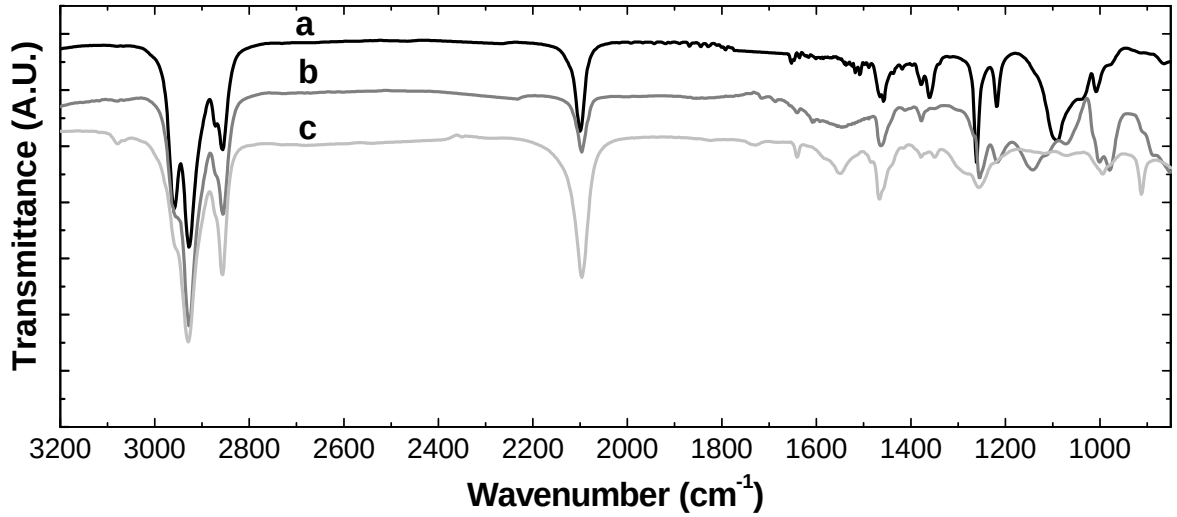

Figure 5.5. FTIR spectra of azide-terminated Si NPs: (a) Si-$(CH_2)_3$-N_3, (b) Si-$(CH_2)_6$-N_3, (c) Si-$(CH_2)_{11}$-N_3.

Due to the lowest oxidation-degree and the highest stability, 11-azido-undecyne-functionalized Si NPs were used for click reaction experiments. They can easily be dried and resuspended in a variety of solvents, and kept at ambient conditions over >4 months without noticeable degradation as observed from the absence of Si-O bands in the IR spectrum and changes in the absorption and fluorescence spectra. Their stability is maintained even under sterilization conditions (T = 121 ^{0}C for 30 min). Si-$(CH_2)_3$-N_3 and Si-$(CH_2)_6$-N_3 NPs did not show such stability. After heating them to ~60 - 80 ^{0}C, the emission spectra already became broader and red tailed, indicating further oxidation. However, when kept in DMF or hexane at 4 ^{0}C, their emission profiles were unchanged for >2 months.

5.3.2. Click reaction on azide-terminated Si NPs

The occurrence of the click reaction is readily ascertained by the complete disappearance of the characteristic absorptions of the azide groups in FTIR (2100 cm^{-1}), and the simultaneous appearance of characteristic vibrational modes (Figure 5.6), specific for the attached molecules: C=O (curve 3b; 1734 cm^{-1}) or NH_2 (curve 3c; 1640 cm^{-1}; broad peak at 3400 cm^{-1}). Finally, curve 3d reveals that acetyl protection of oligosaccharides that are clicked unto the Si NP remains fully intact under these reaction conditions as no broadening of the C=O peak is observed. Stretching vibrations in the 2928-2856 cm^{-1} range are unchanged for all these NPs, revealing the stability of the covalently attached monolayer.

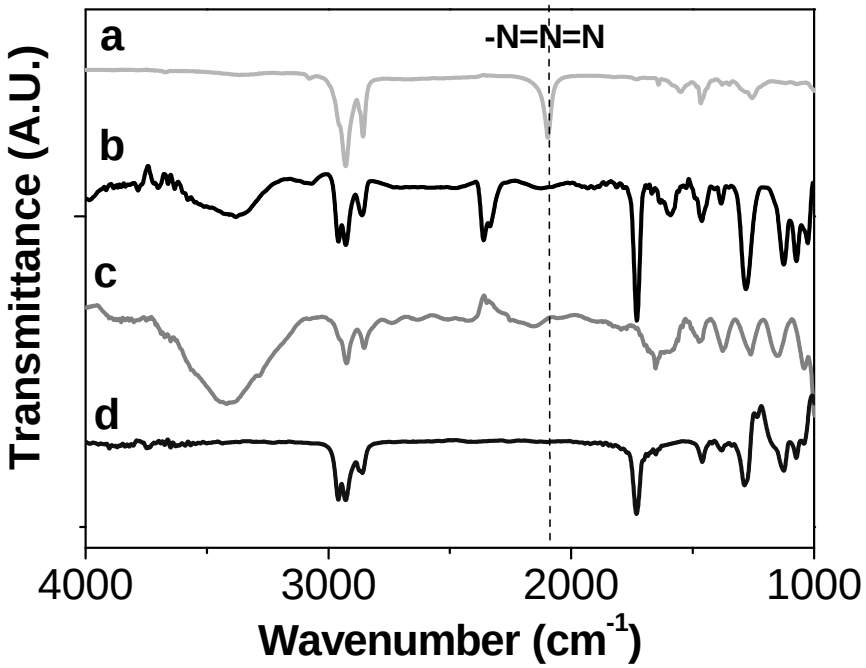

Figure 5.6. FTIR spectra of a) azide-terminated Si NPs; after click reaction with b) undec-10-ynoic acid; c) propargyl amine; d) heptaacetyl-protected lactoside.

Finally, the disappearance in the UV spectrum of the characteristic azide absorption at 290 nm also points to a quantitative conversion of the azide groups to triazole moieties (Figure 5.7).

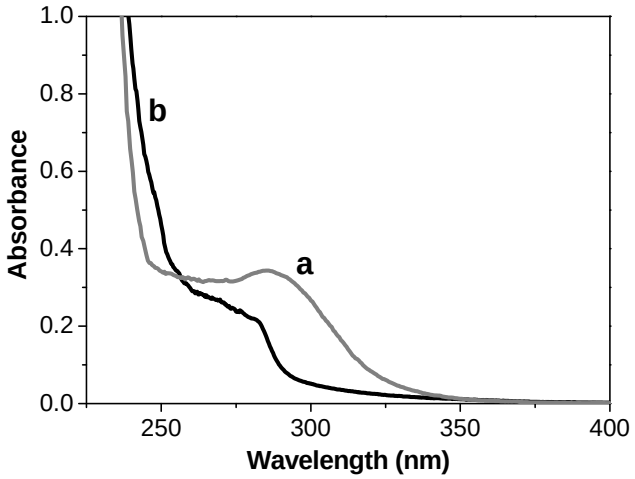

Figure 5.7. Absorption spectra of azide-terminated Si NPs a) before and b) after click reaction; both in hexane.

Emission spectra did not change when undec-10-ynoic acid, and heptaacetyl-protected lactoside were "clicked" to azide-terminated Si NPs. When rhodamine-labeled lactose was attached an additional emission peak of the dye is observed at 575 nm, confirming the attachment of the dye.

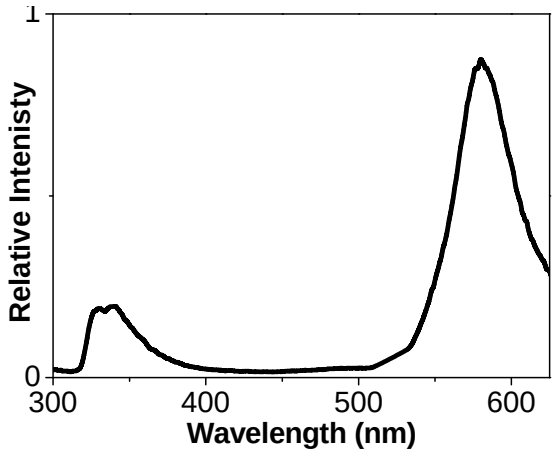

Figure 5.8*:* Emission spectrum of Si-$C_{11}N_3$ NPs clicked with rhodamine labeled lactose in DMF

Interestingly, when propargyl amine was attached to azide-terminated Si NPs, the emission spectrum significantly changed (Figure 5.9), resembling those of amine-terminated Si NPs with an -C_{11} alkyl spacer.[38] Maximal emission intensity centered at 400 nm is obtained when exciting Si NPs with 330 nm. Excitation with higher wavelengths (up to 400 nm) still gave considerable emission, with more red-shifted maxima to 450 - 500 nm.

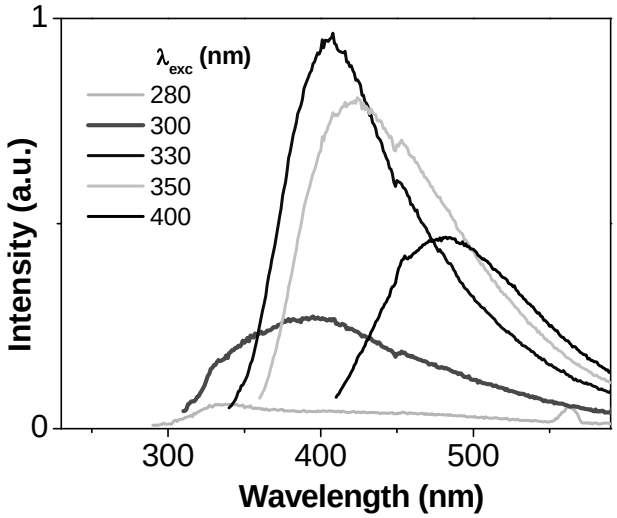

Figure 5.9. Emission spectrum of Si-$C_{11}N_3$ NPs clicked with propargyl amine in DMF. *(See Appendix at the end of the thesis for the color picture)*

This behavior can be useful in the cases when tuning of the emission from UV to blue is needed for certain purposes and can be easily performed only by changing the capping groups from azide to amine.

5.4. Bioimaging

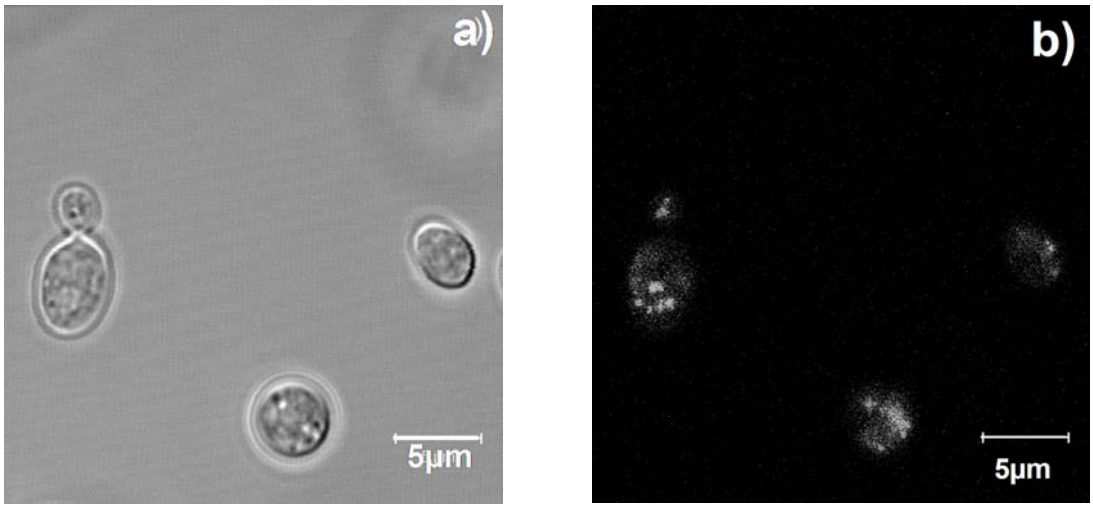

Figure 5.10. Cells of *Rhodotorula glutinis* grown in the presence of RhB Si NPs a) bright field image b) raw data of fluorescence image (λ_{exc} = 488 nm, λ_{em} = 560 - 615 nm). *(See Appendix at the end of the thesis for the color picture)*

Figure 5.10 shows the presence of budding cells, which signifies that the cells are viable and reproducing in the presence of RhB-Si NPs. Exposure to a concentration of

2.2 µM RhB-Si NPs apparently caused no or only a negligible cytotoxicity. Internalization of the RhB-Si NPs is visualized in Figure 5.10b, as detected by live-cell imaging using confocal laser scanning microscopy. Although the RhB-Si NPs were distributed throughout the cell, higher concentrations can be observed directly beneath the cell membrane. This specific localization is in accordance with the morphology of the elaborate mitochondrial network in glycerol-grown yeast cells.[39]

When internalized, rhodamine B has been described to be mainly localized in mitochondria of living eukaryotic cells.[40] Interaction of RhB Si NPs with subcellular material is proposed to be mainly by the easily accessible terminal rhodamine B and to a much less extend by the more shielded and modified lactoside functionality. The (external) concentration of RhB-Si NPs in the growth medium decreased from 2.2 to 1.2 µM RhB after 48 hours cultivation of the yeast, as determined by comparing fluorescence intensities.

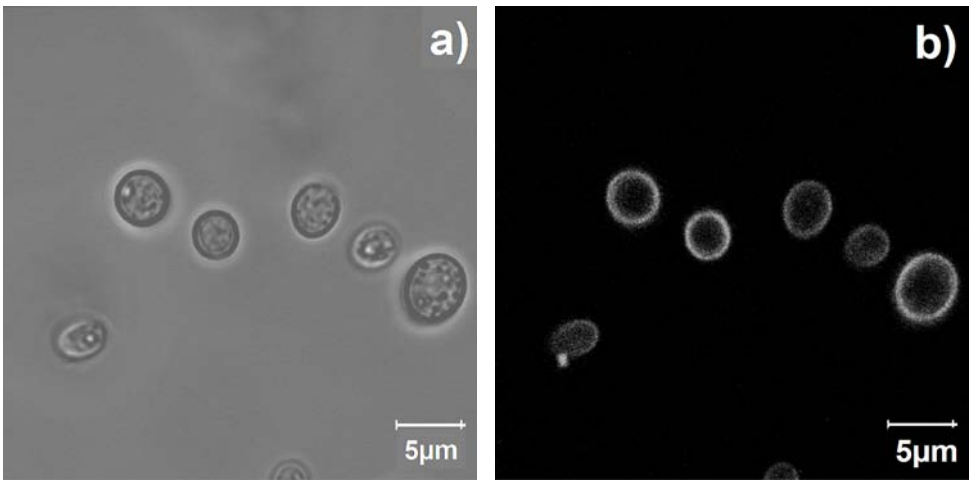

.

Figure 5.11. Cells of *Rhodotorula glutinis* grown in the presence of Rhodamine 123
a) bright-field image b) raw data of fluorescence image (λ_{exc} = 488 nm, λ_{em} = 505 - 530 nm).
(See Appendix at the end of the thesis for the color picture)

Localization and visualization of the intact cell membranes was done by using the cationic dye rhodamine 123 (Figure 5.11).[41,42]

Intact cell membrane indicates that cells are still viable and gives possibility for further study specific staining of only cell membrane, by functionalizing Si NPs with rhodamine 123 instead of rhodamine B.

5.5. Conclusions

We have shown a simple and convenient way to passivate and derivatize surfaces of Si NPs via click chemistry, allowing number complex functionalities to be attached at their periphery via this near-universal anchor – an azide group. This approach allows for the simple and highly flexible production of a large number of novel, chemically modified Si NPs.

Cellular uptake of rhodamine B-labeled Si NPs was demonstrated by using growing cells of the yeast *Rhodotorula glutinis*. It was shown that toxicity of rhodamine B-labeled Si NPs is minimal, because yeast cells were able to grow and multiply in their presence.

Cellular uptake and internal localization under varying physiological conditions can now accordingly be studied in more detail, and with more complex functionalization attached onto the Si NPs. The results of this study open the way for further development of Si NPs as effective delivery vehicles for the transport of biologically active compounds into specific cells of interest.

5.6. References

(1) Veinot, J. G. C., *Chem. Comm.* **2006**, 4160-4168.

(2) Pettigrew, K. A.; Liu, Q.; Power, P. P.; Kauzlarich, S. M., *Chem. Mater.* **2003,** *15*, 4005-4011.

(3) Li, X.; He, Y.; Swihart, M. T., *Langmuir* **2004,** *20*, 4720-4727.

(4) Warner, J. H.; Hoshino, A.; Yamamoto, K.; Tilley, R. D., *Angew. Chem. Int. Ed.* **2005,** *44*, 4550-4554.

(5) Rogozhina, E. V.; Eckhoff, D. A.; Gratton, E.; Braun, P. V., *J. Mater. Chem.* **2006,** *16*, 1421-1430.

(6) Wang, L.; Reipa, V.; Blasic, J., *Bioconjugate Chem.* **2004,** *15*, 409-412.

(7) Hua, F.; Erogbogbo, F.; Swihart, M. T.; Ruckenstein, E., *Langmuir* **2006,** *22*, 4363-4370.

(8) Nelles, J.; Sendor, D.; Ebbers, A.; Petrat, F. M.; Wiggers, H.; Schulz, C.; Simon, U., *Coll. Polym. Sci.* **2007,** *285*, 729-736.

(9) Rostovtsev, V. V.; Green, L. G.; Fokin, V. V.; Sharpless, K. B., *Angew. Chem. Int. Ed.* **2002,** *41*, 2596-2599.

(10) Tornoe, C. W.; Christensen, C.; Meldal, M., *J. Org. Chem.* **2002,** *67*, 3057-3064.

(11) Chan, T. R.; Hilgraf, R.; Sharpless, K. B.; Fokin, V. V., *Org. Lett.* **2004,** *6*, 2853-2855.

(12) Devaraj, N. K.; Decreau, R. A.; Ebina, W.; Collman, J. P.; Chidsey, C. E. D., *J. Phys. Chem. B* **2006,** *110*, 15955-15962.

(13) Lummerstorfer, T.; Hoffmann, H., *J. Phys. Chem. B* **2004,** *108*, 3963-3966.

(14) Collman, J. P.; Devaraj, N. K.; Eberspacher, T. P. A.; Chidsey, C. E. D., *Langmuir* **2006,** *22*, 2457-2464.

(15) Devadoss, A.; Chidsey, C. E. D., *J. Am. Chem. Soc.* **2007,** *129*, 5370-5371.

(16) Collman, J. P.; Devaraj, N. K.; Chidsey, C. E. D., *Langmuir* **2004,** *20*, 1051-1053.

(17) Li, H. M.; Cheng, F. O.; Duft, A. M.; Adronov, A., *J. Am. Chem. Soc.* **2005,** *127*, 14518-14524.

(18) White, M. A.; Johnson, J. A.; Koberstein, J. T.; Turro, N. J., *J. Am. Chem. Soc.* **2006,** *128*, 11356-11357.

(19) Brennan, J. L.; Hatzakis, N. S.; Tshikhudo, T. R.; Dirvianskyte, N.; Razumas, V.; Patkar, S.; Vind, J.; Svendsen, A.; Nolte, R. J. M.; Rowan, A. E.; Brust, M., *Bioconjugate Chem.* **2006,** *17*, 1373-1375.

(20) Fleming, D. A.; Thode, C. J.; Williams, M. E., *Chem. Mater.* **2006,** *18*, 2327-2334.

(21) Voggu, R.; Suguna, P.; Chandrasekaran, S.; Rao, C. N. R., *Chem. Phys. Lett.* **2007,** *443*, 118-121.

(22) Chithrani, B. D.; Ghazani, A. A.; Chan, W. C. W., *Nano Let.* **2006,** *6*, 662-668.

(23) Khan, J. A.; Pillai, B.; Das, T. K.; Singh, Y.; Maiti, S., *ChemBioChem* **2007,** *8*, 1237-

1240.

(24) Thurn, K. T.; Brown, E. M. B.; Wu, A.; Vogt, S.; Lai, B.; Maser, J.; Paunesku, T.; Woloschak, G. E., *Nanoscale Res. Lett.* **2007,** *2*, 430-441.

(25) Kohlwein, S. D., *Microscopy Res. Tech.* **2000,** *51*, 511-529.

(26) Fernandez, N.; Puente, P.; Leal, F., *FEMS Microbiol. Lett.* **1990,** *69*, 7-11.

(27) Munn, A. L., *Biochim. Biophys. Acta, Mol. Basis Dis.* **2001,** *1535*, 236-257.

(28) Kaksonen, M.; Toret, C. P.; Drubin, D. G., *Nature Rev. Molec. Cell Biol.* **2006,** *7*, 404-414.

(29) Glowka, E.; Lamprecht, A.; Ubrich, N.; Maincent, P.; Lulek, J.; Coulon, J.; Leroy, P., *Nanotechnology* **2006,** *17*, 2546-2552.

(30) Cousins, B. G.; Allison, H. E.; Doherty, P. J.; Edwards, C.; Garvey, M. J.; Martin, D. S.; Williams, R. L., *J. App. Microbiol.* **2007,** *102*, 757-765.

(31) Williams, A. T. R.; Winfield, S. A.; Miller, J. N., *Analyst* **1983,** *108*, 1067-71.

(32) Matsunak.S; Morita, S.; Conti, S. F., *Plant Physiology* **1966,** *41*, 1364-1372.

(33) Andersson, H.; Baechi, T.; Hoechl, M.; Richter, C., *J. Microscopy* **1998,** *191*, 1-7.

(34) Bhatta, H.; Goldys, E. M., *FEMS Yeast Res.* **2008,** *8*, 81-87.

(35) Rosso-Vasic, M.; Spruijt, E.; van Lagen, B.; de Cola, L.; Zuilhof, H., *Small*, **2008**, *10, 1835-1841.*

(36) Gilbert;, A.; Baggot, J., *Essentials of Molecular Photochemistry*. Blackwell Scientific Publications: Oxford, 1991.

(37) English, D. S.; Pell, L. E.; Yu, Z. H.; Barbara, P. F.; Korgel, B. A., *Nano Lett.* **2002,** *2*, 681-685.

(38) Rosso-Vasic, M.; Spruijt, E.; Popovic, Z.; Van Lagen, B.; De Cola, L.; Zuilhof, H., *submitted*.

(39) Egner, A.; Jakobs, S.; Hell, S. W., *Proc. Nat. Acad. Sci. U.S.A.* **2002,** *99*, 3370-3375.

(40) Reungpatthanaphong, P.; Dechsupa, S.; Meesungnoen, J.; Loetchutinat, C.; Mankhetkorn, S., *J. Biochem. Bioph. Methods*, **2003,** *57*, 1-16.

(41) Veal, D. A.; Deere, D.; Ferrari, B.; Piper, J.; Attfield, P. V., *J. Immun. Meth.* **2000,** *243*, 191-210.

(42) Ludovico, P.; Sansonetty, F.; Corte-Real, M., *Microbiology* **2001,** *147*, 3335-3343.

Chapter 6

Summary & General Discussion

Abstract – This chapter gives a brief overview of the research results presented in this thesis. Furthermore, some personal views, ideas about possible applications of Si NPs and recommendations for further research are given in the general discussion chapter.

6.1 Summary

Nanotechnology is an emerging multidisciplinary science that involves the formation, investigation and manipulation of nanoobjects (1 - 100 nm). It has a huge potential to revolutionize diverse fields as engineering and medicine since the basis of many different physical processes can now be controlled up to the nanometer-scale and since the nanoworld yields access to novel processes.

For almost two decades, research into semiconductor nanoclusters has been focused on the properties of *quantum dots (QDs)* - semiconductor fragments consisting of hundreds to thousands of atoms.[1] Due to their unique size–range, characteristically on the boundary between quantum mechanics and Newtonian physics, the properties of nanoparticles differ from those of the bulk and of single atoms. Quantum dots have exceptional optical and electronic properties such as: size dependent - tunable light emission wavelengths,[1-3] intense fluorescence,[4-7] resistance against photobleaching[8] and simultaneous excitation of multiple fluorescent colors.[9-12] All these qualities make QDs in many respects superior over organic dyes and fluorescent proteins that are used for bioimaging purposes so far. QDs can be synthesized from a variety of materials with different sizes, shapes and morphologies. The most studied are complex core/shell/coat (CdS/ZnS/silane) QDs which can be produced in a variety of colors (sizes). However, their high intrinsic toxicity and minimal sizes (10 – 20 nm due to their complex structure) are an issue when considering them as candidates for *in vivo* bioimaging. Therefore, a huge interest arose in the possible development of smaller, non-toxic, stable and more versatile nanoparticles (NPs).

On the other side, application of Si was limited only to (micro-)electronics and its photoemission potential has not been realized for years. Due to the indirect band gap in bulk Si, light absorption and emission occur only when the absorption or the emission of a photon and a specific change in a lattice vibration mode occurs simultaneously. Consequently, the photoluminescence of bulk silicon is very weak.

Nonetheless, by creating Si with nanoscale dimensions (silicon nanoparticles), it can be coaxed to emit visible light with relatively high efficiencies. 1-10 nm Si NPs luminesce intensely over a wide range of wavelengths, from UV (for NPs < 2 nm) to IR (NPs > 8 nm).

Silicon surfaces can be well passivated, by creating stable Si-C bonds. The methods to tailor silicon surfaces were developed on porous and planar Si and can also be applied for the functionalization of Si NPs surfaces. Such a coating of Si NPs could prevent surface oxidation. A high luminescence, well-developed surface passivation principles, and a low inherent toxicity of Si initiated the enthusiasm for the research in Si NPs.

The goals of the work described in this thesis are:

- the development and optimization of methods for the preparation of stable and monodisperse Si NPs,
- photophysical characterization of such NPs, also in dependence on their functionalization,
- the exploration of their possible applications, specifically in the realm of bioimaging.

Chapter 1 describes general properties of semiconductor quantum dots and Si NPs, in particular. The origin of Si NPs luminescence is described in detail, and an overview of published methods for the synthesis of Si NPs is given, with a discussion of the advantages and drawbacks of each method.

Experimental work is described in Chapter 2, 3, 4 and 5.

Chapter 2 describes the first gram–scale preparation of highly monodisperse alkyl-terminated Si NPs (diameter of 1.57 ± 0.21 nm) in reverse micelles.[13] Both steady-state and time-resolved absorption and emission techniques, as well as FTIR (Fourier Transform InfraRed Spectroscopy) and XPS (X-ray Photoelectron Spectroscopy) measurements are used to study their photophysical properties and chemical composition in detail. For the first time, due to the relatively efficient synthesis, the molar extinction coefficient of alkyl-terminated Si NPs is experimentally determined to be $\varepsilon_{280} = 9.4 \times 10^3\ M^{-1}cm^{-1}$, only a factor 8 lower than that of CdS and CdSe NPs of that size. The measured quantum yields of emission ranged from 0.12 ($C_{10}H_{21}$ capping) to 0.23 ($C_{16}H_{33}$ capping). TEM measurements confirm the high monodispersity of Si NPs. Also, time-resolved fluorescence anisotropy measurements, displayed a strictly monoexponential decay that can only be indicative of monodisperse, ball-shaped nanoparticles. The thus developed method was further applied to obtain Si NPs with different functionalizations that could be used to develop various applications.

The preparation of very stable and bright water-soluble amine-terminated Si NPs is described in *Chapter 3*. The Si NPs were synthesized with different alkyl-chain lengths between the amine group and the surface of the NP: Si-$C_3H_6NH_2$, Si-$C_6H_{12}NH_2$ and Si-$C_{11}H_{22}NH_2$ NPs.[14] A highly improved synthesis method is presented, and the photophysical characterization of alkyl-amine coated Si NPs, including steady-state and time-resolved fluorescence, as well as STS (Scanning Tunneling Spectroscopy) measurements is discussed. The topography of amine-terminated Si NPs is examined using transmission electron microcopy (TEM) and scanning tunneling microscopy (STM) techniques. TEM measurements indicate a homogeneous size distribution (1.57 ± 0.24 nm). This size was independent of the alkyl spacer length, which excludes effects of the Si NP core size on their optical properties, and also shows that the method used to make

such NPs is very reproducible. Size distribution histograms obtained by TEM and STM display highly similar height distributions. All synthesized amine-terminated Si NPs show a broad continuous absorption between 200 and 380 nm. The absorption spectrum of the 3-amino-propyl-terminated Si NPs has a distinctive broad peak at 300 nm, while for Si NPs with longer alkyl chains between the Si core and the amine group, this peak was not pronounced. The electronic band gap of propyl-amine-terminated Si NPs is determined by STS measurements of individual NPs; ~ 60% of the observed particles have a band gap of ~4 eV, which exactly corresponds to an absorption peak at 300 nm.

All NPs under study displayed an intense, well-defined emission in the 350 – 600 nm range. The emission spectra, and specifically the wavelength at which the maximum emission intensity is observed, depend on the length of the alkyl spacer. With a short (-C_3H_6) spacer the maximum emission is observed in the blue with a maximum centered at 475 nm, when exciting Si NPs with 390 nm. For longer chains the maximum emission gradually shifts to the UV: for the $C_{11}H_{22}$ spacer λ_{exc}^{max} = 320 nm, with the maximum emission is centered at 385 nm. Two factors may contribute to this shift: the amine-to-Si core distance, and a higher degree of oxidation with shorter alkyl chains, as longer alkyl chains may provide a better passivation of the Si NPs surface. A Stokes shift of ~1 eV also points out to the formation of trapped states. The excited-state lifetimes are in the ns range and indicate direct band-gap processes.

The stability of NH_2-terminated Si NPs is exceptionally good over a wide pH range (1 - 13!) and high temperatures (120 °C), which is of great importance for a variety of possible applications including cell contents of various pH values and sterilization conditions. The prepared amine-terminated Si NPs are shown to be highly suitable for bio-imaging studies. They display a very high mobility in water ($D = 3.13 \cdot 10^{-10}$ m^2s^{-1}), and are readily taken up by BV2 nerve cells. After the uptake Si NPs are located in the cell cytosol. For the first time, proliferation of BV2 cells stained with Si NPs is observed by confocal microscopy. The newly formed daughter cells are also stained with Si NPs, indicating their minimal toxicity. In this way, amine-terminated Si NPs can be successfully used for staining multiple cell generations by only staining the mother cells.

The possible use of Si NPs as an active energy donor in energy-transfer processes is described in *Chapter 4.* To that aim, a ruthenium-containing dye was attached to Si NPs, while the chain length of the alkyl spacer between the possible donor and acceptor was varied. In order to examine if an energy transfer occurs, Si NPs emission intensities and lifetimes were measured with and without a Ru dye attached to Si NPs. In this way, it was shown that Si NPs can act as a very efficient energy donor, with energy transfer efficiencies up to 55%. Also, energy transfer efficiency is shown to be distance

dependent. This opens up a venue for numerous applications of Si NPs as efficient energy donors in various systems.

As the fast and efficient synthesis procedure of amine- and alkyl-terminated Si NPs was established, it became highly convenient to functionalize Si NPs via an easy and versatile route. Therefore, *Chapter 5* deals with the development of a method for the production of stable azide-terminated Si NPs and their further functionalization using “click” chemistry. The produced azide-terminated Si NPs were studied by FTIR, steady-state and time-resolved absorption and emission spectroscopy. They absorb light in the UV spectral region and emit light at ~ 350 nm. Stable azide-terminated Si NPs were further functionalized with a number of functional terminal alkynes: undec-10-yn-1-ol, propargyl amine, undec-10-ynoic acid, undec-10-ynyl hepta-O-acetyl lactoside and rhodamine-labeled lactoside. In this way, once synthesized, the azide-terminated Si NPs can be rapidly functionalized with many moieties of interest.

The cellular uptake of rhodamine-labeled Si NPs was successfully demonstrated by using yeast cells (*Rhodotorula glutinis*). Yeast cells were allowed to actually grow in the presence of Si NPs. It was shown by confocal microscopy that rhodamine-labeled Si NPs are located in mitochondria, and no effect on the cells proliferation rate was observed. Our findings clearly demonstrate that Si NPs are biocompatible and can be internalized by growing cells. The cellular uptake and internal localization under varying physiological conditions can now be studied in more detail, and with more complex functionalities attached onto the Si NPs. The results of this study open the way for further progress in research on Si NPs as imaging agents and effective delivery vehicles for the transport of biologically active compounds into specific cells of interest.

6.2 General Discussion and Future Prospects

The results described in the previous chapters represent a good basis to understand the properties of Si NPs. They also give a solution for the synthesis of monodisperse and non-oxidized particles and show possible applications in bioimaging and as efficient energy donors. However, there are several issues that must be addressed before Si NPs become widely used biomarkers and solar cell supplements. They can be categorized in two main directions: impact of Si NPs and modification of Si NPs.

It is already demonstrated that Si has a low intrinsic toxicity, in contrast to Cd, for example. This is a huge advantage of Si NPs when considering their application. Conversely, there are only few studies about toxicity of NPs, in general. While the number of NPs types continues to increase, studies to characterize their effects after exposure and to address their potential toxicity are few in comparison. It is still not very clear what happens with NPs

once they enter the body, where they are stored and how they influence various functions in cells and organism in whole.

For Si NPs to move into the clinical arena, it is important that toxicology research uncovers and understands how multiple factors like their size, composition, coverage, stability, concentration etc. influence the toxicity of NPs so that their undesirable properties can be avoided. Potential areas of Si NPs application in medical purposes are: high-resolution cellular imaging, long-term in vivo observation of cell trafficking, tumor targeting, diagnostics, etc. For all of them it is significant if Si NPs would undergo biodegradation in cellular environment and what cellular degraded Si NPs may induce.[15]

In order to come closer to application of Si NPs for bioimaging, more studies are required. The research we have started on BV2 and yeast cells must be more systematic. This can not be achieved without a strong link between preparative work and toxicology studies.

With respect to the synthesis of Si NPs, it would be extremely useful to extend the method for production of bigger-scale and monodisperse Si NPs to a wide range of sizes (colors). Bigger particles could be made using the same approach (reverse micelles as nanoreactors) but the micelle size (namely surfactant type) and the amount of silicon material should be varied.

This would provide a wider range of applications, especially in bioimaging, where dyes emitting < 600 nm are problematic to use, since biomaterials could be seriously damaged by the UV light needed for their excitation, and because autofluorescence is otherwise a nearly insurmountable problem. Si NPs with significantly higher emission wavelengths could also be used for deep-tissue imaging, as there would be much less interference (absorption) by the surrounding biomaterial.

The use of Si NPs for bioimaging should definitely be examined and extended to a wide variety of cell types, as each of them might display different toxicities. The influence of the functional groups attached to Si NPs should also be examined in detail, because this could also be a source of toxicity and not the Si NPs themselves.

The possibility to direct Si NPs to a specific cell compartment is another area of interest. As we have already shown in Chapter 3 and 5, by attaching amine groups or Rhodamine B to Si NP, they can specifically be located in the cytosol or the mitochondria, respectively. This could be “the way to go” in specific cell labeling and therefore the functionalization range should be significantly expended.

As the Si NPs are proven to be excellent energy donors (Chapter 4) there is a big opportunity in using them as a supplement to Grätzel type of solar cells, in which they could serve as sensitizers to Ru complexes. Their high extinction coefficients and decent emission quantum yields would make them a great candidate for many other energy transfer studies.

In order to increase the energy transfer efficiency, other metal-complexes should be considered as acceptors. Another interesting use of Si NPs would be as a part of white light emitter. This kind of emitter could be made from the already prepared dual-light emitter (blue-red Si NPs – Ru-complex) by attaching a green emitter (another metal complex) to the system.

As we have measured both molar extinction coefficient of alkyl- and amine-terminated Si NPs of the same size, and shown that amine-terminated NPs absorb almost 20 times more light, it would be very interesting to systematically explore how the molar extinction coefficient is changing with a change of the size of Si NPs, and how it depends on the functional groups attached to the Si NPs of each given size. In this way it might be possible to increase the extinction coefficient of functionalized Si NPs even more, while it will 'shine light' on the mechanisms involved in the absorption of photons by such ultrasmall Si clusters.

In addition, a little is known about hydrosilylation reaction mechanism on ultrasmall Si NPs. It is already shown[16] that the UV-blue emitting 1-2 nm Si NPs, can serve as excellent photocatalysts for the reduction and degradation of organic compounds. Therefore, it is very important to examine the effect of small Si NPs, as synthesized by methods described in this thesis, on the terminal alkene or any other compound in their vicinity, and to define how the attachment exactly takes place. For that purpose, highly advanced 2D and ^{29}Si - ^{13}C - ^{1}H NMR techniques should be used. Also, interesting question would be - what happens if the hydrosilylation reaction takes place in the dark or without sonication?

Moreover, the attachment of specifically functionalized Si NPs to metal NPs or metal surfaces would be of interest, as it is known that they can significantly enhance the emission of NPs due to interactions with surface plasmons.[17] This could be highly beneficial for use of Si NPs as various sensors.

Solving some of the above mentioned problems would bring Si NPs closer to commercial applications, as there is a rising interest for their use in many different areas. Practical applications will not come without careful research, but the multidisciplinary nature of nanotechnology may accelerate these goals by combining the great minds of many different fields of science.

The future of exciting and excitable Si NPs is definitely bright!

6.3. References

(1) Alivisatos, A. P. *Science* **1996**, *271*, 933-937.

(2) Kastner, M. A. *Physics Today* **1993**, *46*, 24-31.

(3) Brus, L. *J. Phys. Chem. Solids* **1998**, *59*, 459-465.

(4) Guyot-Sionnest, P.; Hines, M. A. *A. Phys. Lett.* **1998**, *72*, 686-688.

(5) Hines, M. A.; Guyot-Sionnest, P. *J. Phys. Chem.B* **1998**, *102*, 3655-3657.

(6) Eychmuller, A. *J. Phys. Chem. B* **2000**, *104*, 6514-6528.

(7) Willard, D. M.; Carillo, L. L.; Jung, J.; Van Orden, A. *Nano Lett.* **2001**, *1*, 469-474.

(8) Chan, W. C. W.; Nie, S. M. *Science* **1998**, *281*, 2016-2018.

(9) Chan, W. C. W.; Maxwell, D. J.; Gao, X. H.; Bailey, R. E.; Han, M. Y.; Nie, S. M. *Curr. Opin. Biotech.* **2002**, *13*, 40-46.

(10) Chu, M. Q.; Sun, Y.; Liu, G. J. *Mat. Sci. Tech.* **2006**, *22*, 1240-1244.

(11) Gao, X. H.; Chan, W. C. W.; Nie, S. M. *J. Biomed. Optics* **2002**, *7*, 532-537.

(12) Gao, X. H.; Dave, S. R. *Bio-Applic. Nanoparticles* **2007**, *620*, 57-73.

(13) Rosso-Vasic, M.; Spruijt, E.; van Lagen, B.; de Cola, L.; Zuilhof, H. *Small*, **2008**, 10, 1835-1841.

(14) Rosso-Vasic, M.; Spruijt, E.; Popovic, Z.; Overgaag, K.; Van Lagen, B.; Grandidier, B.; Vanmaekelbergh, D.; De Cola, L.; Zuilhof, H. *submitted*.

(15) Lewinski, N.; Colvin, V.; Drezek, R. *Small,* **2008**, *4*, 26-49.

(16) Kang, Z. H.; Tsang, C. H. A.; Wong, N. B.; Zhang, Z. D.; Lee, S. T. *J. Am. Chem. Soc.***2007**, *129*, 12090-12091.

(17) Lakowicz, J. R. *Plasmonics* **2006**, *1*, 5-33.

Samenvatting

Nanotechnologie is een opkomende multidisciplinaire tak van wetenschap die zich bezighoudt met het vormen, onderzoeken en bewerken van nano-objecten (1 - 100 nm). Het heeft een groot potentieel in diverse velden, zoals in de techniek en medische wetenschap, omdat de basis van verschillende fysische processen nu gecontroleerd kan worden op nanometerschaal, en omdat de nanowereld toegang biedt tot nieuwe processen.

Al bijna twintig jaar is het onderzoek naar halfgeleider nanoclusters gefocuseerd op de eigenschappen van *Quantum Dots (QDs)* – halfgeleiderfragmenten bestaande uit honderden tot duizenden atomen.[1] Door hun unieke formaat, karakteristiek gelegen op de grens tussen quantummechanica en Newtoniaanse fysica, verschillen de eigenschappen van de nanodeeltjes ten opzichte van bulkmaterialen en losse atomen. Quantum dots hebben uitzonderlijke eigenschappen, zoals grootte-afhankelijke en programmeerbare emissiegolflengtes,[1-3] intense fluorescentie,[4-7] resistentie tegen fotobleking[8] en gelijktijdige excitatie van meerdere fluorescente kleuren.[9-12] Al deze eigenschappen maakt QDs in vele opzichten superieur ten opzichte van organische kleurstoffen en fluorescente eiwitten, welke tot nu toe voor biologische kleuring veelal worden gebruikt. QDs kunnen gemaakt worden uit een variëteit aan materialen met verschillende groottes, vormen en morfologie. De meest bestudeerde deeltjes zijn complexe kern/schil/coating (CdS/ZnS/silane) nanodeeltjes, die geproduceerd worden met een breed spectrum aan kleuren (groottes). De intrinsieke toxiciteit en minimale groottes (10 - 20 nm, vanwege hun complexe structuur) zijn echter ook belangrijke punten als het gaat om *in vivo* biologische kleuring. Daarom is er een grote interesse ontstaan in de mogelijke ontwikkeling van kleinere, niet-toxische, stabiele en veelzijdig functionaliseerbare nanodeeltjes (NDs).

Aan de andere kant waren de toepassingsmogelijkheden van Si decennia lang gelimiteerd tot (micro-)elektronica. Dat Si ook fluorescent te maken was, is pas zo'n 15 jaar geleden gerealiseerd. Door de indirecte bandgap in bulk Si, kan absorptie of emissie van een foton alleen plaatsvinden als tegelijkertijd een specifieke verandering in de kristalvibratie plaatsvindt. De kans hierop is niet zo groot, en als gevolg hiervan is de fotoluminescentie van bulk silicium erg zwak. Deze beperking wordt opgeheven in Si met nanoschaal dimensies (poreus Si and silicium NDs), waarin de emissie van zichtbaar licht met relatief hoge efficiëntie kan optreden. Si NDs tussen 1-10 nm geven intense luminescentie over een breed spectrum van golflengtes, van het ultraviolette deel van het spectrum (voor NDs < 2 nm) tot het infrarode deel (NDs > ca. 8 nm).

Silicium oppervlakken kunnen goed worden gepassiveerd door het creëren van stabiele Si-C bindingen. De verschillende methoden om siliciumoppervlakken te bewerken die zijn ontwikkeld op poreus en vlak Si kunnen ook worden toegepast voor de functionalisering van

Si ND oppervlakken. Zulke coatings op Si NDs kunnen oxidatie voorkomen. De hoge luminescentie, de goed ontwikkelde oppervlaktepassivatie en de lage inherente toxiciteit hebben het onderzoek naar Si NDs in sterke mate gestimuleerd.

De doelen van het onderzoek dat in dit proefschrift beschreven staat zijn:

- ontwikkeling en optimalisatie van methoden voor het maken van stabiele, monodisperse Si NDs,
- fotofysische karakterisatie van dergelijke NDs, mede in afhankelijkheid van hun functionalisering,
- aanvang maken met evaluatie van gefunctionaliseerde Si NDs voor toepassingen gericht op biologische kleuringen.

Hoofdstuk 1 beschrijft de algemene eigenschappen van halfgeleider QDs en Si NDs in het bijzonder. Vervolgens wordt de oorsprong van de fotoluminescentie gedetailleerd beschreven. Tot slot wordt een overzicht gegeven van de gepubliceerde methoden om Si NDs te maken, met een discussie over de voor- en nadelen van iedere methode.

Het experimentele werk is beschreven in de hoofdstukken 2, 3, 4 en 5.

Hoofdstuk 2 beschrijft de eerste gramschaal synthese van zeer monodisperse, alkylgetermineerde Si NDs (diameter van 1.57 ± 0.21 nm) in omgekeerde micellen.[13] Zowel steady-state en tijdsopgeloste absorptie- en emissietechnieken, FTIR (Fourier Transform InfraRed Spectroscopy) en XPS (X-ray Photoelectron Spectroscopy) zijn gebruikt om de fotofysische eigenschappen en chemische samenstelling in detail te bestuderen. Door de relatief efficiënte synthese was het voor het eerst mogelijk de extinctiecoëfficient van de alkylgetermineerde deeltjes te bepalen op ε_{280}= 9.4 × 10^3 $M^{-1}cm^{-1}$. Deze waarde bleek aantrekkelijk hoog, en o.a. slechts 8 keer lager dan die van CdS en CdSe NDs van dezelfde grootte. De gemeten emissie quantumopbrengst varieert van 0.12 ($C_{10}H_{21}$ terminatie) to 0.23 ($C_{16}H_{33}$ terminatie).Tijdsopgeloste fluorescentie anisotropie metingen laten een strikt monoexponentieel verval zien dat alleen kan komen van monodisperse, bolvormige nanodeeltjes. De ontwikkelde methode is verder toegepast om Si NDs te verkrijgen met verschillende functionaliteiten die verder ontwikkeld kunnen worden voor verschillende toepassingen.

De synthese van zeer stabiele en heldere wateroplosbare aminegetermineerde Si NDs is beschreven in *Hoofdstuk 3*. De Si NDs zijn gemaakt met verschillende lengtes van de alkylketens tussen de aminegroep en het oppervlak van het ND: Si-$C_3H_6NH_2$, Si-$C_6H_{12}NH_2$ en Si-$C_{11}H_{22}NH_2$ NDs.[14] Een sterk verbeterde synthesemethode wordt gepresenteerd, en de fotofysische karakterisatie van alkyl-amine gefunctionaliseerde Si NDs wordt bediscussieerd, inclusief steady-state en tijdsopgeloste fluorescentie en STS (Scanning Tunneling Spectroscopy) metingen. De topografie van de aminegetermineerde Si NDs is bepaald met

behulp van transmissie electron microscopie (TEM) en scanning tunneling microscopie (STM) technieken. De TEM metingen wijzen op een homogene grootte-distributie (1.57 ± 0.24 nm). Deze grootte was onafhankelijk van de alkylketenlengte, die effecten van de Si ND kern op de optische eigenschappen uitsluit, en bovendien laat zien dat de methode om zulke Si NDs te maken zeer reproduceerbaar is. Histogrammen van de distributie van de grootte zoals verkregen uit TEM en STM metingen laten analoge verdelingen zien. Alle gesynthetiseerde amine-getermineerde Si NDs laten een brede absorptie zien tussen 200 en 380 nm. Het absorptiespectrum van de 3-aminopropyl-getermineerde Si NDs laat een duidelijke piek zien bij 300 nm, terwijl voor de Si NDs met langere alkylketens tussen de Si kern en de aminegroep deze piek niet zichtbaar is. De electronische bandgap van de propylaminegetermineerde Si NDs is bepaald met STS metingen van individuele NDs, ~60% van de gemeten deeltjes hebben een bandgap van ~4 eV, dat precies overeenkomt met de absorptiepiek bij 300 nm.

Alle bestudeerde Si NDs laten een intense, goed gedefinieerde emissie zien tussen 350 - 600 nm. De emissiespectra, en specifiek de golflengte bij welke de maximale emissie gemeten wordt, zijn afhankelijk van de lengte van de alkylketen. Met een korte keten ($-C_3H_6$) wordt de maximale emissie gemeten in het blauw, met een maximum bij 475 nm, met excitatie van de Si NDs bij 390 nm. Voor langere ketens schuift de maximale emissie naar het UV-gebied: voor de $C_{11}H_{22}$ alkylketen λ_{exc}^{max} = 320 nm, met een maximale emissie bij 385 nm. Twee factoren dragen bij aan deze verschuiving: de amine-tot-Si kern afstand, en een hogere graad van oxidatie met kortere alkylketens, omdat langere alkylketens een betere passivatie van het oppervlak van de Si NDs kunnen verzorgen. Een Stokes shift van ~1 eV wijst op de formatie van opgesloten toestanden. De levensduur van de aangeslagen toestand is in de orde van ns, en wijst op een directe bandgap proces.

De stabiliteit van NH_2-getermineerde Si NDs is uitzonderlijk goed, over een breed pH gebied (1 - 13!) en tot hoge temperaturen (120 °C), wat erg belangrijk is voor verschillende mogelijke toepassingen, zoals de bepaling van componenten van celleb met verschillende pH-waarden en de optie deze NDs te steriliseren voor gebruik. De gesynthetiseerde aminegetermineerde Si NDs laten zien dat ze erg geschikt zijn voor bio-imaging studies. Ze laten een hoge mobiliteit in water zien ($D = 3.13 \cdot 10^{-10}$ m^2s^{-1}) en worden gemakkelijk opgenomen door BV2-zenuwcellen. Na opname zijn de Si NDs gesitueerd in het cytosol. Voor het eerst is proliferatie van BV2 cellen, gekleurd met Si NDs, geobserveerd., Met confocale microscopie is aangetoond dat ook de nieuwe dochtercellen Si NDs bevatten, wat wijst op een minimale toxiciteit. Op deze manier kunnen de aminegetermineerde Si NDs succesvol gebruikt worden om meerdere generaties cellen te imagen door het kleuren van alleen de moedercel.

Het mogelijke gebruik van Si NDs als actieve energiedonor in energieoverdrachts-processen is beschreven in *Hoofdstuk 4*. Met dat doel is een ruthenium-bevattende kleurstof gekoppeld aan Si NDs, terwijl de ketenlengte tussen de mogelijke donor en acceptor gevarieerd is. Om te bepalen of energieoverdracht plaatsvond, werd de intensiteit van de emissie van de Si NDs en hun fluorescentielevensduur bepaald met en zonder de gekoppelde Ru-kleurstof . Op deze manier is aangetoond dat Si NDs als een zeer efficiënte donor kunnen fungeren, met energieoverdrachtsefficiënties tot 55%. Ook is aangetoond dat de efficiëntie van energieoverdracht afhankelijk is van de afstand. Dit opent een groot aantal mogelijkheden voor toepassingen van de Si NDs als efficiënte energiedonoren in verschillende systemen.

Hoofdstuk 5 behandelt de ontwikkeling van een synthese van stabiele azidegetermineerde Si NDs en de verdere functionalisatie door middel van “click” chemie. De gesynthetiseerde azidegetermineerde Si NDs zijn bestudeerd met FTIR, steady-state en tijdsopgeloste absorptie- en emissiespectroscopie. Ze absorberen licht in het UV-gebied en emitteren bij ~350 nm. Stabiele azidegetermineerde Si NDs zijn gefunctionaliseerd met verschillende terminale alkynen: undecec-10-yn-1-ol, propargylamine, undec-10-ynoic acid, undec10-ynyl lactoside, undec-10-ynyl hepta-O-acetyl lactoside en rhodamine gelabelde lactoside. Op deze manier kunnen de gesynthetiseerde azidegetermineerde Si NDs snel gefunctionaliseerd worden met veel interessante groepen.

De cellulaire opname van rhodamine-gelabelde Si NDs is succesvol gedemonstreerd, gebruik makende van gistcellen *(Rhodotorula glutinis*). De gistcellen zijn gegroeid in de aanwezigheid van Si NDs. Daarna is met confocale microscopie aangetoond dat de rhodamine-gelabelde Si NDs gelocaliseerd zijn in de mitochondriën van de gistcellen, en dat er geen effect op de snelheid van celproliferatie waarneembaar is. Deze resultaten laten duidelijk zien dat de Si NDs compatibel zijn met biologische systemen en door groeiende cellen kunnen worden opgenomen. De cellulaire opname en interne localisatie onder verschillende fysiologische condities kunnen nu in principe in meer detail bestudeerd worden, met meer complexe functionaliteiten gekoppeld aan de Si NDs. De resultaten van deze studie openen de weg voor verdere progressie in het onderzoek naar Si NDs zoals in biologisch toepasbare kleurstoffen en effectieve bezorgsystemen voor het transport van biologisch actieve componenten naar en binnen in specifieke cellen.

References

(1) Alivisatos, A. P. *Science* **1996**, *271*, 933-937.

(2) Kastner, M. A. *Physics Today* **1993**, *46*, 24-31.

(3) Brus, L. *J. Phys. Chem. Solids* **1998**, *59*, 459-465.

(4) Guyot-Sionnest, P.; Hines, M. A. *A. Phys. Lett.* **1998**, *72*, 686-688.

(5) Hines, M. A.; Guyot-Sionnest, P. *J. Phys. Chem.B* **1998**, *102*, 3655-3657.

(6) Eychmuller, A. *J. Phys. Chem. B* **2000**, *104*, 6514-6528.

(7) Willard, D. M.; Carillo, L. L.; Jung, J.; Van Orden, A. *Nano Lett.* **2001**, *1*, 469-474.

(8) Chan, W. C. W.; Nie, S. M. *Science* **1998**, *281*, 2016-2018.

(9) Chan, W. C. W.; Maxwell, D. J.; Gao, X. H.; Bailey, R. E.; Han, M. Y.; Nie, S. M. *Curr. Opin. Biotech.* **2002**, *13*, 40-46.

(10) Chu, M. Q.; Sun, Y.; Liu, G. J. *Mat. Sci. Tech.* **2006**, *22*, 1240-1244.

(11) Gao, X. H.; Chan, W. C. W.; Nie, S. M. *J. Biomed. Optics* **2002**, *7*, 532-537.

(12) Gao, X. H.; Dave, S. R. *Bio-Applic. Nanoparticles* **2007**, *620*, 57-73.

(13) Rosso-Vasic, M.; Spruijt, E.; van Lagen, B.; de Cola, L.; Zuilhof, H. *Small*, **2008**, 10, 1835-1841.

(14) Rosso-Vasic, M.; Spruijt, E.; Popovic, Z.; Overgaag, K.; Van Lagen, B.; Grandidier, B.; Vanmaekelbergh, D.; De Cola, L.; Zuilhof, H. *submitted*.

Curriculum Vitae

Milena Rosso-Vasic was born in Bor, Serbia, on the 12th January 1979. She finished gymnasium “Bora Stankovic” (mathematics and sciences division) in Bor (1994-1998). During primary and high school she won prizes in numerous competitions in chemistry, on republic and international levels (like Bios-Olympiad). While studying Physical Chemistry at the University of Belgrade (1998-2004) she also actively participated in chemistry education programs for talented high-school students in Petnica Science Center, Valjevo, Serbia. Within the specialization in energy conversion and catalysis, she worked on undergraduate research project in the Department of Chemical and Biomolecular Engineering at the University of Illinois, Urbana-Champaign, USA in the summer of 2000 in the Laboratory of Prof. Richard Massel. In 2002 she did her diploma project in the Laboratory for Technical Chemistry, ETH Zurich with Prof. Roel Prins.

In May 2004. she started her PhD project, described in this thesis, at Wageningen University, Laboratory of Organic Chemistry, under joint supervision of Prof. Luisa De Cola and Prof. Han Zuilhof.

Since May 2008, she is working at Albemarle Catalysts Company BV in the Department of Alternative Fuel Technologies.

List of Publications

Omegna, A.; Vasic, M.; van Bokhoven, J. A.; Pirngruber, G.; Prins, R., Dealumination and realumination of microcrystalline zeolite beta: an XRD, FTIR and quantitative multinuclear (MQ) MAS NMR study. *Phys. Chem. Chem. Phys.* **2004**, 6, (2), 447-452.

Rosso-Vasic, M.; Spruijt, E.; van Lagen, B.; de Cola, L.; Zuilhof, H., Alkyl-functionalized oxide-free silicon nanoparticles: synthesis and optical properties. *Small*, **2008**, 10, 1835-1841.

Rosso-Vasic, M.; Spruijt, E.; Popovic, Z.; Overgaag, K.; Van Lagen, B.; Grandidier, B.; Vanmackelenbergh, D.; De Cola, L.; Zuilhof, H., Amine-terminated Silicon Nanoparticles: Synthesis, Optical Properties and their Use in Bioimaging, *submitted*

Rosso-Vasic, M.; Weijers, C.; Spruijt, E.; Pukun, A.; van Lagen, B.; de Cola, L.; Zuilhof, H., Azide-terminated Silicon Nanoparticles: Functionalization using Click Chemistry and Uptake by Growing Yeast Cells, *submitted*.

Rosso-Vasic, M.; de Cola, L.; Zuilhof, H., Efficient Energy Transfer between Silicon Nanoparticles and a Ru-polypyridine complex, *submitted*.

Glossary of Acronyms

A	Acceptor
A.U.	Arbitrary Units
D	Donor
DMF	*N*-dimethylformamide
ET	Energy Transfer
FTIR	Fourier Transform Infrared Spectroscopy
FWHM	Full Width at Half Maximum
HOMO	Highest Occupied Molecular Orbital
ICP-MS	Inductively Coupled Plasma-Mass Spectrometry
IRF	Instrument Response Function
LUMO	Lowest Unoccupied Molecular Orbital
Me	Methyl-
MeOH	Methanol
MWCO	Molecular Weight Cut-Off
NMR	Nuclear Magnetic Resonance Spectroscopy
NP	Nanoparticle
PE 40-60	Petroleum ether fraction boiling between 40 and 60°C
PVDF	Polyvinylidene Fluoride
QD	Quantum Dot
QY	Quantum Yield
RET	Resonance Energy Transfer
Si	Silicon
TEM	Transmission Electron Microscopy
THF	Tetrahydrofuran
TMS	Tetramethylsilane
TOAB	Tetraoctylammonium bromide
UV	Ultraviolet region of the spectral domain
Vis	Visible region of the spectral domain
XPS	X-ray Photoelectron Spectroscopy

Acknowledgments

Four years ago, I entered the fascinating world of nanoscience. This journey has been a great experience and its final outcome is this thesis. I did not go on this trip alone and would like to thank all of you who helped in many different ways to finish this research and made this trip very special.

First of all I would like to thank my supervisors Prof. Han Zuilhof and Prof. Luisa De Cola for recognizing my ambition and giving me the opportunity to work on this project.

Han, thank you for all the discussions and support during the last four years. Your enthusiasm and scientific passion gave me a lot of boost and inspiration during the difficult research times. Also, thanks for the friendly support during the “transition period” from UvA. I learned a lot from you, not only from your explanations, but also from your questions. You taught me how to be accurate and clear, both in writing and in experiments. I would also like to thank you for all the Saturday hours that we spent writing articles and this thesis. With your help, I feel that I have improved my scientific writing skills and I promise to use more articles in my sentences ;-)

Luisa, I would like to thank you for all the inspiring discussions we had. The creativity and talent to form a group (De Cola group) that you have are certainly extraordinary. I very much enjoyed working in your group during my short trips to Munster. Thank you for organizing a wonderful group trip to Lipari, which was a great way to start the PhD chapter of my life!

Barend, I still don’t understand how you had the answer and solution to every question or practical problem I had during the last four years. Thanks for all the help with NMR, FTIR, fluorescence and UV measurements and with all the interpretations. Among all, I would like to thank you for your friendship. Every time there was some problem, you were on my side and I really liked sharing all the good news with you.

Carel, your expertise and really hard work in the last few months of my PhD study made Chapter 5 complete. I would like to thank you for all the discussions we had, the experiments with yeast cells that you have performed, the fluorescence measurements and the writing of a paper/chapter. Every time we spoke about experiments with cells, I learned so much from you and regretted that we did not start this collaboration a bit earlier. You stimulated a lot my interest in biology and in the little beautiful cells and their weird way of life.

When I moved from Belgrade to Wageningen I was really lonely. I missed all my friends and family back home. After 4 years, I am so grateful that I met so many great people here and that we became friends.

Kishore, you were one of the first people to become my friend in Holland. Thanks for your help in the most difficult moment in my life. Also, the first Si NPs were made with your help. I

hope you always stay the way you are now and wish you all the success. This world would be much better place if more people were like you.
Evan, working with you was really great. I enjoyed discussions we had and the way we were getting more and more clues about Si NPs after each experiment. It was nice to collaborate with such a motivated, bright and hardworking person. With your help, Si NPs moved very fast forward and you could recognize many of these findings in the previous pages.
Ahmed, you were always there for scientific advice and as a friend. You taught me so many practical things at the beginning of the PhD that have been really precious for my work. With you in Wageningen, I had an extra parent to take care of me. Thanks for everything.
Louis, my first labmate, thanks for all the help in the lab, especially at the beginning for showing me the way around. I always enjoyed chats at the end of the day while cleaning up for tomorrow's experiments and our trip to Yosemite and around. See you in Leiden;-)
My other labmates, Luc and Jurjen I would like to thank for all the gezelligheid that we had in and outside the lab. Working with you guys was always fun. Our discussions during the lunch, over the table football, helped a lot in setting up experiments and finding many answers that are described in this thesis. Although I did not like you in the beginning☺ I am honored that you will be my paranimphs. (Luc: please don't whistle during my defense!)
Anouk & Jurjen (the cheese fondue buddies), Luc & Janneke , Rosalie & Peter-Paul, thanks to your friendship I feel like home in NL. Rosalie & Anouk, I really enjoyed all the "girls avond's" we had.
Maud and Ioan, thanks for being such great pals, for sharing with us our special day, your friendship and much, much more.
I would also like to thank people from the De Cola group: Fred, Marita, Klaus (thanks for stretching the decays), Tasje, Franti, Anthony, Rene, Fabio's, Tora (the best disco party), Paolo, Ron, Shirinidi, Greg (bubamaro), Ausgeir for making possible for me to measure when I was in Munster (even if it was overlapping with your schedules) or in Amsterdam and for the great time we had on our trips to Lipari and Rome (very special accommodation and great people).
Special thanks goes to Jakob and Loes. Jakob, thanks for all the help with calculations and increasing the resolutions when needed;-). Discussions with you and your calculations improved a lot Chapter 4. Loes, thanks for running the last minute (successful!) experiments for this thesis. Thank you for translating the Summary and all the work we have done together. Have fun with Si NPs and a lot of success!
I would also like to thank the members of the Nanophotonics Flagship in NanoNed program, for all the regular discussions we had and also for giving me the opportunity to present this work at NanoNed conferences. I thank Professors Albert Polman, Rob Zsom and Fred

Brouwer for all the help and ideas. Also, big thanks to Geb Visser who was always interested in this work and was continuously bringing the new ideas. I am also grateful to Prof. Ernst Sudhölter for useful discussions and for finding the time to help us organizing PhD trips and joining us.

Mirjana, Mladjan, Gavrilo, Vesna, Olja, Hans, you made me feel less far from home. Mirjana & Vesna hvala vam za sve savete i prijateljstvo jos od mog drugog dana u Wageningenu. Sada vam konacno verujem da je Wageningen specijalno mesto, mada u pocetku uopste nije delovalo tako. Vi ste dva najbolja Srpska ambasadora na koje sam mnogo ponosna.

I would like to thank all my colleagues from Organic Chemistry: Elly, Aleida, Ronald, Teris, Ton, Melle, Annemarie, Aliaksei, Frank, Elbert, Gregor, Kishore, Ioan, Remko, Agnes, Bin, Ruud, Menglong, TuHa, Feng, Kim, Giedrius, Rokus, Bart, for the pleasant time in the lab. I enjoyed working with you, but also having borrels and lab trips. Also, our PhD trips to California and Sweden I will never forget!

I would like to thank Marcel Giesbers for measuring XPS, Jeanette Smulder for ICP-MS, Adriaan van Aelst and Benedikt Grala for all the hours spent in the search for tiny Si NPs with TEM.

It is important for me to mention the most special place in the world – Petnica Research Center (Serbia) (http://pi.petnica.net). In this wonderful place I grew my passion for science and shared my interest in chemistry with many extraordinary people that are still today my very close friends. Ninocka i Buba, hvala vam za svu podrsku i prijateljstvo tokom poslednjih 12! godina. Petnica je uvek bila svetlo u mraku i zvezda vodilja meni i mnogim prethodnim i buducim generacijama. Bez vaseg entuzijazma i pomoci nasi zivoti bi definitivno imali mnogo drugacije tokove.

Takodje, htela bih da se zahvalim Prof. Veri Dondur koja mi je bila uzor i podrska tokom studiranja i organizovanja praksi u inostranstvu. Bez Vase podrske, entuzijazma i prepoznavanja moje ambicije sigurna sam da bih ove redove pisala negde drugde i mnogo kasnije.

Najvece HVALA dugujem svojoj porodici: Mojim roditeljima, bakama i dekama zahvalna sam za ljubav, vaspitanje i divno detinjstvo. Mama i Minja, vasa ljubav, bezrezervna podrska i razumevanje, bile su mi uvek najveci oslonac, a specijalno tokom poslednje 4 godine. Hvala vam na svemu i sto ste uvek verovale u mene, cak i kada ja nisam. Sa vama je sve lepse, lakse i veselije. Specijalno hvala dugujem i mojim bakama Mirjani i Jeleni. Za svu ljubav i paznju kojom sa bila okruzena od malena, tople dzempere, Politikine Zabavnike i najbolju klopu na svetu. Veliko hvala dugujem mojoj tetki i teci – Svetlani i Milosu Ciricu, sto se cim sletim u Bg osecam kao kod kuce, za svu pomoc tokom studija i za izvanredne kulinarske

ture. Takodje, hvala Maji, Peci, Adriani, Eleni, ujka Ivici, Darku, porodicama Milev, Milosevic i Aleksic. Zbog svih vas uvek volim da se vracam u Srbiju.

Kale, iako prilicno daleko, uvek mi se cini da smo jako blizu i uvek tu jedna za drugu. Iako i sama znas da mi tvoje prijateljstvo neizmerno znaci, zelim da ti se zahvalim na razumevanju, svim razgovorima, ispracanjima i docecima i uvek dobrom provodu.

Zoki, nema tih reci kojima bih mogla da opisem koliko sam ti zahvalna na svemu. Upravo zato sto si ti vec bio u Amsterdamu, od kako sam dosla u NL nikada nisam bila usamljena. Hvala ti za podrsku, prijateljstvo i eksperimente koji su deo ove teze i mnogo toga jos sto definitivno ne moze da stane u par recenica, a verovatno ni u par knjiga.

Tamarice, moja internet drugarice, hvala za prijateljstvo i razumevanje tokom svih ovih godina.

Our summer holidays would not be so nice without my parents in law, as well as Laura, Nathalie and Damien. Thanks for all the good time in Cannes and around.

Michel, thank you for all the support and understanding during the last years and especially the last few months when finishing the thesis became quite intense. Your love and presence make me feel complete and happy, and make all the big problems look like nanoparticles. With you on my side, life is always colorful and fun.

Milena Rosso-Vasic

Wageningen, October 2008

Appendix

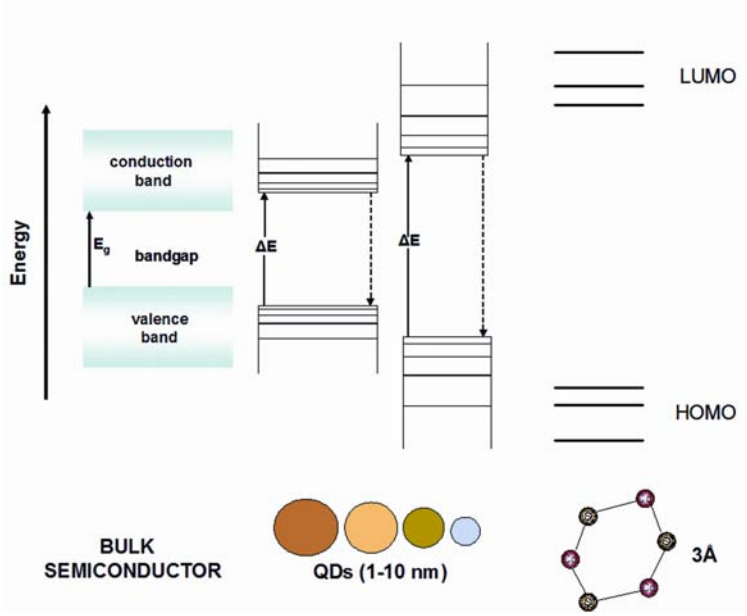

Figure 1.1. Semiconductor energy levels.

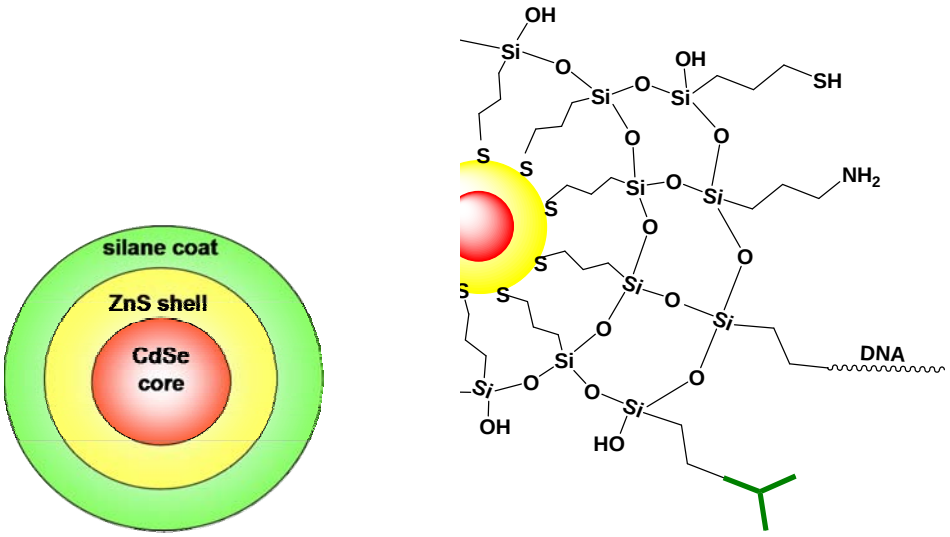

Figure 1.2. Sketch of core/shell/coat quantum dot and some possible functionalizations.

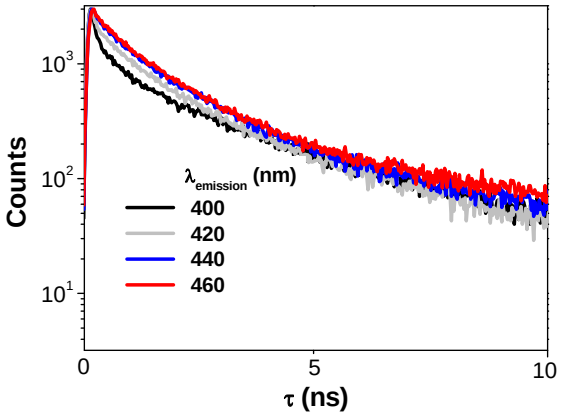

Figure 3.8. Fluorescence time-resolved decays at different emission wavelength for 3-amino-propyl terminated Si NPs in water, λ_{exc} = 372 nm.

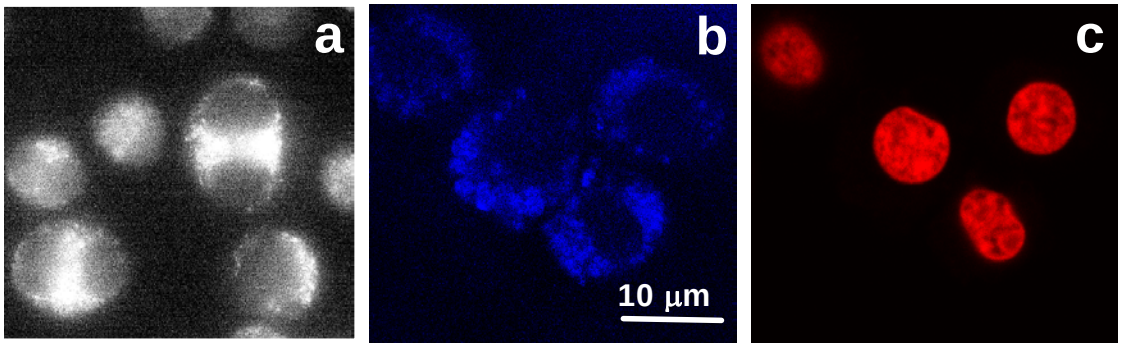

Figure 3.12. a) Epifluorescence image of mitosis of BV2 cells stained with Si NPs under blue light irradiation b) and c) Confocal images of BV2 cells simultaneously stained with Si NPs and DRAQ5.

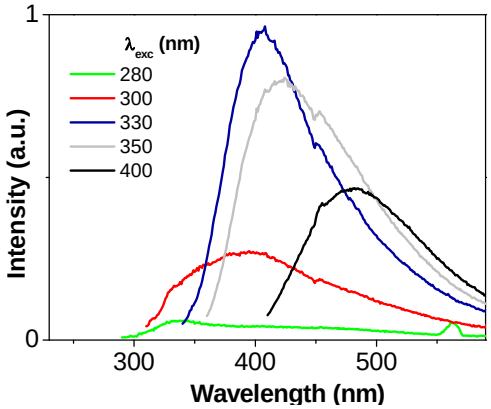

Figure 5.9. Emission spectrum of Si-$C_{11}N_3$ NPs clicked with propargyl amine in DMF.

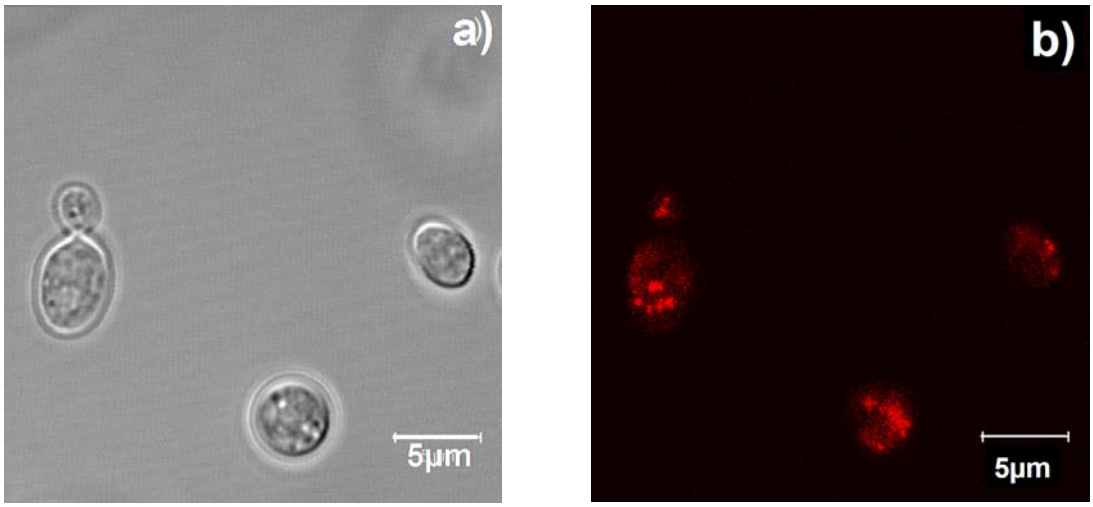

Figure 5.10. Cells of *Rhodotorula glutinis* grown in the presence of RhB Si NPs a) bright field image b) raw data of fluorescence image (λ_{exc} = 488 nm, λ_{em} = 560 - 615 nm).

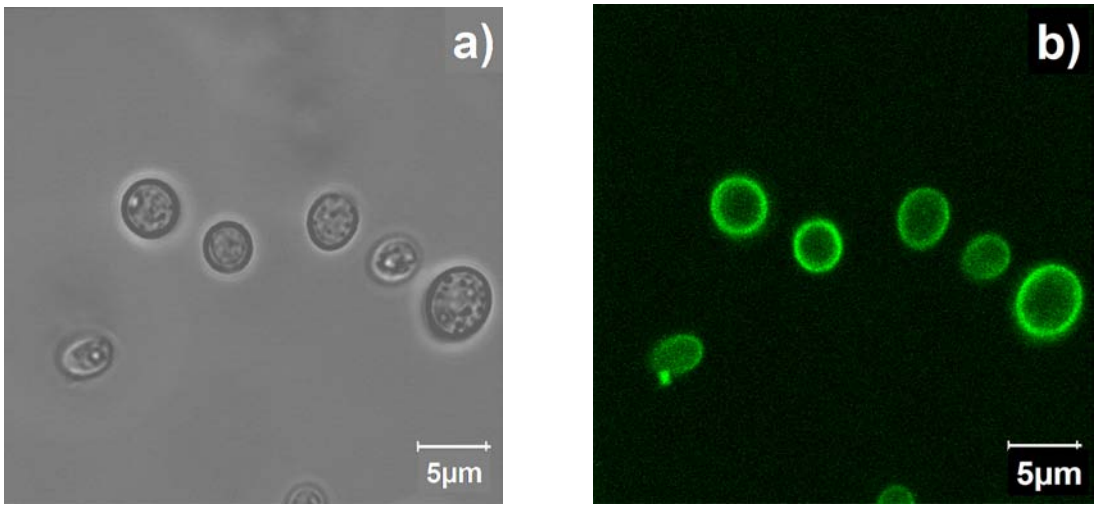

Figure 5.11. Cells of *Rhodotorula glutinis* grown in the presence of Rhodamine 123 a) bright-field image b) raw data of fluorescence image (λ_{exc} = 488 nm, λ_{em} = 505 - 530 nm).

Overview of completed training activities

Discipline specific activities

Courses

BioNano Technology, VLAG, 2005

Surface Analysis Course EPFL, Lausanne, Switzerland, 2006

Fundamentals of Nanotechnology, MESA+, University of Twente, 2006

Principles and Applications of Time-Resolved Fluorescence Spectroscopy, PicoQuant GmbH, Berlin, Germany, 2006

Meetings

Towards molecular electronics University of Ulm, Germany, 2004

Functional Materials for 21st century, University of Edinburgh, UK , 2005

Wageningen Symposium of Organic Chemistry, Wageningen University, 2006

Wageningen Bionanotech. Symposium, 88th Dies Natalis, Wageningen University, 2006

Annual NWO Conference, Lunteren, 2004-2008

Annual NanoNed Conference NanoNed, 2004-2008

General courses

Organising and supervising MSc thesis project, Wageningen University, 2007

IP valorisation course, Veldhoven, 2007

Optionals

Preparation PhD research proposal

PhD study trip, Organized by Laboratory of Organic Chemistry, USA, 2005

PhD study trip, Organized by Laboratory of Organic Chemistry, Sweden, 2007

Literature study, Laboratory of Organic Chemistry, 2004

Group meetings, Laboratory of Organic Chemistry, Wageningen, 2004-2008

The research described in this thesis was financially supported by NanoNed, funded by the Dutch Ministry of Economic Affairs (project WOE.7713).

Design and Layout: Milena Rosso-Vasic

Printed by: Grafisch Bedrijf Ponsen & Looijen BV, Wageningen